Review | Open Access

Microstructures

Zhao et al. Microstructures 2026, 6, 20260136 DOI:10.20517/microstructures.2026.176

# Laser-cladded coatings on titanium alloys: processing-microstructure relationships, phase evolution, and interfacial mechanisms

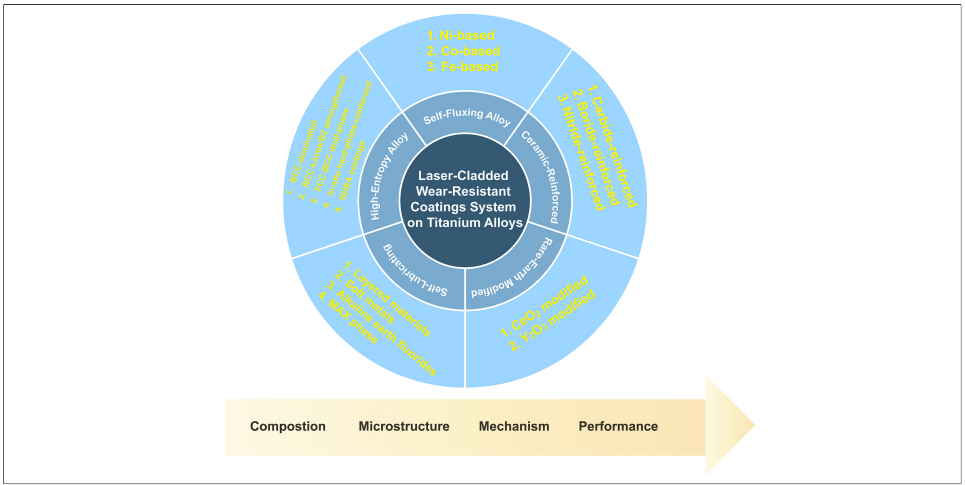
**Yundong Zhao[1], Kaiming Wang[1,2], Jian Gu[3], Yang Li[2], Zixiang Li[2], Xiaotong Pang[1], Zhao Shen[4], Jiang Ju[4], Anping Dong[4], Jun Wang[4], Baode Sun[4]**

**Keywords:**
Titanium alloys, laser cladding, wear-resistant coatings, microstructure design, interfacial behavior, strengthening mechanisms

**Citation:** Zhao, Y.; Wang, K.; Gu, J.; Li, Y.; Li, Z.; Pang, X.; Shen, Z.; Ju, J.; Dong, A.; Wang, J.; Sun, B. Laser-cladded coatings on titanium alloys: processing-microstructure relationships, phase evolution, and interfacial mechanisms. *Microstructures* **2026**, *6*, 20260136. https://dx.doi.org/10.20517/microstructures.2026.176

**Received:** 9 Jul 2026
**First Decision:** 26 Aug 2026
**Revised:** 15 Sep 2026
**Accepted:** 28 Sep 2026
**Published:** 28 Oct 2026

**Academic Editor:**
Huijun Li
**Copy Editor:**
Ping Zhang
**Production Editor:**
Ping Zhang




## Abstract

Titanium (Ti) alloys are attractive for aerospace, biomedical, and advanced engineering applications because they combine high specific strength with excellent corrosion resistance. However, their intrinsically low hardness and poor tribological performance severely limit long-term reliability under frictional loading. Laser cladding provides a promising route for improving Ti alloy surfaces by forming compact, metallurgically bonded coatings whose microstructures can be tailored through rapid laser-induced melting and solidification. This review re-examines recent progress in laser-cladded coatings on Ti alloys from a microstructure-oriented perspective, with particular emphasis on non-equilibrium solidification, phase constitution, interfacial reactions, defect evolution, and structure-dependent degradation during service. Five representative coating systems, namely self-fluxing alloys, ceramic-particle-reinforced composites, rare-earth-oxide-modified coatings, self-lubricating composite coatings, and high-entropy alloy (HEA)

[1]College of Mechanical and Vehicle Engineering, Changsha University of Science and Technology, Changsha 410114, Hunan, China.
[2]The State Key Laboratory of Tribology, Department of Mechanical Engineering, Tsinghua University, Beijing 100084, China.
[3]State Grid Electric Power Engineering Research Institute Co., Ltd., Beijing 100055, China.
[4]School of Materials Science and Engineering, Shanghai Jiao Tong University, Shanghai 200240, China.

**Correspondence to:** Prof. Kaiming Wang, College of Mechanical and Vehicle Engineering, Changsha University of Science and Technology, Changsha 410114, Hunan, China. E-mail: kmwang@csust.edu.cn; Prof. Zhao Shen, Prof. Jiang Ju, Prof. Anping Dong, Prof. Baode Sun, School of Materials Science and Engineering, Shanghai Jiao Tong University, Shanghai 200240, China. E-mail: shenzhao081@sjtu.edu.cn; jujiang1990@sjtu.edu.cn; apdong@sjtu.edu.cn; bdsun@sjtu.edu.cn

coatings, are comparatively discussed not simply in terms of wear performance, but according to their characteristic phase architecture, strengthening pathways, and damage-evolution behavior. Special attention is given to how load transfer, crack initiation, tribofilm stability, oxidation-assisted protection, and delamination resistance are controlled by phase distribution, interface stability, and structural compatibility across multiple length scales. Accordingly, the evolution of laser-cladded coatings is viewed as a shift from isolated hardening or single-purpose functional design to coordinated control of phase configuration, interface reliability, and damage accommodation. Current challenges associated with brittle reaction products, compositional complexity, thermo-mechanical mismatch, and microstructural instability are also discussed. Finally, future directions are proposed toward gradient and multiphase architectures, interface-controlled failure mitigation, advanced microstructural characterization, and data-assisted coating design. This review provides a unified microstructure-based framework for understanding and designing advanced laser-cladded wear-resistant coatings on Ti alloys for demanding tribological environments.

## INTRODUCTION

Ti alloys play an essential role in modern engineering because their low density, high strength-to-weight ratio, and excellent corrosion resistance make them suitable for aerospace structures, marine components, chemical-processing equipment, biomedical devices, and high-end manufacturing applications[1-7]. In recent years, their applications have further expanded into the oil and gas exploration, transportation, and defense sectors, where materials are required to withstand severe wear and corrosive environments[8-10]. Despite these advantages, Ti alloys exhibit relatively low surface hardness and limited wear resistance. Under dry sliding, fretting, or particle-erosion conditions, they are susceptible to adhesive and abrasive wear, leading to accelerated surface degradation and reduced service life[11-14]. This inherent limitation restricts their use in components that demand both lightweight design and high surface durability. Therefore, a major challenge in Ti-alloy surface engineering is to improve wear durability without compromising the alloy's inherent mechanical strength and corrosion resistance.

To overcome these surface-related drawbacks, a range of surface engineering approaches have been explored to improve the friction and wear behavior of Ti alloys. Common approaches include nitriding[15], carburizing[16], thermal spraying[17], magnetron sputtering[18], physical vapor deposition (PVD)[19], and chemical vapor deposition (CVD)[20]. Although conventional surface modification techniques can improve surface hardness to a certain extent, they still suffer from inherent limitations. Thermal spraying and vapor deposition typically produce relatively thin coatings with limited interfacial bonding strength and residual stress issues, whereas thermochemical treatments such as nitriding and carburizing require prolonged processing at elevated temperatures, which may induce substrate distortion. As a result, it remains difficult for these treated surfaces to provide adequate load support and maintain durability during prolonged service[21,22]. Laser cladding therefore provides an advanced surface engineering technique capable of fabricating thick, dense coatings with strong metallurgical bonding on Ti alloys. During laser cladding, the laser beam locally melts the feedstock powder and a shallow region of the substrate, producing a transient molten pool that solidifies rapidly into a dense coating with refined microstructures[23-25]. Compared with conventional deposition methods, laser cladding offers advantages including controllable dilution, low porosity, enhanced interfacial adhesion, and reduced substrate distortion[26,27]. These features make it a versatile and effective strategy for improving the wear, corrosion, and oxidation resistance of Ti alloys under demanding service conditions. Table 1 further compares these methods with respect to coating characteristics, bonding mechanisms, advantages, and limitations.

Recent studies have increasingly explored laser-cladded wear-resistant coatings on Ti alloys to improve surface hardness, wear durability, and stability at elevated temperatures. A variety of coating systems have been developed, including self-fluxing alloys, ceramic particle-reinforced composites, rare-earth

**Table 1. Comparison of typical surface modification methods for Ti alloys**

| Methods | Main characteristics | Bonding type | Main advantages | Major limitations | Ref. |
|---|---|---|---|---|---|
| Nitriding | Diffusion-based process modifying surface layer | Diffusion | High surface hardness, good wear resistance, integral bonding without delamination | Very thin layer, long processing time, high temperature may cause substrate distortion | [28,29] |
| Carburizing | Diffusion of carbon atoms into surface | Diffusion | Improves hardness and wear resistance | Requires extremely high temperature, may form brittle phases | [16,28] |
| Thermal spraying | Deposition of molten/semi-molten particles | Mechanical | Thick coating, high deposition rate, wide material selection | Porous structure, weak mechanical bonding, possible delamination | [17,30] |
| Magnetron sputtering | Atom-by-atom deposition in a vacuum | Physical/atomic | Dense film, precise control of thickness and composition | Low deposition efficiency, high equipment cost | [18,31] |
| PVD | Vaporization and condensation in vacuum | Physical/atomic | Low processing temperature, dense coating; good adhesion | Thin coating, high residual stress, limited load capacity | [19,32] |
| CVD | Chemical reaction of gaseous precursors | Chemical/diffusion | Excellent conformality, dense, pure coatings | Very high temperature, toxic precursors; slow process | [20,32] |
| Laser cladding | Local melting of alloy powders and substrate | Metallurgical | Strong metallurgical bonding, low dilution, dense microstructure, low porosity | High residual stress, cracking tendency | [24,27] |

PVD: Physical vapor deposition; CVD: chemical vapor deposition.

oxide-modified coatings, self-lubricating composites, and high-entropy alloys (HEAs)[22]. These systems rely on distinct strengthening principles: self-fluxing Ni-based alloys utilize B and Si to promote *in situ* hard phase formation and metallurgical bonding[33]; ceramic reinforcements such as TiC, tungsten carbide (WC), and $TiB_2$ provide rigid load-bearing frameworks[34]; rare-earth oxides refine microstructures and regulate interfaces[35]; solid lubricants including $MoS_2$ and $CaF_2$ reduce interfacial shear stress[36]; and HEA coatings achieve structural stability through multi-principal-element solid solutions[21]. To clarify their intrinsic relationships and performance trade-offs, Figure 1 presents a framework-level comparative radar map that schematically correlates material design concepts with relative mechanical, tribological, interfacial, and functional characteristics of five major classes of laser-cladded wear-resistant coatings on Ti alloys. Each dimension represents a characteristic aspect of coating behavior, such as load-bearing capability, wear resistance, interfacial stability, lubrication or oxidation-related functionality, and structural adaptability, as summarized from representative findings in the literature. It should be noted that this figure is intended as a qualitative comparative illustration rather than a strict quantitative evaluation. The core message conveyed by Figure 1 is that different coating systems exhibit distinct balances between hardness, toughness, interfacial compatibility, and functional performance, thereby reflecting the evolution of coating design from single-function strengthening toward synergistic regulation of microstructure, interface integrity, and service behavior. This comparative perspective enables the identification of both evolutionary trends and inherent limitations among different coating systems.

Despite substantial progress in laser-cladded wear-resistant coatings on Ti alloys, existing studies remain largely fragmented and system-specific, with limited efforts to establish a unified mechanistic understanding across different coating architectures. Most previous reviews primarily focus on individual material systems or performance improvements, while the intrinsic relationships among microstructure construction, interfacial stability, load-bearing capability, and wear degradation behavior have not been systematically clarified. In particular, the evolution of coating design from single-mechanism strengthening toward multi-mechanism synergistic regulation, which represents a fundamental paradigm shift in surface engineering, has not been comprehensively analyzed.

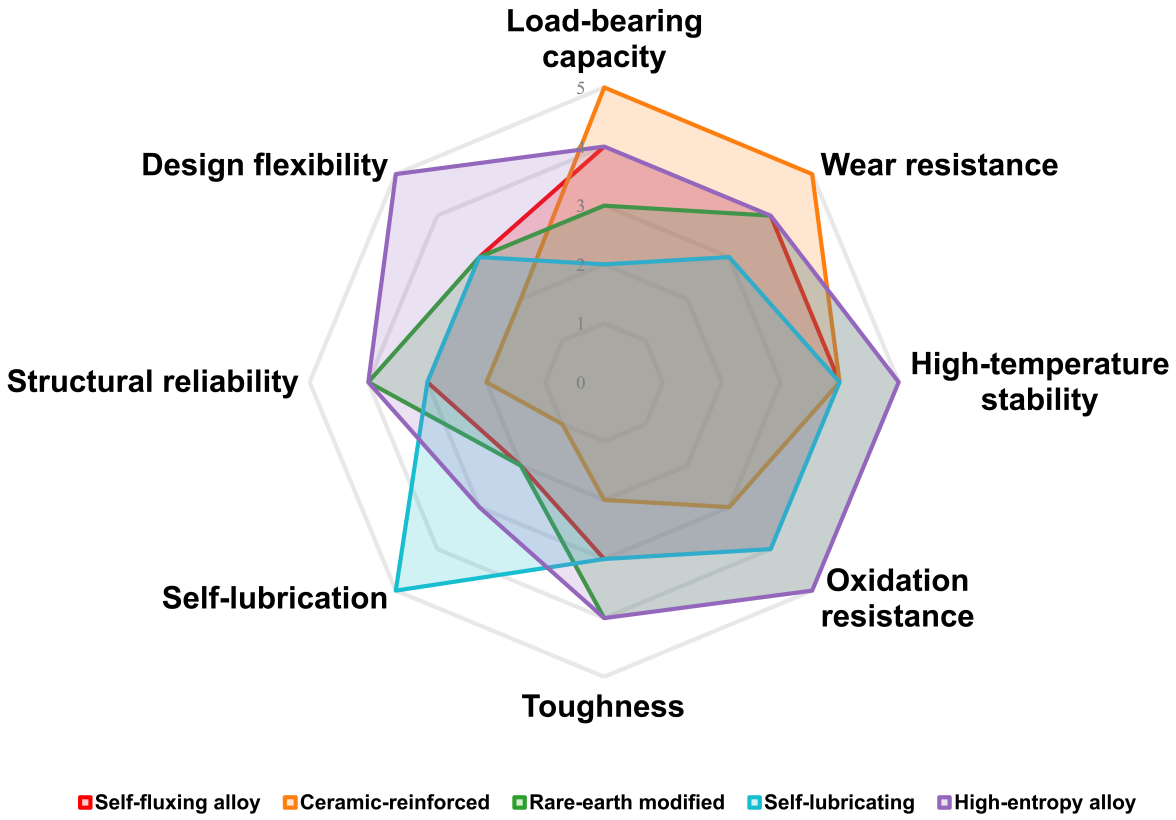



**Figure 1.** Comparative radar map of performance profiles for five major wear-resistant coating systems on Ti alloys.

In this context, the present review reinterprets laser-cladded wear-resistant coatings on Ti alloys through a microstructure-based framework. Compared with existing reviews that mainly focus on individual coating systems or general performance improvements, this review emphasizes the intrinsic relationships among processing conditions, microstructural evolution, phase constitution, interfacial reactions, defect evolution, and wear degradation behavior. Rather than primarily cataloguing material systems and tribological properties, it examines how non-equilibrium solidification, phase selection, interfacial reactions, and defect evolution govern coating integrity and wear degradation. Five representative classes of wear-resistant coatings, including self-fluxing alloys, ceramic-particle-reinforced composites, rare-earth-oxide-modified coatings, self-lubricating composite coatings, and high-entropy alloy coatings, are comparatively discussed in terms of phase constitution, characteristic structural architecture, and dominant failure pathways. Particular emphasis is placed on mechanistic evidence revealed by multiscale characterization, including grain evolution, reinforcement morphology and distribution, interface stability, crack initiation, and subsurface damage development. Wear behavior is therefore treated not as an isolated property outcome, but as the consequence of structure-controlled load transfer, damage accommodation, tribofilm evolution, and failure-path propagation. Current challenges and future opportunities are further analyzed with emphasis on gradient architectures, multiphase cooperative design, interface-dominated failure control, and characterization-guided optimization. On this basis, this review seeks to establish a unified microstructure-oriented framework for understanding and designing advanced laser-cladded wear-resistant coatings on Ti alloys.

## FUNDAMENTALS AND CRITICAL CHALLENGES OF LASER CLADDING ON TI ALLOYS

### Process principle and non-equilibrium solidification behavior

In laser cladding, a focused laser beam locally melts pre-placed or continuously delivered powder together with a shallow region of the Ti substrate, producing a transient molten pool. Representative thermal-field

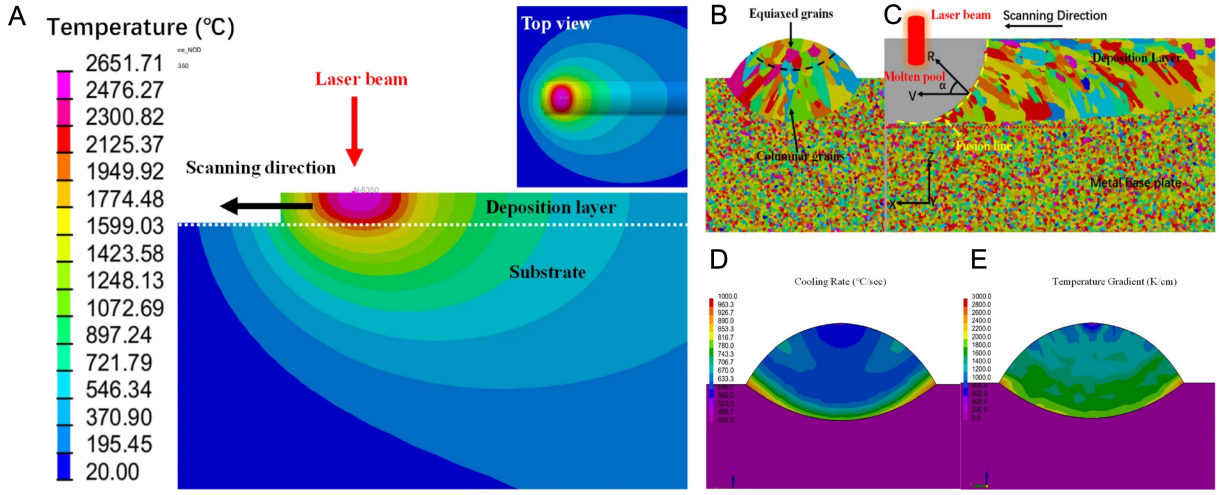



**Figure 2.** Thermal-field evolution, grain-growth behavior, and solidification characteristics of Ti6Al4V during laser-based deposition. (A) Simulated temperature field and molten-pool characteristics during single-track deposition; (B) transverse-section grain morphology showing columnar and equiaxed grains; (C) longitudinal-section grain-growth morphology along the scanning direction; (D) cooling-rate distribution within the molten pool; and (E) temperature-gradient distribution within the molten pool. This figure is adapted from Ref.[37]. Licensed under CC-BY 4.0.

evolution and solidification characteristics of Ti6Al4V under laser-based deposition are shown in Figure 2, including the temperature distribution, grain-growth morphology, cooling rate, and temperature gradient. Under such processing conditions, rapid melting and solidification promote the formation of non-equilibrium microstructures, which are typically characterized by refined grains, microsegregation, supersaturated solid-solution matrices, metastable phases, and *in situ* reaction products[39]. Laser cladding differs from many conventional surface treatments in its localized heat input, adjustable dilution, short processing time, limited heat-affected zone (HAZ), and ability to form metallurgical bonding with the Ti substrate. These characteristics make it a particularly suitable method for Ti-alloy surface modification[22,39].

For Ti alloy substrates, this non-equilibrium solidification behavior has a dual effect. On the one hand, rapid solidification promotes grain refinement, metastable phase formation, and fine dispersion of reinforcing phases, which are beneficial for hardness and wear resistance. On the other hand, it may intensify elemental segregation, constitutional supercooling, dendritic heterogeneity, and local enrichment of brittle reaction products. These features can generate spatially heterogeneous mechanical properties and unstable crack-propagation paths. Therefore, the key issue is not merely to exploit rapid solidification for strengthening, but to control the solidification pathway so that refined microstructures are obtained without forming continuous brittle networks or highly segregated interfacial regions.

In Ti-alloy claddings, solidification often starts epitaxially from the substrate, leading to columnar grains adjacent to the bonding interface and more equiaxed grains toward the upper region of the coating[40,41]. As shown in Figure 2, the resulting grain morphology is closely related to the spatial variation in cooling rate and temperature gradient within the molten pool. During this process, constitutional supercooling may develop in front of the advancing solid/liquid interface, promoting columnar-to-equiaxed transition (CET) when newly formed equiaxed nuclei progressively restrict the continued growth of columnar grains[24,27]. The final growth mode is mainly controlled by the balance between the thermal gradient (G) and the solidification rate (R), which governs the transition from planar growth to cellular and dendritic morphologies[42].

### Microstructural evolution, Ti-induced interfacial reactions, and cracking susceptibility

The solidification-driven features not only define the microstructural morphology but also dictate subsequent phase evolution, element segregation, and strengthening behavior across various coating systems. Because atomic diffusion is strongly restricted during rapid solidification, solutes may be retained unevenly within the solidifying coating, resulting in microsegregation and metastable solid-solution formation[43-46]. These microstructural characteristics significantly influence the hardness, toughness, and wear resistance of the cladding layer.

Notwithstanding these advantages, Ti alloys exhibit intrinsic chemical and thermo-mechanical characteristics that make coating formation particularly challenging. Ti's high chemical reactivity promotes interfacial chemical ordering and intermetallic compound formation through reactions with transition metals, ceramic-forming elements, and oxygen, while the large mismatch in thermal expansion generates high residual stresses during rapid heating and cooling[47-49]. During the short molten-pool lifetime, dilution from the Ti substrate may trigger non-equilibrium interfacial reactions, leading to the formation of Ti-Ni, Ti-Fe, Ti-Co, Ti-Si, TiC, TiB, TiN, or oxide-containing reaction products depending on the coating composition[22,50,51]. These products are not inherently beneficial or detrimental. Finely dispersed or discontinuous reaction phases may enhance metallurgical bonding and local hardening, whereas continuous or coarse brittle reaction layers reduce interfacial deformability and become preferential sites for crack initiation and delamination. Therefore, interfacial reaction products should be evaluated according to their morphology, continuity, thickness, and compatibility with the adjacent matrix, rather than simply being regarded as strengthening phases.

Residual stress represents another critical challenge specific to laser cladding on Ti alloys. The combined influence of intermetallic compound formation and residual stress greatly increases the cracking susceptibility of laser-cladded coatings[52,53]. Severe thermal gradients and rapid solidification during laser processing generate tensile stresses in the cladding layer, which are intensified by the mismatch in thermophysical and mechanical properties at the interface. When brittle intermetallic compounds or continuous ceramic networks are present, residual stress tends to concentrate at grain boundaries (GBs), phase interfaces, and dilution-affected regions, thereby promoting hot cracking, cold cracking, or interfacial spallation. This explains why coatings with higher hardness do not necessarily exhibit better wear resistance if their stress-accommodation capacity and interfacial toughness are insufficient. Accordingly, controlling interfacial reactions, mitigating residual stresses, and optimizing elemental partitioning remain key challenges for coating design.

### Design strategies and relevance to coating systems

To overcome persistent metallurgical and thermo-mechanical challenges, particularly Ti-induced interfacial reactions, brittle reaction-layer formation, residual stress accumulation, and cracking, recent research has progressively shifted from passive process optimization toward active material system design. This transition reflects the recognition that adjusting processing parameters alone cannot fundamentally resolve the inherent incompatibilities between coating materials and Ti substrates.

The five coating systems discussed in the following sections, namely self-fluxing alloys, ceramic particle-reinforced composites, rare-earth-modified coatings, self-lubricating coatings, and HEAs, embody distinct materials design pathways developed to mitigate these inherent conflicts. However, each strategy inevitably introduces trade-offs, including hardness-toughness imbalance, interfacial chemical reactivity, and lubrication instability under complex service conditions. Consequently, coating reliability is governed not by a single strengthening mechanism but by the coordinated regulation of compositional design, phase architecture, and interfacial stability.

Collectively, these approaches establish a unified conceptual framework linking processing thermodynamics, microstructural evolution, and multi-mechanism strengthening behavior. This framework provides the scientific basis for the comparative analyses presented in the subsequent sections and underscores the necessity of synergistic design beyond isolated performance enhancement.

## TRADITIONAL ALLOY-BASED COATINGS: SELF-FLUXING SYSTEMS

Self-fluxing alloys are among the earliest and most technologically mature categories of hard-facing materials. Their defining feature is the deliberate incorporation of boron (B) and silicon (Si) into the alloy composition, which act as fluxing elements during melting[54,55]. These elements depress the liquidus temperature, improve powder wettability, and promote melt spreading, thereby enhancing metallurgical bonding. Based on matrix chemistry, self-fluxing alloys are generally classified into Ni-, Co-, and Fe-based systems[56-58]. Their enhanced hardness and tribological performance are mainly attributed to solid-solution hardening of the γ-Ni or γ-Co matrix, together with dispersion reinforcement from *in situ* carbides and borides, including $Cr_7C_3$, $Cr_{23}C_6$, $Fe_3C$, and $TiB_2$[59,60].

More importantly, the strengthening effect of self-fluxing alloys is closely associated with the formation, distribution, and crystallographic identity of *in situ* carbides and borides rather than with matrix hardening alone. Such matrix/hard-phase coexistence establishes a load-bearing microstructural framework that underpins the wear-resistant performance of self-fluxing coatings. From a microstructural viewpoint, the key issue is not only the presence of hard phases, but also their continuity, dispersion state, and interface compatibility with the γ matrix, since these factors directly affect load transfer efficiency, crack initiation sensitivity, and damage accommodation during sliding contact. Owing to the synergy between metallurgical fluidity and *in situ* hard-phase formation, self-fluxing alloys have been widely applied in laser cladding to produce wear-resistant coatings, particularly on steel and Ni/Co-based substrates, and are increasingly being investigated for surface modification of Ti alloys. Tribological performance of representative laser-cladded self-fluxing coatings on Ti alloy substrates is summarized in Table 2. Overall, the tabulated results show that self-fluxing alloy coatings generally increase the hardness of Ti alloy substrates and, in most cases, reduce the coefficient of friction (COF) and wear loss. The table also indicates that the extent of improvement varies among Ni-based, Co-based, and Fe-based systems, and that wear behavior often shifts from substrate-dominated adhesive/abrasive damage toward more stable abrasive or oxidative regimes after cladding.

### Nickel-based coatings

Nickel-based self-fluxing alloy coatings are among the most extensively investigated systems in wear- and corrosion-resistant surface engineering due to their mature engineering foundation and favorable comprehensive performance[66,67]. Compared with Fe-based counterparts, Ni-based alloys exhibit superior toughness and corrosion resistance while retaining relatively high hardness. In contrast to Co-based systems, they offer lower material cost and a wider processing window[49,68]. Consequently, Ni-based self-fluxing coatings are widely considered as versatile materials capable of balancing mechanical performance and economic efficiency across diverse service conditions.

In terms of compositional design, typical Ni-based self-fluxing alloys are built around a γ-Ni solid-solution matrix. B, together with Si, is introduced to lower the melting temperature and improve melt fluidity, while Cr and C favor *in situ* precipitation of carbides and borides[33,61]. Rapid cooling during laser cladding promotes the formation of a solid solution, borides, carbides, and minor Ni-Si intermetallic compounds. This multiphase constitution reflects a typical non-equilibrium phase-selection process in laser cladding, in which rapid melting, dilution with the Ti substrate, and subsequent solidification jointly determine the formation of borides, carbides, and intermetallic products. In this sense, the wear behavior of Ni-based self-fluxing coatings should also be interpreted in relation to phase evolution and interfacial reaction pathways.

**Table 2. Tribological performance of laser-cladded self-fluxing alloy coatings on Ti alloys**

| Substrate | Self-fluxing alloy base | Coating material | Tribological results of substrates | | | | Tribological results of coatings | | | | Ref. |
|---|---|---|---|---|---|---|---|---|---|---|---|
| | | | Microhardness | COF | Wear losses | Mechanism | Microhardness | COF | Wear losses | Mechanism | |
| Ti6Al4V | Nickel-based | Ni40 | 314 $HV_{0.3}$ | 0.71 | 6.1 × $10^{-7}$ $mm^3/(N·m)$ | Adhesive Abrasive | 490 $HV_{0.3}$ | 0.69 | 1.4 × $10^{-7}$ $mm^3/(N·m)$ | Fatigue Adhesive | [33] |
| Ti6Al4V | Nickel-based | Ni50 | 314 $HV_{0.3}$ | 0.71 | 6.1 × $10^{-7}$ $mm^3/(N·m)$ | Adhesive Abrasive | 609 $HV_{0.3}$ | 0.62 | 0.5 × $10^{-7}$ $mm^3/(N·m)$ | Fatigue Abrasive | [33] |
| Ti6Al4V | Nickel-based | Ni60 | 314 $HV_{0.3}$ | 0.71 | 6.1 × $10^{-7}$ $mm^3/(N·m)$ | Adhesive Abrasive | 708 $HV_{0.3}$ | 0.57 | 1.38 × $10^{-7}$ $mm^3/(N·m)$ | Fatigue Abrasive | [33] |
| Ti6Al4V | Nickel-based | Ni60 | 361 $HV_1$ | 0.63 | 115 mg | Adhesive | 837 $HV_1$ | 0.40 | 21 mg | Abrasive | [61] |
| Ti6Al4V | Nickel-based | Ni60, Cu | 391 $HV_{0.5}$ | 0.457 | 4.30 × $10^{-4}$ $mm^3/(N·m)$ | Adhesive | 781 $HV_{0.5}$ | 0.498 | 3.11 × $10^{-4}$ $mm^3/(N·m)$ | Abrasive | [62] |
| Ti6Al4V | Cobalt-based | TC4 + 10 wt.% Co12 | 350 $HV_{0.5}$ | N/A | N/A | N/A | 559 $HV_{0.5}$ | 0.48(RT) | 52.1 × $10^{-5}$ $mm^3/(N·m)$ | Abrasive | [63] |
| | | | | | | | | 0.48(300 °C) | 36.7 × $10^{-5}$ $mm^3/(N·m)$ | | |
| | | | | | | | | 0.385(500 °C) | 3.83 × $10^{-5}$ $mm^3/(N·m)$ | | |
| | | TC4 + 20 wt.% Co12 | | | | | 545 $HV_{0.5}$ | 0.44(RT) | 56.8 × $10^{-5}$ $mm^3/(N·m)$ | Adhesive Oxidative | |
| | | | | | | | | 0.485(300 °C) | 21.9 × $10^{-5}$ $mm^3/(N·m)$ | | |
| | | | | | | | | 0.39(500 °C) | 0.775 × $10^{-5}$ $mm^3/(N·m)$ | | |
| | | TC4 + 30 wt.% Co12 | | | | | 569 $HV_{0.5}$ | 0.405(RT) | 44.2 × $10^{-5}$ $mm^3/(N·m)$ | Adhesive Oxidative | |
| | | | | | | | | 0.465(300 °C) | 24.2 × $10^{-5}$ $mm^3/(N·m)$ | | |
| | | | | | | | | 0.35(500 °C) | 4.89 × $10^{-5}$ $mm^3/(N·m)$ | | |
| Ti6Al4V | Cobalt-based | Co42, $B_4C$, SiC, $Y_2O_3$ | 350 $HV_{0.2}$ | N/A | 6.63 × $10^{-1}$ $mm^3·min^{-1}$ | Adhesive | 1,314 $HV_{0.2}$ | N/A | 6.38 × $10^{-2}$ $mm^3·min^{-1}$ | Abrasive | [64] |
| Ti6Al4V | Cobalt-based | Stellite 6 | 272 HV | 0.379 | 18.5 mg | N/A | 542 HV | 0.22 | 7.8 mg | N/A | [65] |
| Ti6Al4V | Iron-based | FeNiCrBSiC Ti, SiC | 350 $HV_1$ | 0.437 | 1.092 $mm^3$ | Adhesive Abrasive | 1,843 $HV_1$ | 0.202 | 0.0567 $mm^3$ | Oxidative | [51] |

COF: Coefficient of friction; RT: room temperature.

This multiphase architecture, characterized by a continuous tough matrix reinforced by dispersed hard phases, enables an effective balance among hardness, toughness, and crack resistance. Representative studies further indicate that the effect of compositional optimization in Ni-based self-fluxing coatings is not monotonic. Fan *et al.*[33] showed that increasing the Cr and B contents from Ni40 to Ni60 promoted the formation of carbide- and boride-type hard phases, thereby increasing coating

hardness and reducing the COF. However, the wear resistance did not improve monotonically, and the Ni50 coating exhibited the best overall tribological performance[33]. This behavior suggests that the optimum reinforcement level is governed not simply by hardness, but by the balance between hard-phase strengthening and microstructural integrity. At moderate hard-phase fractions, dispersed carbides and borides can effectively share the contact load and suppress matrix plowing, while the γ-Ni matrix still retains sufficient deformability to alleviate local stress concentration. By contrast, when the hard-phase fraction increases further, the reinforcing phases tend to become coarser and less mechanically compatible with the surrounding matrix, which promotes particle fracture, interfacial decohesion, and abrasive debris generation during sliding[33,69]. In this case, the hard phases no longer act only as load-bearing units, but also as potential crack-initiation and micro-cutting sources. Therefore, the better overall behavior of the Ni50 coating can be understood as the result of a more favorable balance between reinforcement efficiency and damage tolerance, whereas the inferior wear behavior of Ni60 reflects the transition from beneficial hard-phase dispersion to excessive brittle reinforcement.

Mechanistically, Ni-based self-fluxing coatings resist wear through the combined contribution of matrix hardening and load support by dispersed hard phases. The γ-Ni matrix accommodates part of the applied stress through plastic deformation, thereby mitigating local stress concentration and delaying crack initiation, while dispersed carbides and borides sustain the majority of the contact load and suppress plowing and micro-cutting wear[33,70]. Consistent with this mechanism, Wang *et al.*[61] fabricated a laser-cladded Ni60 coating on TC4 Ti alloy, where *in situ*-formed TiC and $Cr_3C_2$ increased the hardness to 837 $HV_1$ (~2.3 times that of the substrate). The synergistic strengthening reduced material loss from 115 mg to 21 mg and shifted the dominant wear mechanism from severe adhesive wear to mild abrasive wear, highlighting the effectiveness of multiphase strengthening.

### Cobalt-based coatings

Cobalt-based self-fluxing alloy coatings, typically represented by the Stellite series, are widely applied in demanding service environments, including aircraft-engine parts, gas-turbine components, and high-temperature valve seats due to their superior high-temperature mechanical stability and wear reliability[71]. Although their material cost exceeds that of Fe- and Ni-based counterparts, Co-based alloys provide distinct advantages under severe operating conditions, particularly in retaining hardness at elevated temperatures, resisting adhesive wear, and tolerating thermal fatigue[71,72].

Microstructurally, Co-based self-fluxing alloys generally consist of a face-centered cubic (FCC) Co solid solution matrix reinforced by dispersed Cr-rich carbides, predominantly $Cr_7C_3$ and $M_{23}C_6$[64,65]. This phase constitution is also a result of non-equilibrium solidification and interfacial dilution during laser cladding, in which rapid cooling and local compositional redistribution govern the selection, dispersion, and stability of carbide phases within the FCC Co matrix. The FCC Co matrix exhibits good plastic deformability and strain accommodation at elevated temperatures, thereby alleviating stress concentration during thermal cycling. Simultaneously, high-melting-point carbides form a rigid, load-bearing skeleton that preserves structural integrity under frictional loading[63,65]. Representative studies have further clarified these strengthening mechanisms. Liu *et al.*[65] fabricated a Stellite 6 coating on TC4 Ti alloy via laser cladding and reported a microstructure composed of an FCC γ-Co matrix with dispersed $M_{23}C_6$, $Cr_7C_3$, TiC, and $CoC_x$ phases. The incorporation of Fe, Ni, and C stabilized the γ-Co structure during thermal cycling, enhancing strain accommodation through lattice distortion under residual tensile stress. From a crystallographic perspective, this stabilization is important because it implies that the matrix can retain a deformation-tolerant crystal structure under thermal and mechanical loading, thereby reducing the tendency for premature crack initiation at stress-concentrated regions. This synergistic matrix-carbide architecture resulted in an average microhardness of 542 HV, significantly reducing the COF relative to TC4.

From a tribological perspective, Co-based self-fluxing coatings exhibit strong resistance to adhesive and fatigue wear, particularly at elevated temperatures. During high-temperature sliding, the Co matrix exhibits pronounced work-hardening, enabling continuous renewal of load-bearing regions via surface plastic deformation. In parallel, Cr-rich and Co oxides formed at the friction interface form a dense, stable tribo-oxide layer that mitigates adhesive failure. Shi *et al.*[63] reported that Co12 coatings undergo a transition from abrasive wear at room temperature (RT) to oxidation-dominated wear at elevated temperatures. At 500 °C, the formation of a dense glaze layer reduced the COF to approximately 0.35 via third-body rolling, resulting in wear resistance superior to that at RT.

### Iron-based coatings

Fe-based self-fluxing systems are mainly valued for their cost advantage, since their material cost is usually much lower than that of Ni- or Co-based coatings, while they can still offer high hardness and good abrasive-wear resistance at RT[73].

From a microstructural design perspective, boron (B) functions not only as a fluxing element but also as a key regulator of reinforcing phase evolution. Because B has low solubility in the metallic matrix and diffuses slowly in hard phases, local B enrichment can reduce the energy barrier for phase formation and promote phase transformation. Conventional Fe-based hardfacing materials tend to form brittle carbides such as $M_2C$, MC, or $M_6C$. With suitable B addition, however, the activity of carbon in the melt increases, which promotes $M_3C$-type eutectic precipitation, such as $Fe_3C$, with relatively better fracture toughness[74].

In Fe-based hardfacing coatings, Feng *et al.*[74] reported that increasing B content induces a transition of reinforcing phases from NbC or $Cr_{23}C_6$ carbides toward $Fe_3C$-type carbides. When the B content reached 0.75%, a $Fe_3C$ + γ-Fe eutectic microstructure was formed, enabling the microhardness to exceed 900 $HV_{0.5}$. Under rapid solidification, a skeletal architecture composed of blocky or plate-like $M_7C_3$ and $Fe_2B$ phases developed, supported by a martensitic or bainitic composite matrix. This multiphase framework exhibits strong room-temperature wear resistance[75].

Despite these advantages, Fe-based self-fluxing coatings are seldom applied to Ti alloys due to severe metallurgical incompatibility and thermophysical mismatch at elevated temperatures. Owing to the strong Ti-Fe affinity, laser cladding induces the rapid formation of brittle interfacial Ti-Fe intermetallics, while significant thermal expansion mismatch generates tensile residual stresses upon cooling, frequently resulting in cracking or even coating failure[76]. Even when crack-free coatings are achieved, a fundamental performance conflict persists: Ti alloys are commonly employed in medium- to high-temperature environments, whereas Fe-based coatings undergo rapid matrix softening and loss of wear resistance above approximately 400 °C, limiting their practical applicability for Ti substrates.

Nevertheless, Fe can serve as a reactive alloying element to modify *in situ* phase evolution in Ti-based systems. Zhao *et al.*[51] fabricated a Ti-40SiC transition layer on TC4, followed by a Ti-xFe-80SiC working layer with varying Fe contents (0-15 vol.%). Their results showed that Fe addition altered the reaction pathway of the Ti-Si-C system. At higher Fe contents (10 and 15 vol.%), an ultra-hard $TiFeSi_2$ phase formed *in situ*, significantly enhancing coating performance[51]. Furthermore, Fe-based alloys improved wettability and self-fluxing behavior, effectively reducing pores and cracks. As the Fe content increased, defect density within the coating decreased markedly [see Figure 3]. These findings indicate that controlled Fe incorporation can tailor phase evolution and construct ultra-hard wear-resistant architectures, offering an alternative design strategy for Ti-based composite coatings.

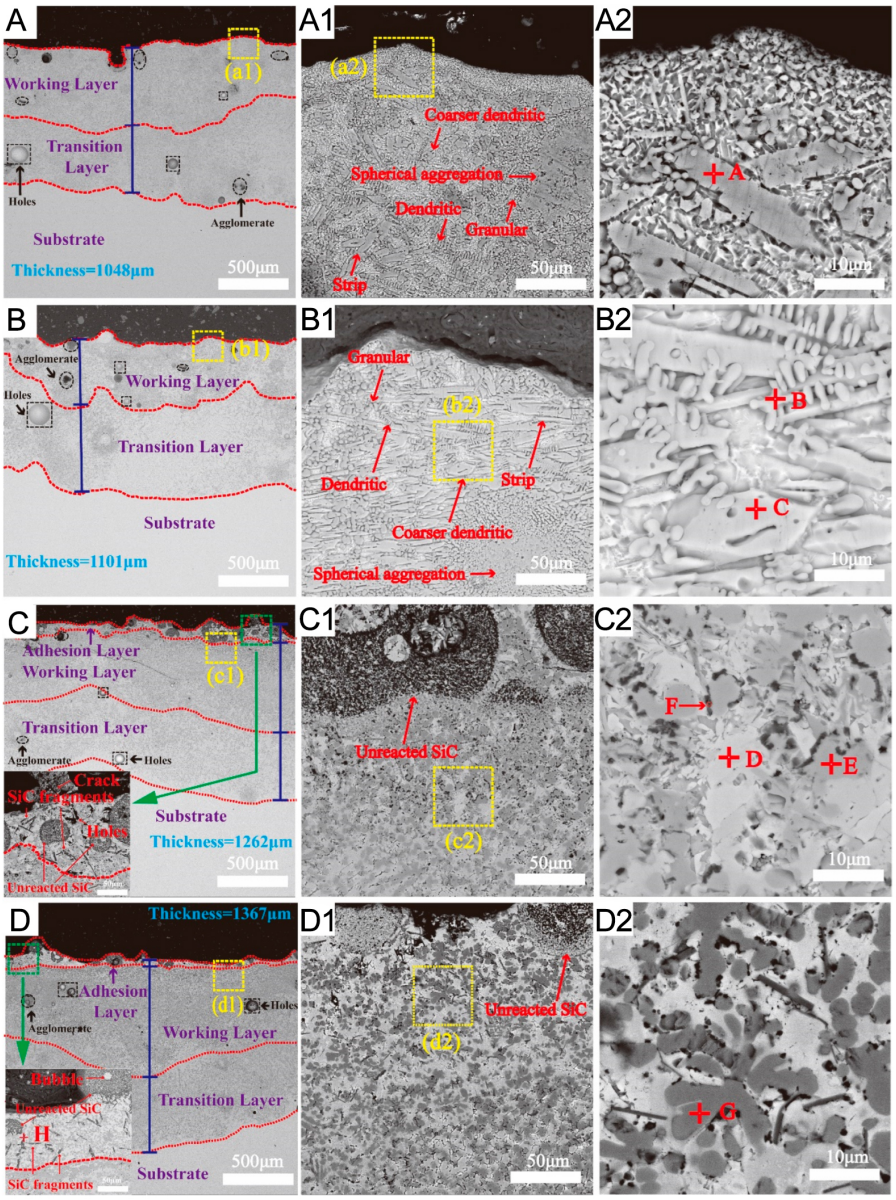



**Figure 3.** SEM images of the cross-sectional microstructure of the coatings: (A) WL-F0; (B) WL-F5; (C) WL-F10; (D) WL-F15; ($A_1$-$D_1$) Higher-magnification views of the regions in (A-D), respectively; ($A_2$-$D_2$) Further enlargements of ($A_1$-$D_1$), respectively. This figure is adapted from Ref.[51]. Licensed under CC-BY 4.0. SEM: Scanning electron microscopy.

Overall, self-fluxing systems are typically characterized by a ductile metallic matrix, such as γ-Ni- or γ-Co-based phases, reinforced by *in situ* formed carbides and/or borides generated during rapid solidification. Their wear-resistant performance mainly originates from the synergistic effects of matrix-supported stress accommodation, hard-phase load bearing, and strong metallurgical bonding.

Although self-fluxing systems are important in surface engineering because they can provide good resistance to both wear and corrosion, their inherent limitations become pronounced when applied to highly reactive substrates such as Ti alloys[48,49]. The drawbacks of traditional self-fluxing coatings on Ti substrates mainly arise from three mutually reinforcing factors.

First, the high-volume fraction of carbides and borides required to improve wear resistance inevitably increases microstructural brittleness and reduces impact toughness, making self-fluxing alloy coatings susceptible to cracking[63]. As shown in Figure 4A, cracking can be observed in a representative Ni-based

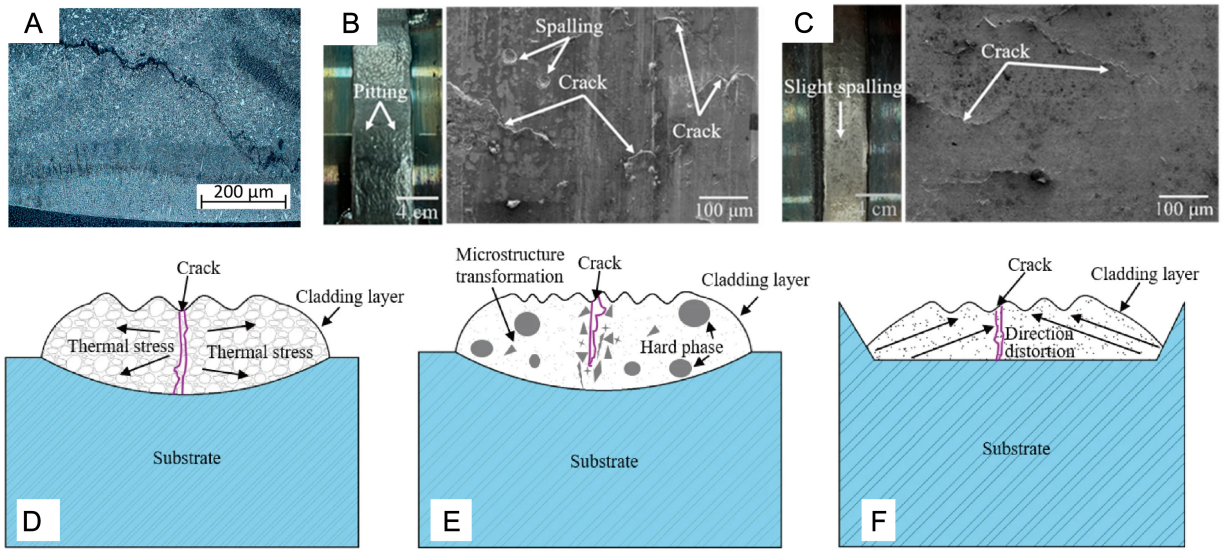



**Figure 4.** Cracking, spalling, and stress-induced failure mechanisms of laser-cladded self-fluxing alloy coatings. (A) Crack morphology in a Ni-based self-fluxing alloy coating; (A) is adapted from Ref.[69]. Licensed under CC-BY 4.0; (B) worn surface morphology of a Fe-based coating showing pitting, spalling, and cracking; (C) worn surface morphology of a Co-based coating showing slight spalling and cracking; (B and C) are adapted from Ref.[77]. Licensed under CC-BY 4.0; (D-F) schematic illustrations of crack formation induced by thermal stress, organizational stress, and restraint stress, respectively. (D-F) are adapted from Ref.[81]. Licensed under CC-BY 4.0.

self-fluxing alloy coating[69]. For Fe- and Co-based coatings, worn surface morphologies further reveal pitting, spalling, peeling, and cracking, indicating that crack formation is closely coupled with tribological damage during sliding contact [Figure 4B and C][77]. Second, reactions between Ti and transition metals promote the formation of brittle Ti-Ni, Ti-Co, and Ti-Fe intermetallic compounds near the coating/substrate interface, which favor crack nucleation and interfacial debonding[78-80]. Third, mismatches in thermal expansion and elastic properties generate high tensile residual stresses under steep thermal gradients. As schematically illustrated in Figure 4D-F, crack formation can be associated with thermal stress, organizational stress, and restraint stress. These stresses accelerate interfacial damage and crack propagation. Although optimized powder feeding and process control can partially suppress cracking, process-parameter optimization alone cannot fully resolve the intrinsic incompatibility between conventional self-fluxing alloys and Ti substrates.

Taken together, these limitations have driven the development of composite and multiphase coatings that integrate ceramic load-bearing frameworks, rare-earth oxide grain refiners, solid-lubricant phases, and high-entropy matrices. These strategies aim to balance hardness, toughness, lubrication, and interfacial stability through synergistic microstructural design, forming the basis for the following sections on ceramic reinforcement, rare-earth modification, self-lubricating coatings, and HEA systems.

## CERAMIC PARTICLE-REINFORCED COMPOSITE COATINGS

To address the brittleness and interfacial mismatch often encountered in conventional self-fluxing coatings, ceramic-reinforced composite coatings have been developed as an important route for strengthening Ti-alloy surfaces. In these coatings, hard ceramic phases are incorporated into a metallic matrix to improve load support and resistance to abrasive damage in the cladded layer while reshaping its internal phase architecture.

In such systems, ceramic reinforcements are introduced either *ex situ* as pre-existing stable particulates or formed *in situ* through reaction-assisted cladding processes, for example, via reactions between Ti and C-, B-, or N-containing precursors[82-84]. The resulting microstructure typically consists of a metallic matrix

reinforced by dispersed or interconnected ceramic phases. Among the reported reinforcements, carbides, borides, and nitrides are the most representative because they combine high hardness, chemical stability, and relatively good compatibility with Ti-based matrices.

The tribological performance of representative laser-cladded *in situ* and *ex situ* ceramic-reinforced coatings on Ti alloy substrates is summarized in Tables 3 and 4. Overall, the results indicate that ceramic reinforcement enhances coating hardness and wear resistance relative to the Ti substrate. The tribological performance is governed not only by hard-phase strengthening but also by the type, fraction, distribution, and interface compatibility of the ceramic phases. Optimal performance is typically achieved at intermediate reinforcement levels rather than at the highest ceramic content. This common trend reflects the transition from a dispersed load-bearing reinforcement architecture to a more connected and damage-sensitive brittle structure at excessive ceramic contents.

### Carbide-reinforced systems

Carbide reinforcements are primarily introduced to suppress severe abrasive and erosive wear by constructing a high-hardness load-bearing skeleton within the cladding layer. This strategy is particularly effective under wear regimes dominated by micro-cutting and plowing, provided that the service temperature remains within a range where the metallic matrix retains sufficient strength[102,103].

Carbide-reinforced coatings can be produced either by *ex situ* incorporation of stable carbides (e.g., TiC, WC, and SiC) or via *in situ* formation during reaction-assisted cladding. *In situ* TiC typically forms because of the strong chemical affinity between Ti and C, for example, via reactions involving graphite, $B_4C$, or carbide-containing powders[85-87]. WC may partially dissolve in the molten pool and reprecipitate as (Ti, W)C-type carbides, while SiC can react with Ti to generate TiC, accompanied by Ti-Si intermetallic or silicide phases, depending on local composition and thermal history[94,104,105]. Representative TiC-, SiC-, and WC-reinforced coating microstructures and their hard-phase-assisted wear-resistance mechanisms are summarized in Figure 5, highlighting the important role of carbide ceramics in microstructural strengthening and load-bearing protection. These phase reactions show that carbide reinforcement in laser cladding is closely associated with non-equilibrium solidification and local solute redistribution in the molten pool. The final reinforcing architecture is governed by the competition among dissolution, interfacial reaction, and carbide reprecipitation during rapid cooling.

The morphology, size, and spatial distribution of carbide phases critically govern coating behavior and damage tolerance. Wei *et al.*[106] synthesized *in situ* TiC/Ti composite coatings on Ti6Al4V using graphene as a carbon precursor. With increasing carbon content, the TiC morphology evolved from short, fibrous structures to near-spherical particles, accompanied by increases in volume fraction and hardness. This microstructural transition improved wear resistance by enhancing load sharing and stabilizing the matrix. Such observations indicate that carbide efficiency is controlled not simply by phase fraction, but by whether the carbide phase remains finely dispersed or develops into a more continuous load-bearing framework.

Consistently, increasing the TiC fraction together with grain refinement leads to higher microhardness and a reduced COF, as reflected by the systematic variation in hardness and COF with SiC content. Fine carbide particles promote Orowan strengthening and increase dislocation density through thermal-misfit effects, whereas coarser carbides enhance the effective composite modulus and share contact loads[107-109]. During sliding, a well-developed carbide skeleton stabilizes the near-surface deformation layer and can shift the wear mode from severe adhesive or oxidative wear to controlled abrasive wear, thereby reducing wear-track depth and counter-body damage[110-113]. Wear-track profiles and wear-rate measurements further indicate the existence of an optimal carbide fraction: moderate reinforcement maximizes load sharing and minimizes

**Table 3. Summary of tribological properties of *in situ* ceramic-reinforced coatings on Ti alloy substrates**

| Substrate | *In situ* formed ceramic phase | Coating material | Tribological results of substrates | | | | Tribological results of coatings | | | | Ref. |
|---|---|---|---|---|---|---|---|---|---|---|---|
| | | | Microhardness | COF | Wear losses | Mechanism | Microhardness | COF | Wear losses | Mechanism | |
| Ti6Al4V | TiC | TA2, Ti6Al4V, Graphene | 311 $HV_{0.2}$ | 0.258 | 0.20 g | N/A | 413 $HV_{0.2}$ | 0.236 | 0.15 g | N/A | [85] |
| Ti6Al4V | TiC | Ti6Al4V, $Cr_3C_2$ | 284 $HV_{0.2}$ | 0.453 | $1.85 \times 10^{-4}$ $mm^3/(N \cdot m)$ | Abrasive Adhesive Oxidative | 552 $HV_{0.2}$ | 0.407 | $1.43 \times 10^{-4}$ $mm^3/(N \cdot m)$ | Abrasive Oxidative | [86] |
| Ti6Al4V | TiC | Ti6Al4V + 2 wt.% SiC | 352 $HV_{0.2}$ | 0.627 | $4.18 \times 10^{-4}$ $mm^3/(N \cdot m)$ | Abrasive Adhesive Oxidative | 653 $HV_{0.2}$ | 0.574 | $3.48 \times 10^{-4}$ $mm^3/(N \cdot m)$ | Abrasive Adhesive Oxidative | [87] |
| | | Ti6Al4V + 4 wt.% SiC | | | | | 686 $HV_{0.2}$ | 0.513 | $2.37 \times 10^{-4}$ $mm^3/(N \cdot m)$ | | |
| | | Ti6Al4V + 6 wt.% SiC | | | | | 727 $HV_{0.2}$ | 0.472 | $1.25 \times 10^{-4}$ $mm^3/(N \cdot m)$ | | |
| | | Ti6Al4V + 8 wt.% SiC | | | | | 726 $HV_{0.2}$ | 0.505 | $2.09 \times 10^{-4}$ $mm^3/(N \cdot m)$ | | |
| Ti6Al4V | TiN | NiCrAlY | 330 $HV_{0.5}$ | N/A | N/A | Adhesive Abrasive | 653 $HV_{0.5}$ | 0.317 | $0.125 \times 10^{-4}$ $mm^3/(N \cdot m)$ | Abrasive Adhesive Oxidative | [88] |
| Ti6Al4V | Ti (C, N) | TiN, Ti, graphite, In625 | 437 $HV_{0.3}$ | 0.656 | $3.72 \times 10^{-5}$ $mm^3$ | N/A | 584 $HV_{0.3}$ | 0.544 | $5.41 \times 10^{-6}$ $mm^3$ | N/A | [82] |
| Ti6Al4V | TiB | Ti6Al4V, $TiB_2$ | 364 $HV_{0.2}$ | N/A | 0.3783 g/min | Abrasive | 747 $HV_{0.2}$ | N/A | 0.0216 g/min | Abrasive | [84] |
| Ti6Al4V | TiC + TiB | Ti, $B_4C$ | 340 $HV_{0.2}$ | N/A | N/A | N/A | 1,224 $HV_{0.2}$ | N/A | N/A | N/A | [89] |
| Ti6Al4V | TiC + TiB | Ti, $B_4C$ | N/A | N/A | N/A | N/A | 896 $HV_{0.2}$ | 0.16 | $1.02 \times 10^{-1}$ $mm^3$ | Fatigue Abrasive | [90] |
| Ti6Al4V | TiN + TiB | Ti, h-BN, $Y_2O_3$ | 370 $HV_{0.5}$ | 0.458 | 7.14 $mm^3$ | Adhesive Abrasive | 891 $HV_{0.5}$ | 0.167 | 0.30 $mm^3$ | Abrasive | [91] |
| Ti6Al4V | TiC + TiN | $Cr_3C_2$ | 343 HV | 0.56 | $5.21 \times 10^{-8}$ $mm^3/(N \cdot m)$ | Abrasive Adhesive Oxidative | 959 HV | 0.23 | $3.85 \times 10^{-8}$ $mm^3/(N \cdot m)$ | Abrasive Oxidative | [92] |

COF: Coefficient of friction.

material removal, while excessive ceramic content deteriorates structural integrity and promotes crack initiation. Wang *et al.*[87] further confirmed these strengthening mechanisms in SiC-reinforced Ti-based composite coatings fabricated on Ti6Al4V via laser cladding. Rapid SiC dissolution and strong Ti-C affinity promoted *in situ* TiC formation as the dominant reinforcing phase, while residual SiC and reaction products provided heterogeneous nucleation sites. Enhanced carbon activity and melt-pool convection promoted TiC growth into dendritic and flower-like morphologies, resulting in refined microstructures and significantly improved hardness. The resulting improvement in tribological performance therefore arose not only from increased hardness, but also from grain refinement, load transfer by TiC, and stabilization of the near-surface deformation layer.

**Table 4. Summary of tribological properties of laser-cladded *ex situ* ceramic-particle-reinforced coatings on Ti alloy substrates**

| Substrate | *Ex situ* added ceramic particles | Other coating material | Tribological results of substrates | | | | Tribological results of coatings | | | | Ref. |
|---|---|---|---|---|---|---|---|---|---|---|---|
| | | | Microhardness | COF | Wear losses | Mechanism | Microhardness | COF | Wear losses | Mechanism | |
| Ti6Al4V | TiC | Ni60 | N/A | N/A | 22.5 mg | N/A | 850 $HV_{0.5}$ | N/A | 6.5 mg | N/A | [93] |
| Ti6Al4V | WC | Ni60 | 365 $HV_{0.5}$ | N/A | 27.6 mg | Adhesive Abrasive | 1142 $HV_{0.5}$ | 0.43 | 5.6 mg | Adhesive Abrasive | [94] |
| Ti6Al4V | SiC | N/A | 330 HV | 0.45 | N/A | Adhesive Abrasive | 950 HV | 0.13 | N/A | Fatigue Abrasive | [95] |
| Ti6Al4V | $B_4C$ | Ti6Al4V | 366 $HV_{0.3}$ | N/A | 1,745.1 mg | Abrasive | 583 $HV_{0.3}$ | N/A | 683.8 mg | Abrasive | [96] |
| Ti6Al4V | TiCN | NiCrBSiFeC | N/A | N/A | N/A | N/A | 974 $HV_{0.2}$ | 0.186 | $9.22 \times 10^{-2}$ $mm^3$ | Abrasive | [97] |
| Ti6Al4V | TiBCN | Ti | 350 HV | 0.32 | 6.71 mg | N/A | 1,596 HV | 0.18 | 1.22 mg | N/A | [98] |
| Ti6Al4V | $TiB_2$ | Ti | 332 $HV_{0.2}$ | N/A | N/A | N/A | 725 $HV_{0.2}$ | N/A | N/A | N/A | [99] |
| Ti6Al4V | TiC + SiC | Ni60 | 330 HV | 0.8 | $4.31 \times 10^{-6}$ $mm^3/(N{\cdot}mm)$ | Abrasive | 840 HV | N/A | $2.55 \times 10^{-6}$ $mm^3/(N{\cdot}mm)$ | Abrasive Adhesive Oxidative | [100] |
| Ti6Al4V | TiC + WC | Ti6Al4V | 330 HV | N/A | N/A | N/A | 450 HV | N/A | N/A | N/A | [101] |

COF: Coefficient of friction.

Despite the substantial hardness enhancement provided by carbide reinforcements, wear resistance does not increase monotonically with reinforcement content. The key factor is not the carbide fraction itself, but whether the reinforcing phase remains finely dispersed and mechanically compatible with the surrounding matrix. At moderate reinforcement levels, TiC particles can effectively share contact stresses, suppress matrix plowing, and stabilize the near-surface deformation layer during sliding, thereby improving wear resistance[87,100,114]. However, once the carbide content exceeds an optimal range, the reinforcing architecture gradually loses its damage tolerance. Particle agglomeration, incomplete melting, and pore formation become more pronounced, while the growing continuity and coarsening of the hard phase increase local stress concentration[87,114]. Under such conditions, the carbide phase no longer acts only as a load-bearing constituent, but also becomes a preferred site for crack initiation and brittle fracture. Cai *et al.*[114] reported that increasing the TiC content in TiC-reinforced Ni60 composite coatings reduced both wear resistance and flexural strength, indicating that excessive, coarse TiC particles can promote brittle failure rather than further strengthening. Similarly, Wang *et al.*[87] showed that excessive SiC addition during *in situ* TiC formation led to crack development because agglomerated particles and associated pores created stress-concentration zones under rapid solidification. Therefore, the deterioration in wear performance at excessive carbide contents originates fundamentally from the microstructural transition of the coating from a dispersed strengthening architecture to a defect-assisted brittle network.

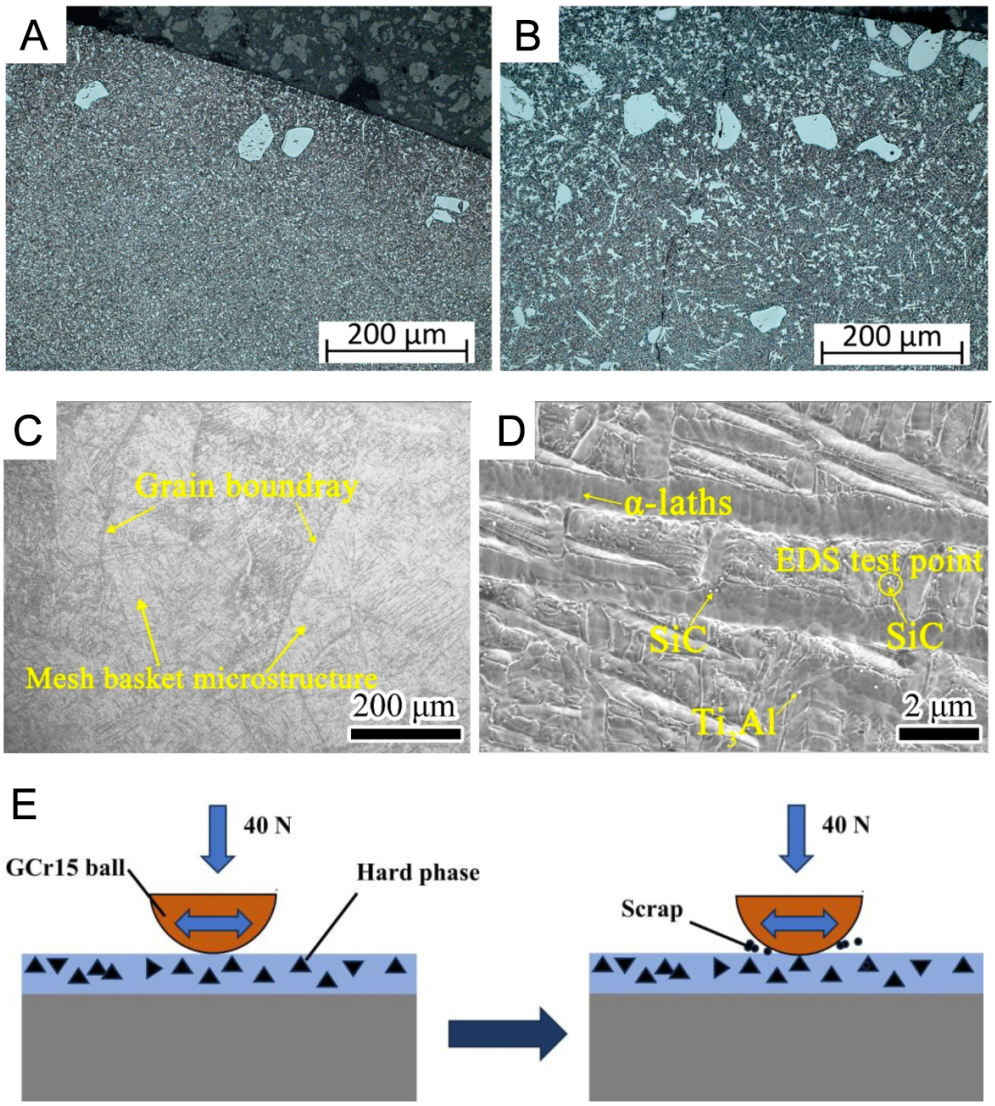



**Figure 5.** Representative microstructures and wear-resistance mechanism of carbide-reinforced laser-cladded composite coatings. (A and B) Cross-sectional microstructures of TiC-reinforced coatings; (A and B) are adapted from Ref.[69]. Licensed under CC-BY 4.0; (C) cross-sectional morphology and basket-weave microstructure of a SiC-containing laser-cladded coating; (D) high-magnification SEM image showing α-laths, residual SiC particles, and $Ti_3Al$ phase in the SiC-containing coating; (C and D) are adapted from Ref.[36]. Licensed under CC-BY 4.0; (E) schematic illustration of the WC-assisted wear-resistance mechanism during sliding contact. (E) is adapted from Ref.[94]. Licensed under CC-BY 4.0. SEM: Scanning electron microscopy; WC: tungsten carbide.

These findings indicate that the effectiveness of carbide reinforcement is controlled by the balance between hard-phase strengthening and structural integrity. Accordingly, the design of carbide-reinforced composite coatings should focus on controlling phase fraction, particle morphology, and distribution uniformity, for example, through compositional gradient design, controlled particle-size distribution, or the incorporation of ductile binder phases, to retain high load-bearing capacity while mitigating brittleness. More fundamentally, carbide-reinforced coatings are effective only when phase constitution, reinforcing morphology, and defect distribution are jointly optimized to prevent the hard ceramic framework from evolving into a continuous brittle crack-initiation path.

## Boride-reinforced systems

Boride reinforcements are introduced to enhance hardness while retaining higher fracture tolerance compared with carbide-dominated architectures[115,116]. For Ti alloys, the $TiB/TiB_2$ system is particularly attractive because the *in situ* formation of TiB whiskers or needles can generate a semi-continuous

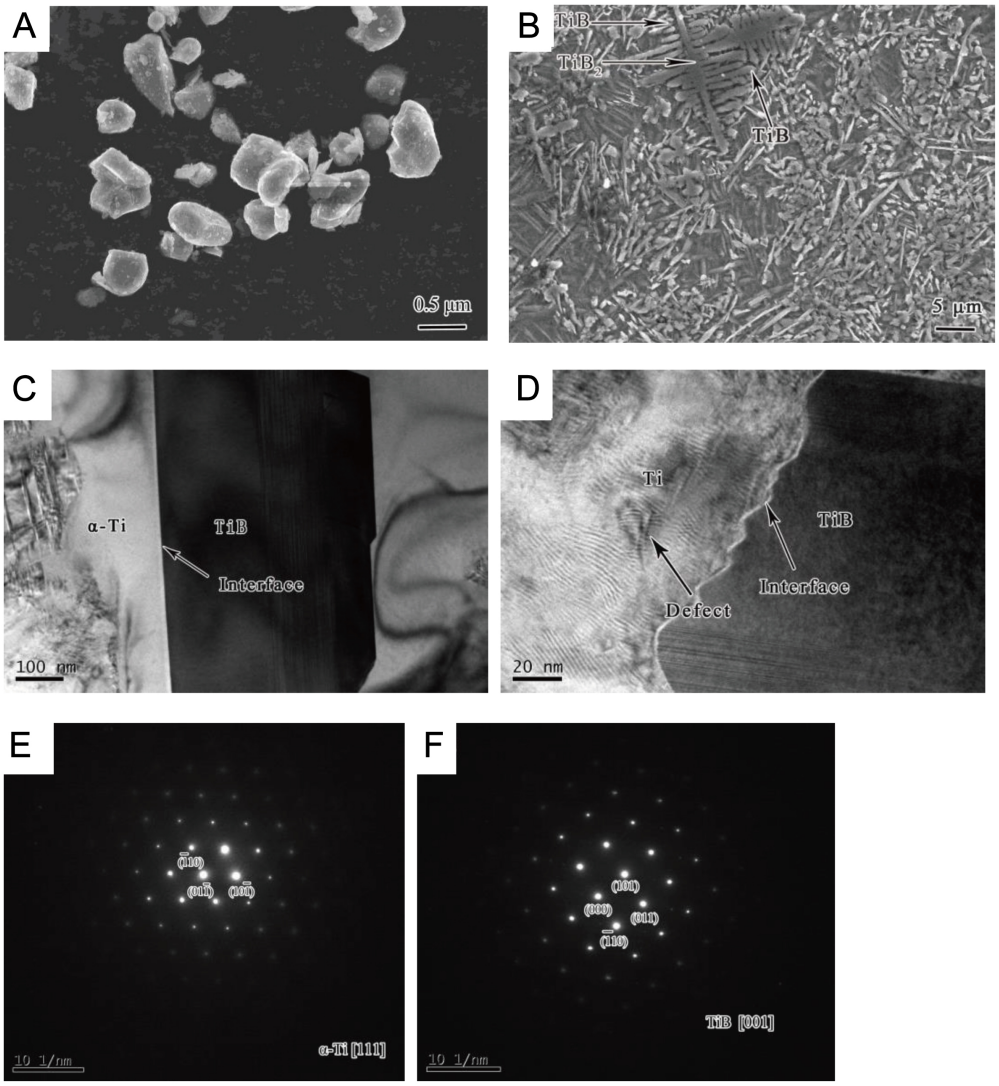



**Figure 6.** Representative microstructures and interfacial crystallography of TiB/$TiB_2$-reinforced laser-cladded composite coatings. (A) Morphology of $TiB_2$ particles; (B) microstructure showing TiB and residual $TiB_2$ phases in the coating; (C and D) TEM images showing the α-Ti/TiB interfacial characteristics; (E and F) SAED patterns corresponding to the α-Ti matrix and TiB phase, respectively. This figure is adapted from Ref.[99]. Licensed under CC-BY 4.0. TEM: Transmission electron microscopy; SAED: selected-area electron diffraction.

reinforcing framework, enabling efficient load transfer while mitigating crack propagation under impact-sensitive wear and thermal cycling[84,115,117,118].

Boride-reinforced coatings are fabricated either through *ex situ* addition of $TiB_2$ particulates or via *in situ* reactions from B-containing precursors such as $B_4C$, BN, or elemental B during laser cladding. Typical microstructures exhibit a multiscale architecture containing primary TiB, eutectic TiB whiskers, and residual $TiB_2$ embedded within an α-Ti matrix. As shown in Figure 6, scanning electron microscopy (SEM) and transmission electron microscopy (TEM) observations reveal TiB/$TiB_2$-reinforced microstructures and the interfacial characteristics between α-Ti and TiB, while the corresponding selected-area electron diffraction (SAED) patterns further confirm the crystallographic characteristics of the α-Ti matrix and TiB phase. These interfacial features are closely related to load transfer and crack-propagation behavior in boride-reinforced coatings. Representative studies have demonstrated the feasibility of gradient and composite designs; for example, Lin *et al.*[99] produced a gradient coating containing 30% $TiB_2$/Ti on Ti alloy substrates, while Li *et al.*[84] prepared multiple TiB-reinforced titanium matrix composite coatings via *in situ* laser cladding to improve wear performance.

The hallmark of TiB-reinforced claddings lies in the development of a multiscale whisker network inside a rapidly solidified matrix. High thermal gradients near the substrate promote epitaxial growth and columnar alignment of TiB whiskers, whereas reduced gradients and solute redistribution favor more equiaxed morphologies in upper regions[83]. Clean interfaces and favorable wettability between TiB whiskers and Ti-rich matrices facilitate effective load transfer and suppress interfacial decohesion during wear[119,120]. With increasing $TiB_2$ addition, the microstructure evolves from fine eutectic whiskers to a mixed architecture containing primary TiB and residual $TiB_2$ particles. Moderate reinforcement levels generate an interlocked whisker-like TiB framework that enhances load transfer and effectively impedes crack propagation. In this condition, the TiB phase acts as a crack-deflection and crack-bridging unit, forcing propagating cracks to change direction or become blunted, thereby improving fracture toughness and wear resistance. However, with further increases in boride content, the morphology and spatial distribution of TiB change significantly. Coarsening and local connectivity of whiskers may gradually develop into a quasi-continuous brittle network. Under such conditions, the role of TiB shifts from inhibiting crack propagation to facilitating it, as cracks can propagate preferentially along or through the interconnected boride structure. This transition from crack-deflection-dominated behavior to crack-propagation-assisted failure is responsible for the observed reduction in fracture toughness and wear resistance at excessive reinforcement levels[84].

Beyond simple load transfer, TiB networks contribute to crack deflection, bridging, and pull-out resistance, as the interlocking skeleton redistributes local stresses[121,122]. Wear cross-sectional analyses further reveal a gradual transition in wear mechanism: from matrix-dominated plastic deformation to skeleton-controlled abrasion with increasing reinforcement content. The whisker architecture also induces back-stress hardening, as deformation incompatibility between whiskers and the matrix generates geometrically necessary dislocations that improve the strength-ductility synergy[123,124]. Compared with TiC, TiB exhibits a closer thermal-expansion match with Ti and higher intrinsic fracture tolerance, thereby reducing susceptibility to thermal cracking during processing and service[125,126].

However, excessive boron activity or overly high $TiB_2$ addition can lead to whisker coarsening, increased melt viscosity, clustering, and lack-of-fusion defects, thereby elevating crack susceptibility[127]. Schematic analyses suggest that while moderate TiB content forms an interlocked network capable of effectively distributing contact stresses, excessive reinforcement results in brittle phase continuity and particle fracture. Consistent with this trend, Wang *et al.*[128] reported that although increasing $TiB_2$ content improved microhardness in laser melting deposition coatings on TiAl alloys, fracture toughness decreased markedly at high addition levels.

An effective design window for boride-reinforced coatings requires controlled whisker aspect ratio and spacing, avoidance of continuous brittle networks, and regulation of thermal gradients through optimized energy density, track overlap, and preheating when necessary. These factors govern not only hardness development but also the stability of the whisker framework and the coating's capacity to relieve stress before premature cracking occurs. The goal is to obtain a better balance among hardness, crack resistance, and structural reliability.

### Nitride-reinforced systems

Nitride reinforcements are introduced to enhance wear resistance under oxidative and high-temperature conditions while reducing friction through chemically stable, low-shear interfaces[129,130]. Among them, TiN is particularly suitable for Ti substrates because it combines high hardness and thermal stability with relatively good fracture tolerance and wettability, making it favorable for constructing stable hard-phase architectures in Ti-based cladding layers[131,132].

TiN-containing cladding layers are typically fabricated through three principal routes: (i) direct *ex situ* incorporation of TiN into the cladding powder[133]; (ii) laser-assisted *in situ* nitriding under $N_2$-rich shielding gas or reactive atmospheres[131]; (iii) introduction of nitrogen-containing precursors, such as boron nitride (BN) or $Si_3N_4$, which react with molten Ti to form TiN during cladding[134]. In precursor-assisted systems, BN can simultaneously introduce boron into the melt pool, resulting in the concurrent formation of TiB as a secondary reinforcement. Under such conditions, TiN, Ti(C,N), sub-stoichiometric titanium nitrides, and nano-scale TiB may coexist, producing a composite nitride-boride architecture that contributes to microstructural refinement and improved tribological performance[134].

Rapid solidification during laser cladding promotes the formation of fine TiN particles within the Ti matrix. Optimal performance is generally associated with a fine and discontinuous distribution of TiN-based phases, which enhances second phase strengthening and nitrogen-induced solid-solution strengthening while avoiding continuous brittle nitride bands[83]. In BN-derived systems, TiB can interlock with TiN particles and help deflect or arrest cracks, thereby reducing the crack sensitivity of otherwise brittle TiN-rich regions[135,136].

Fine TiN dispersions increase dislocation density, promote grain refinement, and improve load-bearing capacity. In addition, chemically stable nitride surfaces can facilitate the formation of oxide- or oxynitride-rich tribofilms, which reduce interfacial shear stress during sliding[83,137]. However, excessive nitride or nitride-boride content may cause particle coarsening, brittle connectivity, porosity, and localized corrosion or cracking, especially under strong compositional gradients or repeated cladding passes. Therefore, the effectiveness of nitride reinforcement depends not only on phase fraction, but also on the size, continuity, and spatial distribution of nitride-containing regions within the coating.

The primary risks associated with nitride systems include nitrogen-related porosity and residual-stress-driven cracking under steep thermal gradients and thermomechanical mismatch[138,139]. Accordingly, an effective design window requires balancing nitrogen activity to ensure adequate TiN formation while maintaining melt-pool stability to prevent gas entrapment. Control of particle fraction, spatial distribution, and thermal gradients through powder design, shielding strategy, and energy-density optimization is essential for achieving structural integrity and long-term reliability. From a microstructural standpoint, the key challenge is to retain the strengthening benefits of nitride phases while preventing defect accumulation, brittle connectivity, and interfacial instability during processing and service.

Overall, ceramic-particle-reinforced coatings are characterized by metallic matrices containing dispersed or interconnected carbide, boride, and/or nitride phases that provide substantial improvements in hardness and load-bearing capacity. Their tribological performance nevertheless depends strongly on reinforcement fraction, spatial distribution, and matrix/ceramic interface stability, because excessive phase connectivity may reduce damage tolerance and compromise coating integrity. These limitations have encouraged the incorporation of complementary regulatory mechanisms, including rare-earth grain refinement, self-lubricating phases, and high-entropy matrices, to achieve more balanced and stable service performance.

## MICROSTRUCTURE MODIFICATION BY RARE-EARTH OXIDES ($CeO_2$, $Y_2O_3$, *ETC*.)

In contrast to self-fluxing alloys and ceramic-particle-reinforced coatings, which primarily improve wear resistance through rigid, hard-phase load-bearing frameworks, rare-earth oxides in laser-cladded Ti coatings primarily function by regulating melt-pool behavior, solidification processes, and interfacial reactions. Rather than serving as primary load-bearing constituents, trace additions of rare-earth oxides refine grains, scavenge impurities, suppress defect formation, and enhance coating-substrate bonding. These effects improve the microstructural basis of wear resistance and long-term service stability[140,141]. Representative

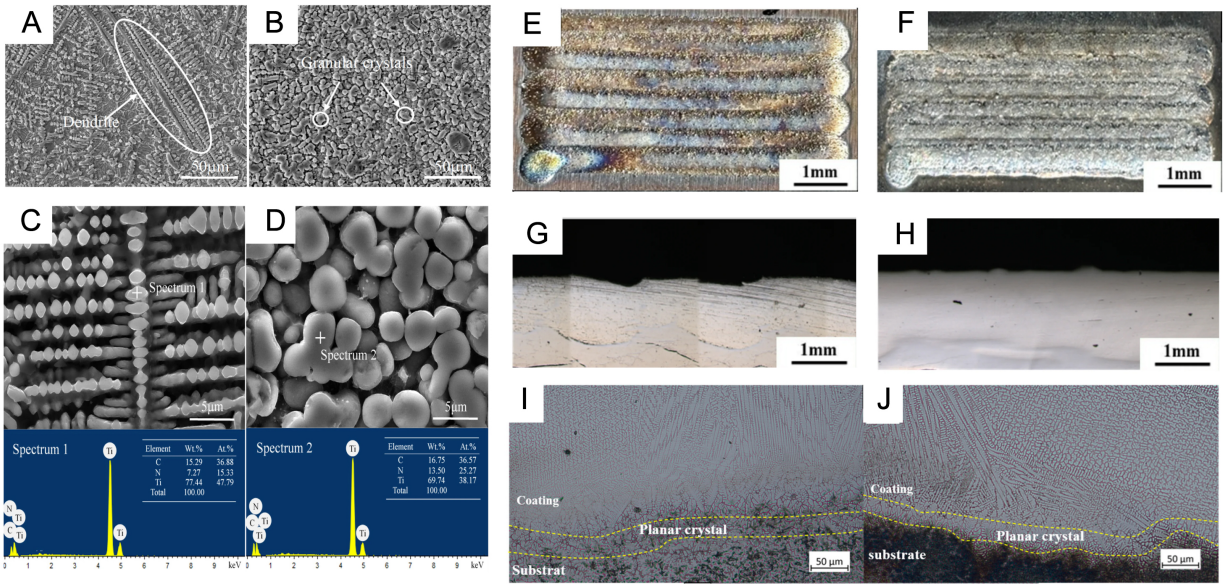



**Figure 7.** Rare-earth oxide-induced microstructural refinement and forming-quality improvement in laser-cladded coatings. (A-D) $CeO_2$-induced microstructural transformation and compositional characteristics: (A and C) coatings without $CeO_2$ modification and (B and D) coatings with $CeO_2$ modification. (A-D) are adapted from Ref.[142]. Licensed under CC-BY 4.0; (E-J) Effect of $Y_2O_3$ content on coating morphology and bonding-zone microstructure: (E and F) Macroscopic morphologies of coatings with 0% and 3% $Y_2O_3$; (G and H) Cross-sectional morphologies of coatings with 0% and 3% $Y_2O_3$; (I and J) Bonding-zone microstructures of coatings with 2% and 3% $Y_2O_3$. (E-J) are adapted from Ref.[143]. Licensed under CC-BY 4.0.

effects of $CeO_2$ and $Y_2O_3$ modification on microstructural refinement and coating-forming quality are summarized in Figure 7.

Among the rare-earth oxides investigated, $CeO_2$ and $Y_2O_3$ have been most extensively studied in laser-cladded wear-resistant Ti coatings owing to their high thermal stability, processing reliability, and comparatively well-understood modification mechanisms.

The tribological performance of representative rare-earth-oxide-modified laser-cladded coatings on Ti alloy substrates is summarized in Table 5. In summary, moderate additions of rare-earth oxides generally improve hardness and tribological stability, whereas excessive additions do not necessarily lead to further improvement. The table also suggests that their beneficial effect is mainly associated with microstructural refinement and interface regulation rather than direct load-bearing reinforcement.

## $CeO_2$-modified coatings

As a typical active rare-earth oxide, $CeO_2$ is often introduced into Ti-alloy coating systems not as a primary load-bearing phase, but to regulate microstructural evolution. Its design objective is to optimize melt-pool behavior, solidification dynamics, and interfacial stability during laser cladding. $CeO_2$ possesses good thermal stability and sufficient chemical activity, which allows it to participate in melt purification and interfacial reactions[149]. In addition, the reversible $Ce^{3+}/Ce^{4+}$ redox capability mitigates the detrimental effects of oxygen on coating integrity, thereby indirectly enhancing wear resistance and long-term service stability[150,151].

During laser cladding, $CeO_2$ is typically introduced via *ex situ* powder addition. Owing to its high melting point, $CeO_2$ particles remain largely solid or partially dissolved in the molten pool, where they may undergo local reduction or interfacial reactions[142]. A portion of Ce segregates toward GBs and melt-pool edges, reacting with impurity elements such as O and S to reduce their effective concentration[152]. Simultaneously, $CeO_2$ particles and reaction products promote grain refinement and modify solidification pathways[149].

**Table 5. Summary of tribological properties of rare-earth-oxide-modified laser-cladded coatings on Ti alloy substrates**

| Substrate | Rare-earth oxides | Coating material | Tribological results of substrate | | | | Tribological results of coatings | | | | Ref. |
|---|---|---|---|---|---|---|---|---|---|---|---|
| | | | Microhardness | COF | Wear losses | Mechanism | Microhardness | COF | Wear losses | Mechanism | |
| Ti811 | $CeO_2$ | TC4 + Ni60 + 0 wt.% $CeO_2$ | ~380 $HV_{0.5}$ | 0.67 | 287.63 × $10^{-3}$ $mm^3$ | N/A | ~646 $HV_{0.5}$ | 0.36 | 121.23 × $10^{-3}$ $mm^3$ | N/A | [50] |
| | | TC4 + Ni60 + 1 wt.% $CeO_2$ | | | | | ~771 $HV_{0.5}$ | 0.28 | ~74.37 × $10^{-3}$ $mm^3$ | | |
| | | TC4 + Ni60 + 2 wt.% $CeO_2$ | | | | | ~790 $HV_{0.5}$ | 0.25 | ~63.14 × $10^{-3}$ $mm^3$ | | |
| | | TC4 + Ni60 + 3 wt.% $CeO_2$ | | | | | ~730 $HV_{0.5}$ | 0.31 | ~79.24 × $10^{-3}$ $mm^3$ | | |
| | | TC4 + Ni60 + 4 wt.% $CeO_2$ | | | | | ~695 $HV_{0.5}$ | 0.33 | ~85.37 × $10^{-3}$ $mm^3$ | | |
| Ti6Al4V | $CeO_2$ | TiCN + $SiO_2$ + 0 wt.% $CeO_2$ | 340 $HV_{0.2}$ | N/A | ~2.75 $mm^3$ | Plastic deformation | 1,050 $HV_{0.2}$ | N/A | ~0.075 $mm^3$ | Fatigue | [142] |
| | | TiCN + $SiO_2$ + 3 wt.% $CeO_2$ | | | | | 1,230 $HV_{0.2}$ | | ~0.065 $mm^3$ | Abrasive | |
| Ti6Al4V | $CeO_2$ | Ni60 + Cu + Ti | 340 $HV_1$ | 0.73 | 65.5 mg | Adhesive Abrasive | N/A | 0.33 | 2.5 mg | N/A | [144] |
| | | Ni60 + Cu + Ti + 8 wt.% $B_4C$ | | | | | 1,078 $HV_1$ | 0.28 | 1.8 mg | Abrasive | |
| | | Ni60 + Cu + Ti + 8 wt.% $B_4C$ + 3 wt.% $CeO_2$ | | | | | 1,105 $HV_1$ | 0.25 | 1.2 mg | Abrasive | |
| Ti6Al4V | $Y_2O_3$ | Ti6Al4V | 396 $HV_{0.5}$ | 0.526 | 9.17 × $10^{-4}$ $mm^3/(N·m)$ | Adhesive Abrasive | 411 $HV_{0.5}$ | 0.49 | 8.25 × $10^{-4}$ $mm^3/(N·m)$ | Adhesive Abrasive | [145] |
| | | Ti6Al4V + 2 wt.% $Y_2O_3$ | | | | | 455 $HV_{0.5}$ | 0.524 | 10.02 × $10^{-4}$ $mm^3/(N·m)$ | Abrasive | |
| Ti6Al4V | $Y_2O_3$ | NiCr-$Cr_3C_2$ + TC4 + Ni-$MoS_2$ + 0 wt.% $Y_2O_3$ | 350 HV | 0.51 ± 0.02 | ~3.91 × $10^{-4}$ $mm^3/(N·m)$ | N/A | 541 $HV_{10}$ | 0.44 | 3.21 × $10^{-4}$ $mm^3/(N·m)$ | Abrasive Oxidative | [146] |
| | | NiCr-$Cr_3C_2$ + TC4 + Ni-$MoS_2$ + 2 wt.% $Y_2O_3$ | | | | | ~506 $HV_{10}$ | ~0.42 | 3.30 × $10^{-4}$ $mm^3/(N·m)$ | | |
| | | NiCr-$Cr_3C_2$ + TC4 + Ni-$MoS_2$ + 4 wt.% $Y_2O_3$ | | | | | ~431 $HV_{10}$ | 0.39 | 3.01 × $10^{-4}$ $mm^3/(N·m)$ | | |
| | | NiCr-$Cr_3C_2$ + TC4 + Ni-$MoS_2$ + 6 wt.% $Y_2O_3$ | | | | | ~415 $HV_{10}$ | ~0.47 | ~3.84 × $10^{-4}$ $mm^3/(N·m)$ | | |
| | | NiCr-$Cr_3C_2$ + TC4 + Ni-$MoS_2$ + 8 wt.% $Y_2O_3$ | | | | | 420 $HV_{10}$ | N/A | N/A | | |
| Ti6Al4V | $Y_2O_3$ | TC4 + WC + Ni-$MoS_2$ + 0 wt.% $Y_2O_3$ | 395 $HV_{0.5}$ | 0.4716 | 4.52 × $10^{-4}$ $mm^3/(N·m)$ | Adhesive | 626 $HV_{0.5}$ | 0.5563 | 3.95 × $10^{-4}$ $mm^3/(N·m)$ | Abrasive | [147] |
| | | TC4 + WC + Ni-$MoS_2$ + 1 wt.% $Y_2O_3$ | | | | | 589 $HV_{0.5}$ | 0.5316 | 3.71 × $10^{-4}$ $mm^3/(N·m)$ | | |
| | | TC4 + WC + Ni-$MoS_2$ + 2 wt.% $Y_2O_3$ | | | | | 575 $HV_{0.5}$ | 0.5234 | 3.65 × $10^{-4}$ $mm^3/(N·m)$ | | |
| | | TC4 + WC + Ni-$MoS_2$ + 3 wt.% $Y_2O_3$ | | | | | 565 $HV_{0.5}$ | 0.4791 | 3.49 × $10^{-4}$ $mm^3/(N·m)$ | | |
| | | TC4 + WC + Ni-$MoS_2$ + 4 wt.% $Y_2O_3$ | | | | | 548 $HV_{0.5}$ | 0.4915 | 3.63 × $10^{-4}$ $mm^3/(N·m)$ | | |

| | | | | | | | | | | | |
|---|---|---|---|---|---|---|---|---|---|---|---|
| Ti6Al4V | $La_2O_3$ | Ti + B + 0 wt.% $La_2O_3$<br>Ti + B + 1 wt.% $La_2O_3$<br>Ti + B + 2 wt.% $La_2O_3$<br>Ti + B + 3 wt.% $La_2O_3$ | 330 HV | ~0.92 | N/A | Adhesive | ~1,050 HV<br>~1,150 HV<br>~1,180 HV<br>~1,210 HV | ~0.89<br>~0.82<br>~0.91<br>~0.64 | N/A | Abrasive | [148] |

COF: Coefficient of friction.

Microstructural modification following $CeO_2$ addition commonly manifests as reduced columnar grain fractions and increased equiaxed grains or fine dendrites, thereby improving structural uniformity. Wang *et al.*[142] reported that introducing 3 wt.% nano-$CeO_2$ into TiCN/$SiO_2$ composite coatings produced a refined and compact microstructure, increasing microhardness to 1,230 $HV_{0.2}$ and reducing wear volume loss by 14% in simulated body fluid. In the absence of $CeO_2$, coarse dendritic grains dominated the coating thickness, whereas $CeO_2$ addition significantly refined dendrites and improved microstructural homogeneity. GB Ce segregation suppressed continuous brittle phase formation and reduced defect density, thereby enhancing coating stability[153]. Additionally, Gong *et al.*[154] observed that 3 wt.% $CeO_2$ addition to Ni60A coatings on TC4 yielded crack-free, pore-free layers with a microhardness of 1,164 HV.

The regulatory effect of $CeO_2$ exhibits a distinct concentration window. At excessive addition levels, its ability to effectively regulate melt-pool dynamics and microstructural refinement becomes progressively limited. Instead, particle agglomeration, localized embrittlement, and increased substrate dilution may occur, replacing the beneficial refinement effect observed at moderate additions[50,155]. Liu *et al.*[50] demonstrated that moderate $CeO_2$ addition eliminated characteristic herringbone cracks and promoted TiC spheroidization, transforming dendritic TiC morphologies into more homogeneous granular structures. However, with further increases in $CeO_2$ content, microstructural coarsening was observed[149]. Elemental analyses revealed Ce enrichment along TiC dendrites, consistent with Ti-Ce mutual solubility at elevated temperatures under non-equilibrium cladding conditions. This indicates that excessive Ce alters the solidification pathway, shifting it from refinement-dominated behavior toward dendritic growth, thereby weakening the beneficial effects observed at intermediate additions.

Additional studies indicate that excessive $CeO_2$ may increase the dilution rate by enhancing melt-pool fluidity, which in turn leads to reduced hardness at high addition levels[144]. Consequently, the effectiveness of $CeO_2$ modification is intrinsically limited to a controlled compositional window. Since $CeO_2$ does not directly participate in primary load bearing, its primary role lies in regulating microstructural evolution and defect formation, rather than providing direct mechanical reinforcement. Therefore, its beneficial effect depends on maintaining a balance between refinement efficiency and structural stability through synergistic interaction with both hard phases and the metallic matrix.

### $Y_2O_3$-modified coatings

The primary objective of $Y_2O_3$-modified coatings is to enhance microstructural stability, interfacial bonding quality, and reliability at high temperatures. Compared with $CeO_2$, $Y_2O_3$ exhibits higher thermal stability and greater chemical inertness, making it particularly suitable for elevated-temperature and complex service environments[35,156]. Rather than acting as an active melt regulator, $Y_2O_3$ primarily serves as a structural stabilizer, strengthening the microstructural foundation of

wear-resistant coatings through grain-boundary regulation and interfacial control.

During laser cladding, $Y_2O_3$ particles are typically introduced as dispersed solids. Owing to their high melting point and limited solubility, they largely remain undissolved within the molten pool, while a small fraction of Y undergoes limited diffusion and interfacial reactions. $Y_2O_3$ particles preferentially segregate at GBs and exert a pinning effect that inhibits grain growth. Although heterogeneous nucleation has been proposed in earlier interpretations, lattice-misfit analyses indicate that the dominant mechanism is grain-boundary pinning and dragging rather than nucleation-rate enhancement[35]. This restriction on solid-liquid interface migration promotes significant grain refinement, leading to transformation from coarse columnar structures to fine equiaxed grains or dendrites and resulting in a denser, more homogeneous microstructure[157].

Experimental evidence supports this mechanism. Zhang *et al.*[145] reported that $Y_2O_3$ addition to laser-cladded Ti6Al4V coatings completely suppressed pore formation and improved overall forming quality. The refined microstructure, predominantly composed of acicular α'-Ti, exhibited disrupted β-Ti GB continuity due to adsorption and pinning effects. Elemental mapping and lattice mismatch evaluation revealed Y and O enrichment along original β-Ti grain boundaries, while the lattice mismatch between $Y_2O_3$ and β-Ti exceeded 12%, excluding effective heterogeneous nucleation. These findings confirm that refinement originates primarily from grain-boundary pinning rather than increased nucleation.

Beyond microstructural refinement, $Y_2O_3$ improves interfacial bonding and crack resistance. By regulating interfacial reactions, it reduces the thickness of brittle interfacial layers and alleviates residual stress concentration, thereby enhancing structural stability during service. Zhang *et al.*[157] demonstrated that $Y_2O_3$ addition in TiC-Ti6Al4V composite coatings induced the formation of numerous tertiary dendrites and improved metallurgical bonding. The semi-coherent epitaxial relationship between TiC particles and the β-Ti matrix further strengthened interfacial adhesion, thereby improving resistance to dislocation motion and delamination under frictional loading. Likewise, surface and cross-sectional observations revealed that moderate $Y_2O_3$ additions suppressed crack formation and porosity, significantly enhancing coating integrity[146].

As with $CeO_2$, the strengthening effect of $Y_2O_3$ exhibits a concentration-dependent window. Moderate additions refine the microstructure and, by enhancing structural stability, indirectly improve wear resistance. However, excessive $Y_2O_3$ content leads to particle agglomeration, localized embrittlement, and surface instability. At high concentrations, crack reappearance and localized surface collapse have been observed, indicating that over-addition disrupts the beneficial pinning mechanism and compromises mechanical integrity. Hence, $Y_2O_3$ functions most effectively as a microstructural regulator when combined with hard reinforcing phases, enabling a better balance among hardness, toughness, and high-temperature reliability.

In summary, rare-earth-oxide-modified coatings are characterized by refined, dense, and more homogeneous microstructures resulting from the regulation of melt-pool behavior, solidification, and interfacial reactions. Their principal contribution lies in improving microstructural quality and interfacial stability rather than providing direct load-bearing reinforcement. Consequently, although rare-earth oxides can enhance the structural basis of wear resistance, they have limited ability to directly regulate friction or suppress severe wear under high loads, dry sliding, or elevated temperatures.

For this reason, coating design strategies have gradually extended beyond structural stabilization toward more active control over friction and wear. One promising direction is to design self-lubricating coating systems by incorporating solid lubricants into wear-resistant matrices, enabling stable transfer films to form during sliding to reduce COF and suppress adhesive wear.

At the same time, increasingly demanding service environments require coating systems with more comprehensive performance. Because a single strengthening mechanism is often insufficient to simultaneously satisfy the demands for wear resistance, thermal stability, and environmental adaptability, HEA coatings have attracted growing attention. Through multi-principal-element alloying, high mixing entropy effects, and enhanced structural stability, these systems offer unique potential for synergistically improving wear resistance, thermal stability, and environmental tolerance under complex service conditions, and therefore represent an important emerging direction in Ti alloy surface modification.

## FUNCTIONAL COMPOSITE COATINGS WITH SELF-LUBRICATING CAPABILITY

Although traditional ceramic-reinforced coatings exhibit excellent wear resistance, they often maintain relatively high COF. Elevated friction leads to excessive heat generation, increased energy dissipation, and a greater tendency toward adhesive wear[158]. These limitations become particularly critical under extreme service conditions, including high-temperature and vacuum environments, where conventional liquid lubrication is impractical.

To address these challenges, self-lubricating composite coatings have been developed as an advanced design approach. In such systems, solid lubricating phases are dispersed within a hard wear-resistant matrix, enabling the coating to function both as a load-bearing framework and as a reservoir for interfacial lubrication. This dual-function architecture facilitates friction reduction while preserving structural integrity. From a microstructural standpoint, the effectiveness of these coatings depends on the compatibility between lubricating phases and the supporting matrix, as well as on the spatial distribution and stability of the lubricating domains during sliding. As summarized in Figure 8, representative self-lubricating laser-cladded coatings may contain TiS-, $WS_2$-, $Ti_2S$-, and $Ti_2SC$-based lubricating constituents, together with TiW-, TiC-, $Ti_2Ni$-, and α-Ti-related supporting or reinforcing phases.

The tribological performance of representative laser-cladded self-lubricating coatings and MAX-phase-based self-lubricating coatings on Ti alloy substrates is summarized in Tables 6 and 7. MAX phases, a family of layered ternary carbides and nitrides generally represented by the formula $M_{n+1}AX_n$. Both tables show that the incorporation of lubricating phases generally lowers friction and improves wear resistance, while MAX-phase-based systems further combine lubrication with structural load-bearing capability. The results also indicate that the tribological benefit depends on the stability and continuity of the transfer film or tribofilm, rather than on lubricant content alone.

### Solid lubricant synergistic composite coatings

Currently, solid lubricants applied to Ti alloy surfaces mainly include layered materials such as graphite, h-BN, $MoS_2$, and $WS_2$; soft metals including Ag, Au, and Cu; and alkaline-earth fluorides such as $CaF_2$ and $BaF_2$.

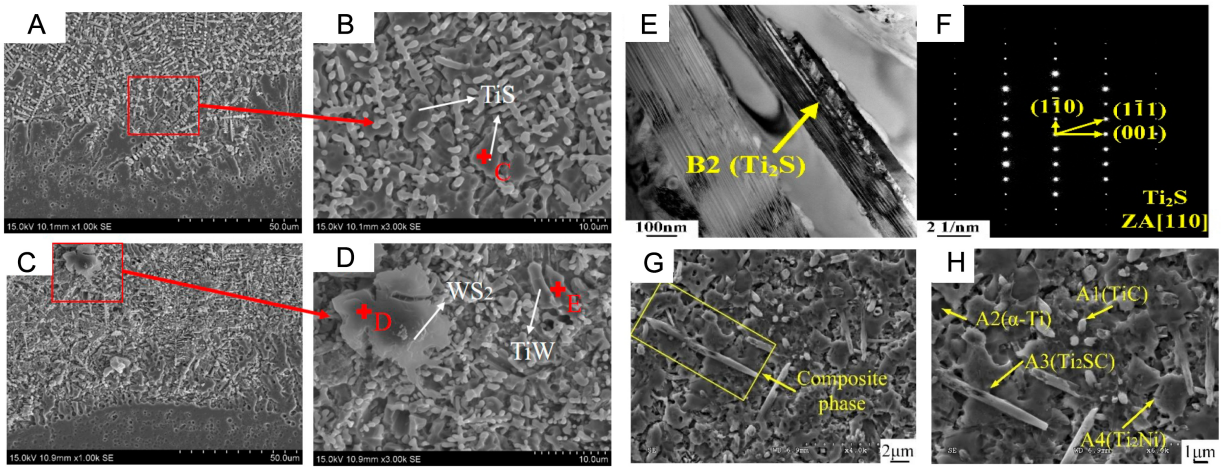



**Figure 8.** Microstructural characteristics of multiphase self-lubricating laser-cladded composite coatings. (A and B) SEM microstructures showing TiS-containing phases in the coating; (C and D) SEM microstructures showing $WS_2$ and TiW phases in the coating; (A-D) are adapted from Ref.[159]. Licensed under CC-BY 4.0; (E) TEM image showing a $Ti_2S$-containing layered structure; (F) corresponding SAED pattern of the $Ti_2S$ phase; (E and F) are adapted from Ref.[160]. Licensed under CC-BY 4.0; (G and H) SEM microstructures showing composite phases, including α-Ti, TiC, $Ti_2SC$, and $Ti_2Ni$ phases. (G and H) are adapted from Ref.[161]. Licensed under CC-BY 4.0. SEM: Scanning electron microscopy; TEM: transmission electron microscopy; SAED: selected-area electron diffraction.

### *Layered materials*

Layered materials represent the earliest and most extensively studied class of solid lubricants in self-lubricating coatings for Ti alloys. Their lubrication mechanism originates from weak van der Waals bonding between adjacent atomic layers within their lamellar crystal structures. During sliding, these materials readily undergo interlaminar shear along basal planes, which helps develop continuous or partially continuous transfer films at the contact interface. Such films significantly reduce interfacial shear resistance and mitigate adhesive wear and micro-cutting, which are common in Ti alloys under dry sliding conditions. Therefore, the effectiveness of layered lubricants depends not only on their intrinsic low-shear crystal structure, but also on their ability to form and maintain a stable tribofilm during service.

Liu *et al.*[159] prepared a series of TiN/$WS_2$ + h-BN/NiCrBSi self-lubricating coatings with different $WS_2$/h-BN ratios to evaluate the effect of solid-lubricant composition on wear behavior. As shown in Figure 9, the optimized coating exhibited a shallower and flatter wear scar, indicating that an appropriate $WS_2$/h-BN balance can reduce material removal during sliding.

The temperature-dependent evolution of tribofilms in graphene-containing coatings provides a representative example. Zhang *et al.*[165] reported that tribological performance is governed by the composition and architecture of the interfacial film. At room temperature, the tribofilm mainly consists of graphene nanosheets with a small amount of oxides. SEM, elemental mapping, and Raman analyses confirmed the formation of a dense carbon-rich transfer film that preserves the lamellar structure of graphene within the wear track. This low-shear barrier minimizes direct metal contact and suppresses adhesive wear.

At elevated temperatures, however, the tribofilm composition undergoes a pronounced transition. X-ray photoelectron spectroscopy (XPS) analysis at 600 °C revealed the dominance of oxide phases, including CuO, $Cr_2O_3$, $CoWO_4$, $TiO_2$, and $SiO_2$. Although graphene retains partial lubricating functionality, oxide products become the primary load-bearing and protective constituents. The resulting graphene-oxide composite tribofilm enhances oxidation resistance and stabilizes the sliding interface. Therefore, lubrication

**Table 6. Summary of tribological properties of laser-cladded self-lubricating coatings on Ti alloy substrates**

| Substrate | Self-lubricating components | Experimental environment | Coating material | Tribological results of substrates | | | | Tribological results of coatings | | | | Ref. |
|---|---|---|---|---|---|---|---|---|---|---|---|---|
| | | | | Microhardness | COF | Wear losses | Mechanism | Microhardness | COF | Wear losses | Mechanism | |
| Ti6Al4V | Ag | RT (30N) | | | | 64.6 × $10^{-5}$ $mm^3$/(N·m) | | | | 7.45 × $10^{-5}$ $mm^3$/(N·m) | Abrasive | |
| | | 300 °C (30N) | TC4 + 18.5 wt.%Co12 + 8 wt.%Ag | 350 HV | N/A | 53.1 × $10^{-5}$ $mm^3$/(N·m) | Abrasive | 598 $HV_{0.5}$ | N/A | 3.08 × $10^{-5}$ $mm^3$/(N·m) | Abrasive Oxidative | [162] |
| | | 500 °C (30N) | | | | 18.7 × $10^{-5}$ $mm^3$/(N·m) | | | | 0.846 × $10^{-5}$ $mm^3$/(N·m) | Oxidative | |
| Ti6Al4V | $MoS_2$ | N/A | TC4 + Ni-$MoS_2$ + 15 wt.% WC | 332 $HV_{0.5}$ | 0.4184 | 4.608 × $10^{-4}$ $mm^3$/(N·m) | Adhesive | 746 $HV_{0.5}$ | 0.5807 | 1.245 × $10^{-4}$ $mm^3$/(N·m) | Abrasive | [160] |
| Ti6Al4V | $MoS_2$ | N/A | NiCrBSi + 0 wt.% $MoS_2$ | 364 $HV_{0.2}$ | N/A | N/A | N/A | 911 $HV_{0.2}$ | 0.6477 | 2.035 × $10^{-5}$ $mm^3$/(N·m) | N/A | [163] |
| | | | NiCrBSi + 4 wt.% $MoS_2$ | | | | | 874 $HV_{0.2}$ | 0.5881 | 2.136 × $10^{-5}$ $mm^3$/(N·m) | | |
| | | | NiCrBSi + 6 wt.% $MoS_2$ | | | | | 820 $HV_{0.2}$ | 0.5521 | 1.963 × $10^{-5}$ $mm^3$/(N·m) | | |
| | | | NiCrBSi + 8 wt.% $MoS_2$ | | | | | 899 $HV_{0.2}$ | 0.5218 | 1.208 × $10^{-5}$ $mm^3$/(N·m) | | |
| | | | NiCrBSi + 10 wt.% $MoS_2$ | | | | | 873 $HV_{0.2}$ | 0.4539 | 0.895 × $10^{-5}$ $mm^3$/(N·m) | | |
| Ti6Al4V | $WS_2$ | N/A | NiCrBSi | 370 $HV_{0.2}$ | 0.4134 | ~20 × $10^{-6}$ $mm^3$/(N·m) | Plastic deformation | 1,006 $HV_{0.2}$ | 0.46 | ~5 × $10^{-6}$ $mm^3$/(N·m) | Abrasive | [164] |
| | | | NiCrBSi + 30 wt.% TiN | | | | | 927 $HV_{0.2}$ | 0.4304 | ~10 × $10^{-6}$ $mm^3$/(N·m) | | |
| | | | NiCrBSi + 30 wt.% TiN + 10 wt.% $WS_2$ | | | | | 860 $HV_{0.2}$ | 0.402 | ~20 × $10^{-6}$ $mm^3$/(N·m) | | |
| | | | NiCrBSi + 30 wt.% TiN + 20 wt.% $WS_2$ | | | | | 842 $HV_{0.2}$ | 0.36 | ~10 × $10^{-6}$ $mm^3$/(N·m) | | |
| | | | NiCrBSi + 30 wt.% TiN + 30 wt.% $WS_2$ | | | | | 870 $HV_{0.2}$ | 0.3826 | ~20 × $10^{-6}$ $mm^3$/(N·m) | | |

| | | | | | | | | | | | | |
|---|---|---|---|---|---|---|---|---|---|---|---|---|
| Ti6Al4V | Cu + Graphene | RT | Stellite6-10Cu + 0.6 wt.% Graphene | 321 $HV_{0.5}$ | 0.56 | 245 × $10^{-5}$ $mm^3/(N·m)$ | Adhesive Abrasive | 455 $HV_{0.5}$ | 0.25 | 7.61 × $10^{-5}$ $mm^3/(N·m)$ | Adhesive Oxidative | [165] |
| | | | Stellite6-10Cu + 1.2 wt.% Graphene | | | | | 658 $HV_{0.5}$ | 0.27 | 4.42 × $10^{-5}$ $mm^3/(N·m)$ | | |
| | | | Stellite6-10Cu + 1.8 wt.% Graphene | | | | | 465 $HV_{0.5}$ | 0.42 | 8.14 × $10^{-5}$ $mm^3/(N·m)$ | | |
| | | | Stellite6-10Cu + 2.4 wt.% Graphene | | | | | 483 $HV_{0.5}$ | 0.46 | 9.91 × $10^{-5}$ $mm^3/(N·m)$ | | |
| | | 600 °C | | | 0.47 | 121 × $10^{-5}$ $mm^3/(N·m)$ | | | 0.39 | 92.9 × $10^{-5}$ $mm^3/(N·m)$ | | |
| | | | | | | | | | 0.33 | 43.9 × $10^{-5}$ $mm^3/(N·m)$ | | |
| | | | | | | | | | 0.51 | 61.2 × $10^{-5}$ $mm^3/(N·m)$ | | |
| | | | | | | | | | 0.58 | 80.3 × $10^{-5}$ $mm^3/(N·m)$ | | |
| Ti6Al4V | Graphene oxide (GO) | N/A | CoCrMo + 0 wt.%GO | 391 HV | 0.626 | 3.826 × $10^{-4}$ $mm^3/(N·m)$ | N/A | 762 HV | 0.515 | 16.52 × $10^{-5}$ $mm^3/(N·m)$ | N/A | [166] |
| | | | CoCrMo + 0.2 wt.% GO | | | | | 912 HV | 0.44 | 9.64 × $10^{-5}$ $mm^3/(N·m)$ | | |
| | | | CoCrMo + 0.5 wt.% GO | | | | | 1,008 HV | 0.375 | 5.54 × $10^{-5}$ $mm^3/(N·m)$ | | |
| | | | CoCrMo + 0.8 wt.% GO | | | | | 920 HV | 0.429 | 8.89 × $10^{-5}$ $mm^3/(N·m)$ | | |
| | | | CoCrMo + 1.1 wt.% GO | | | | | 806 HV | N/A | N/A | | |
| | | | CoCrMo + 1.4 wt.% GO | | | | | 738 HV | N/A | N/A | | |
| Ti6Al4V | $CaF_2$ | RT | NiCr/$Cr_3C_2$ + 20 wt.% $CaF_2$ | ~300 $HV_{0.2}$ | ~0.425 | ~38 × $10^{-5}$ $mm^3/(N·m)$ | Abrasive Adhesive | 1,013 $HV_{0.2}$ | ~0.325 | ~7 × $10^{-5}$ $mm^3/(N·m)$ | Abrasive | [167] |
| | | 300 °C | | | ~0.35 | ~25 × $10^{-5}$ $mm^3/(N·m)$ | | | ~0.3125 | ~5 × $10^{-5}$ $mm^3/(N·m)$ | Abrasive Oxidative | |
| | | 600 °C | | | ~0.37 | ~17.5 × $10^{-5}$ $mm^3/(N·m)$ | | | ~0.21 | ~2.5 × $10^{-5}$ $mm^3/(N·m)$ | Generation of transfer films | |
| Ti6Al4V | h-BN | RT | TC4 + 1 wt.% h-BN | 350 $HV_{0.5}$ | N/A | N/A | N/A | 497 $HV_{0.5}$ | ~0.29 | 7.48 × $10^{-4}$ $mm^3/(N·m)$ | Plastic deformation Abrasive Adhesive | [168] |
| | | | TC4 + 2 wt.% h-BN | | | | | 552 $HV_{0.5}$ | ~0.36 | 9.92 × $10^{-4}$ $mm^3/(N·m)$ | | |
| | | | TC4 + 3 wt.% h-BN | | | | | 605 $HV_{0.5}$ | ~0.47 | 6.87 × $10^{-4}$ $mm^3/(N·m)$ | | |
| | | 300 °C | | | | | | | ~0.355 | 6.83 × $10^{-4}$ $mm^3/(N·m)$ | | |
| | | | | | | | | | ~0.38 | 3.53 × $10^{-4}$ $mm^3/(N·m)$ | Oxidative | |
| | | | | | | | | | ~0.375 | 4.93 × $10^{-4}$ $mm^3/(N·m)$ | | |
| | | | | | | | | | ~0.33 | 3.92 × $10^{-4}$ $mm^3/(N·m)$ | | |
| | | 600 °C | | | | | | | ~0.29 | 1.61 × $10^{-4}$ $mm^3/(N·m)$ | Oxidative | |
| | | | | | | | | | ~0.32 | 2.48 × $10^{-4}$ $mm^3/(N·m)$ | | |

| | | | | | | | | | | | | |
|---|---|---|---|---|---|---|---|---|---|---|---|---|
| | | | NiCrBSi + 30 wt.% TiN + 15 wt.% $WS_2$ | | | | | 860 ± 13 $HV_{0.2}$ | 0.4323 | | | |
| | | | NiCrBSi + 30 wt.% TiN + 15 wt.% h-BN | | | | | 842 ± 16 $HV_{0.2}$ | 0.4291 | | | |
| Ti6Al4V | $WS_2$ + h-BN | N/A | NiCrBSi + 30 wt.% TiN + 5 wt.% $WS_2$ + 10 wt.% h-BN | 370 $HV_{0.2}$ | 0.8 | N/A | Abrasive | 870 ± 15 $HV_{0.2}$ | 0.3458 | N/A | Abrasive<br>Adhesive<br>Oxidative | [159] |
| | | | NiCrBSi + 30 wt.% TiN + 7.5 wt.% $WS_2$ + 7.5 wt.% h-BN | | | | | 1,006 ± 7 $HV_{0.2}$ | 0.3948 | | | |
| | | | NiCrBSi + 30 wt.% TiN + 10 wt.% $WS_2$ + 5 wt.% h-BN | | | | | 927 ± 20 $HV_{0.2}$ | 0.4072 | | | |
| | | RT | | | | | | | 0.9834 | ~$10^{-5}$ $mm^3/(N·m)$ | Microscopic cutting | |
| Ti6Al4V | Ag + $MoS_2$ | 300 °C | Ni60 + 8 wt.% $MoS_2$ + 5 wt.% Ag | 330 $HV_{0.2}$ | N/A | N/A | N/A | 824 $HV_{0.2}$ | 0.9602 | | Abrasive | [169] |
| | | 600 °C | | | | | | | 0.5662 | N/A | Adhesive | |
| | | 800 °C | | | | | | | 0.5048 | 4.85 × $10^{-6}$ $mm^3/(N·m)$ | Oxidative | |

COF: Coefficient of friction; RT: room temperature; h-BN: hexagonal boron nitride; WC: tungsten carbide.

is governed mainly by a graphene-dominated low-shear mechanism at room temperature but shifts toward an oxide-dominated protective mechanism at high temperature. This transition reflects an intrinsic trade-off between shear accommodation and chemical stability in layered lubricants and indicates that lubrication in such systems is controlled by the temperature-dependent evolution of tribofilm chemistry and architecture.

Similar synergistic behavior has been reported for $MoS_2$-containing systems. Qu *et al.*[163] observed that when $MoS_2$ content exceeded 6 wt.%, sliding-induced reactions generated a dense $TiS_2$ surface layer, which facilitated the formation of a stable oxide film. The $TiS_2$ layer reduced friction, while the oxide layer provided structural protection, cumulatively suppressing micro-cutting and reducing wear loss. This result further suggests that the lubricating function of layered phases is often coupled with interfacial reaction products rather than being solely determined by the original lubricant phase.

Despite their effectiveness at moderate temperatures, layered materials exhibit limited thermal and chemical stability. Graphite and $MoS_2$ are susceptible to oxidation or decomposition in oxygen-rich environments at elevated temperatures, leading to diminished lubrication performance. Consistent with this limitation, Zhang *et al.*[165] reported higher COF and wear rates at elevated temperatures than at RT, indicating that the long-term effectiveness of layered lubricants depends not only on their low-shear crystal structure but also on the stability and continuity of the tribofilm formed under service conditions.

**Table 7. Summary of tribological properties of laser-cladded MAX-phase-based self-lubricating coatings on Ti alloy substrates**

| Substrate | Self-lubricating components | Experimental environment | Coating material | Tribological results of substrates | | | | Tribological results of coatings | | | | Ref. |
|---|---|---|---|---|---|---|---|---|---|---|---|---|
| | | | | Microhardness | COF | Wear losses | Mechanism | Microhardness | COF | Wear losses | Mechanism | |
| Ti6Al4V | $Ti_3SiC_2$ | RT | Co | 370 $HV_{0.5}$ | 0.477 | 16.035 × $10^{-6}$ $mm^3/(N·m)$ | Plastic deformation | 818 $HV_{0.5}$ | 0.471 | 4.133 × $10^{-6}$ $mm^3/(N·m)$ | Abrasive Oxidative | [170] |
| | | | Co-$Ti_3SiC_2$ | | | | | 907 $HV_{0.5}$ | 0.525 | 2.903 × $10^{-6}$ $mm^3/(N·m)$ | | |
| | | | Co-$Ti_3SiC_2$-Cu | | | | | 787 $HV_{0.5}$ | 0.146 | 0.176 × $10^{-6}$ $mm^3/(N·m)$ | | |
| | | 600 °C | | N/A | N/A | 34.114 × $10^{-7}$ $mm^3/(N·m)$ | Plastic deformation Oxidative | N/A | N/A | 5.612 × $10^{-7}$ $mm^3/(N·m)$ | Adhesive Oxidative | |
| | | | | | | | | | | 3.092 × $10^{-7}$ $mm^3/(N·m)$ | | |
| | | | | | | | | | | 3.802 × $10^{-7}$ $mm^3/(N·m)$ | | |
| Ti6Al4V | $Ti_3SiC_2$ | RT | Ni60 + 5 wt.% $Ti_3SiC_2$ | | 0.51 | 35.96 × $10^{-5}$ $mm^3/(N·m)$ | Plastic deformation Adhesive Abrasive | 1,101 $HV_{0.5}$ | 0.39 | 3.07 × $10^{-5}$ $mm^3/(N·m)$ | Plastic deformation Abrasive | [171] |
| | | | Ni60 + 10 wt.% $Ti_3SiC_2$ | | | | | 1,037 $HV_{0.5}$ | 0.41 | 1.45 × $10^{-5}$ $mm^3/(N·m)$ | | |
| | | | Ni60 + 15 wt.% $Ti_3SiC_2$ | | | | | 907 $HV_{0.5}$ | 0.42 | 1.26 × $10^{-5}$ $mm^3/(N·m)$ | | |
| | | 300 °C | | 350 $HV_{0.5}$ | 0.49 | 25.99 × $10^{-5}$ $mm^3/(N·m)$ | Plastic deformation Abrasive Oxidative | N/A | 0.35 | 1.47 × $10^{-5}$ $mm^3/(N·m)$ | Plastic deformation Oxidative | |
| | | | | | | | | | 0.45 | 0.96 × $10^{-5}$ $mm^3/(N·m)$ | | |
| | | | | | | | | | 0.46 | 0.84 × $10^{-5}$ $mm^3/(N·m)$ | | |
| | | 600 °C | | | 0.47 | 15.18 × $10^{-5}$ $mm^3/(N·m)$ | Plastic deformation Adhesive Oxidative | N/A | 0.30 | 0.77 × $10^{-5}$ $mm^3/(N·m)$ | Plastic deformation Oxidative | |
| | | | | | | | | | 0.44 | 0.62 × $10^{-5}$ $mm^3/(N·m)$ | Abrasive Oxidative | |
| | | | | | | | | | 0.40 | 0.63 × $10^{-5}$ $mm^3/(N·m)$ | | |
| Ti6Al4V | $Ti_2AlC$ | RT | TC4-TiC | 320 ± 3 $HV_{0.5}$ | N/A | N/A | N/A | 482 ± 4 $HV_{0.5}$ | 0.486 | 2.35 × $10^{-6}$ $mm^3/(N·m)$ | Plastic deformation | [172] |
| | | | TC4-TiC-$Ti_2AlC$ | | | | | 535 ± 3 $HV_{0.5}$ | 0.366 | 1.48 × $10^{-6}$ $mm^3/(N·m)$ | Oxidative | |
| | | 500 °C | | | | | | N/A | 0.270 | 1.83 × $10^{-6}$ $mm^3/(N·m)$ | Oxidative | |
| | | | | | | | | | 0.267 | 0.92 × $10^{-6}$ $mm^3/(N·m)$ | Oxidative | |
| Ti6Al4V | $Ti_2AlC$ | N/A | TC4 | 320 $HV_{0.5}$ | N/A | N/A | Plastic deformation Adhesive Abrasive | 341 $HV_{0.5}$ | 0.486 | 25.46 × $10^{-5}$ $mm^3/(N·m)$ | Abrasive Oxidative | [173] |
| | | | TC4 + 5 wt.% $Ti_2AlC$ | | | | | 372 $HV_{0.5}$ | 0.457 | 22.35 × $10^{-5}$ $mm^3/(N·m)$ | | |
| | | | TC4 + 10 wt.% $Ti_2AlC$ | | | | | 383 $HV_{0.5}$ | 0.382 | 8.87 × $10^{-5}$ $mm^3/(N·m)$ | | |
| | | | TC4 + 15 wt.% $Ti_2AlC$ | | | | | 389 $HV_{0.5}$ | 0.415 | 12.13 × $10^{-5}$ $mm^3/(N·m)$ | | |

COF: Coefficient of friction; MAX: MAX phases, a family of layered ternary carbides and nitrides generally represented by the formula $M_{n+1}AX_n$; RT: room temperature.

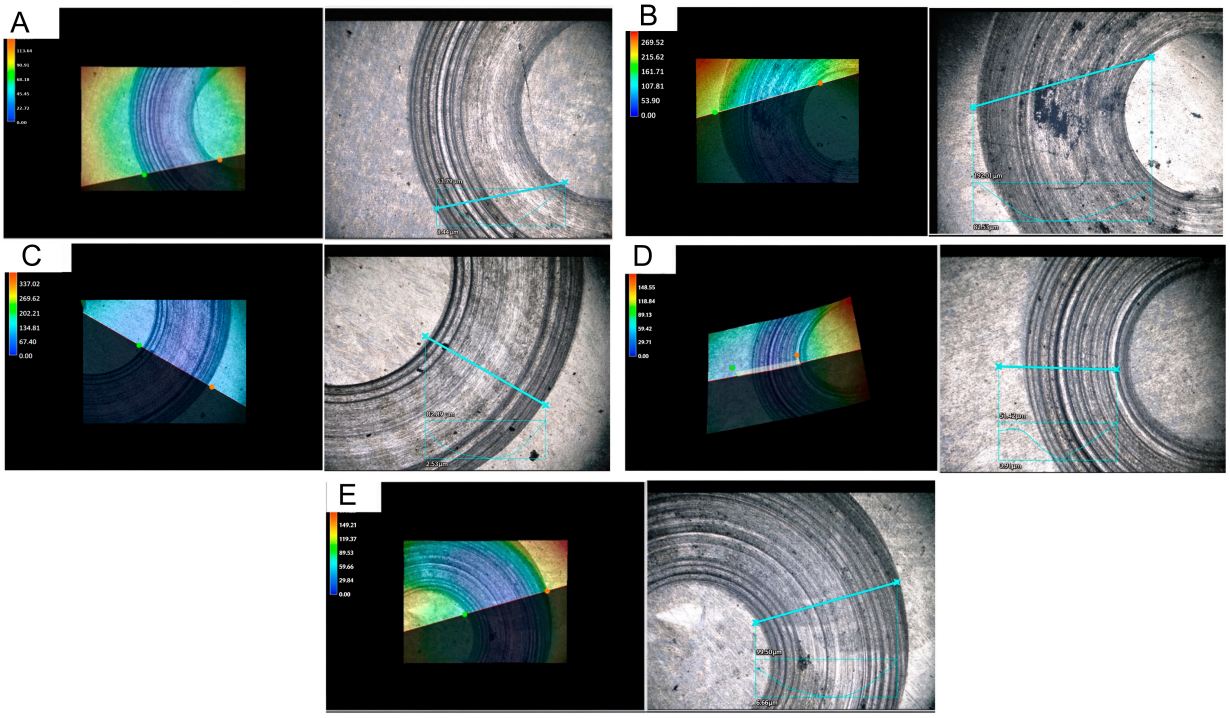



**Figure 9.** Wear-scar morphology and wear volume of TiN/$WS_2$ + h-BN/NiCrBSi self-lubricating coatings with different solid-lubricant compositions. (A-E) Wear-scar morphologies and wear volumes of coatings 1-5 obtained by 3D microscopy, respectively. Coatings 1-5 were prepared with different $WS_2$/h-BN ratios while maintaining NiCrBSi and TiN as the matrix and hard reinforcing phases. This figure is adapted from Ref.[159]. Licensed under CC-BY 4.0. h-BN: Hexagonal boron nitride.

### *Soft metals*

Compared with layered lubricants, soft metals exhibit superior lubrication stability and environmental adaptability at intermediate to high temperatures. Noble metals such as Ag maintain effective friction-reduction capability over a broad temperature range, owing to their high ductility and chemical stability[162,174,175]. In self-lubricating laser-cladded coatings, their function is not to serve as rigid reinforcing phases, but to provide a deformable metallic constituent that can dynamically redistribute to the sliding interface under thermo-mechanical loading. Under frictional heating and contact stress, soft metallic phases undergo plastic flow and interfacial migration. This deformation-driven redistribution allows metal particles to extrude from the coating interior, fill surface microcracks and pores, and progressively form a continuous ductile lubricating film. The resulting metallic transfer layer accommodates interfacial shear and suppresses adhesive wear by reducing direct metal-to-metal contact. This process is therefore governed by the mobility and replenishment of the metallic phase during sliding, rather than by static phase dispersion alone.

Shi *et al.*[162] investigated the tribological behavior of Ag-containing self-lubricating coatings at RT, 300 °C, and 500 °C under loads of 10 and 30 N. At higher load levels, frictional heating and contact stress significantly increased, accelerating silver diffusion and surface accumulation. As sliding proceeded, Ag progressively precipitated and spread across the worn surface, forming a stable lubricating transfer film that effectively reduced interfacial shear stress.

The beneficial effect of Ag thus arises from a sliding-induced redistribution process, in which subsurface soft-metal reservoirs continuously feed the contact interface and sustain local shear accommodation.

At elevated temperatures, matrix softening further promoted ductile deformation and enhanced the formation of stable friction-induced oxides. The synergistic interaction between the ductile Ag transfer film

and the protective oxide layers improved wear resistance under high-load, high-temperature conditions. In this type of system, lubrication stability depends on whether the metallic phase can maintain sufficient interfacial coverage while remaining mechanically supported by the surrounding wear-resistant matrix. Once the supply or retention of the metallic transfer layer becomes inadequate, friction reduction and anti-wear protection deteriorate simultaneously.

### *Alkaline earth fluorides*

The lubrication and anti-wear performance of alkaline-earth fluorides such as $CaF_2$ and $BaF_2$ is primarily governed by their temperature-dependent softening behavior[174]. As temperature increases, their shear strength decreases markedly, enabling plastic deformation and interfacial spreading under frictional stress. In intermediate to high-temperature environments, these materials become activated at the sliding interface and progressively form a continuous lubricating film. This film accommodates interfacial shear, suppresses adhesive wear, and mitigates severe oxidative damage.

Alkaline-earth fluorides possess high melting points, strong chemical stability, and excellent oxidation resistance, allowing stable lubrication within a typical service temperature range of 400 to 800 °C. These characteristics make them particularly suitable for high-temperature applications where layered lubricants may degrade. Xiang *et al.*[167] fabricated $CaF_2$-containing wear-resistant composite coatings on TC4 substrates and evaluated their tribological behavior at different temperatures. They reported that $CaF_2$ undergoes a brittle-to-ductile transition above 400 °C, forming a ductile phase with low shear strength. Under elevated temperature and sustained contact stress, $CaF_2$ is readily sheared and spreads across the interface, forming a stable transfer film. This layer effectively separates the coating from the counterface, replacing direct contact with sliding along a lubricating film. As a result, interfacial shear stress was significantly reduced, and the coating exhibited its lowest COF at 600 °C, which highlights the importance of temperature-activated film formation in determining the lubrication behavior of fluoride-containing systems.

### *Composite lubricant*

Although single solid lubricants, such as layered materials, soft metals, and alkaline-earth fluorides, can effectively reduce friction and wear under specific service conditions, each class has inherent limitations. Layered materials are susceptible to oxidation and degradation at elevated temperatures; soft metals possess limited load-bearing capacity under high contact stresses; and alkaline-earth fluorides provide insufficient lubrication at low temperatures. These constraints restrict the operational temperature range and mechanical adaptability of single-phase lubricating systems.

To overcome these limitations, composite self-lubricating coatings have been developed by synergistically incorporating multiple lubricating phases into laser-cladded Ti alloy coatings. Such multi-phase designs enable continuous lubrication across low, intermediate, and high temperature regimes while maintaining sufficient load-bearing capacity and structural stability. Furthermore, these coatings rely on microstructural coupling between lubricating constituents and supporting phases, enabling reduced interfacial shear without sacrificing the integrity of the load-bearing framework. The integration of lubricating and hard-reinforcing phases enables simultaneous friction reduction and enhanced wear resistance.

For example, Qu *et al.*[169] fabricated Ni-based Ag/$MoS_2$ self-lubricating composite coatings on Ti6Al4V substrates. The coating microstructure consisted of a $Ti_2Ni$/TiNi matrix reinforced by TiC and $TiB_2$ phases, together with *in situ*-generated $Ti_2SC$ lubricating constituents. At elevated temperatures of 600 to 800 °C, synergistic interactions among Ag, $MoS_2$, and tribochemical products such as $MoO_3$ and silver molybdates promoted the formation of a dense and stable lubricating film. This composite tribofilm substantially

lowered friction and reduced wear, with the high-temperature wear rate decreasing by nearly one order of magnitude compared with that at RT.

Moreover, Kumar *et al.*[176] prepared Cu/$MoS_2$ composite self-lubricating coatings via laser cladding. The resulting multi-phase microstructure exhibited hardness values two to three times that of the substrate while maintaining stable load-bearing capability. During sliding, $MoS_2$ and Cu phases reduced interfacial shear resistance, decreasing the COF from approximately 0.5 for the substrate to 0.33 for the coating. The synergistic interaction between lubricating phases and hard reinforcements effectively suppressed micro-cutting and micro-plowing, thereby improving wear resistance under low-to-medium loads. Here, the beneficial effect arises from phase complementarity: the hard matrix constrains plastic damage, whereas the lubricating phases continuously regulate interfacial shear by forming films and accommodating localized shear.

In summary, self-lubricating coatings on Ti alloys are typically characterized by a dual-functional architecture in which solid lubricating phases are incorporated into a wear-resistant matrix. Depending on the lubricant type, such phases may be introduced as layered materials, soft metals, alkaline-earth fluorides, or multi-lubricant composite systems. Their tribological advantage mainly arises from the synergistic interaction between matrix-supported load bearing and the formation of low-shear transfer films or tribofilms during sliding, which can reduce friction, suppress adhesive wear, and stabilize the contact interface over a range of service temperatures. However, the effectiveness of these systems strongly depends on the thermal and chemical stability, spatial distribution, and release behavior of the lubricating phases. In particular, layered lubricants are vulnerable to oxidation or decomposition at elevated temperatures, soft metals may suffer from limited load-bearing capability, and fluorides often exhibit insufficient lubrication at low temperatures. Although composite lubricant designs can broaden the service window, excessive lubricant addition or poor phase compatibility may still reduce hardness, weaken structural integrity, or impair long-term lubrication stability.

### MAX phase ceramic self-lubricating coatings

Beyond conventional self-lubricating systems based on externally introduced lubricant phases, a further developmental trend in Ti alloy surface engineering involves shifting toward coatings that intrinsically combine wear resistance with self-lubricating capability. This strategy promotes the design of synergistic composite coatings that combine rigid ceramic frameworks with solid lubricating constituents. Within such architectures, hard ceramic phases provide structural load-bearing support, while high-temperature-resistant lubricants such as $MoS_2$, $WS_2$, h-BN, or $CaF_2$ regulate interfacial shear. The ultimate objective is to construct surfaces capable of resisting abrasive wear while adaptively forming lubricating films during sliding.

In this context, MAX phases represent a unique class of nanolaminated ceramics that intrinsically integrate hardness and lubricity. These materials follow the general formula $M_{n+1}AX_n$, where M is an early transition metal, A is a group A element, and X represents carbon or nitrogen [see Figure 10][177,178]. Their crystal structure consists of alternating M-X octahedral layers and A-element atomic layers stacked along the c-axis. Strong M-X covalent bonds confer high hardness and load-bearing capability, whereas weaker metallic M-A bonds enable interlayer shear. This layered architecture allows MAX phases to act simultaneously as structural reinforcements and internal lubricating planes, helping adaptive transfer films form during sliding without requiring external lubricants[177,179]. As a result, MAX phases offer a rare combination of mechanical robustness and frictional adaptability[180]. Unlike conventional lubricant-containing coatings, whose lubricating function is directly rooted in their crystallographic architecture, these coatings are particularly relevant to a microstructure-centered interpretation of self-lubricating behavior.

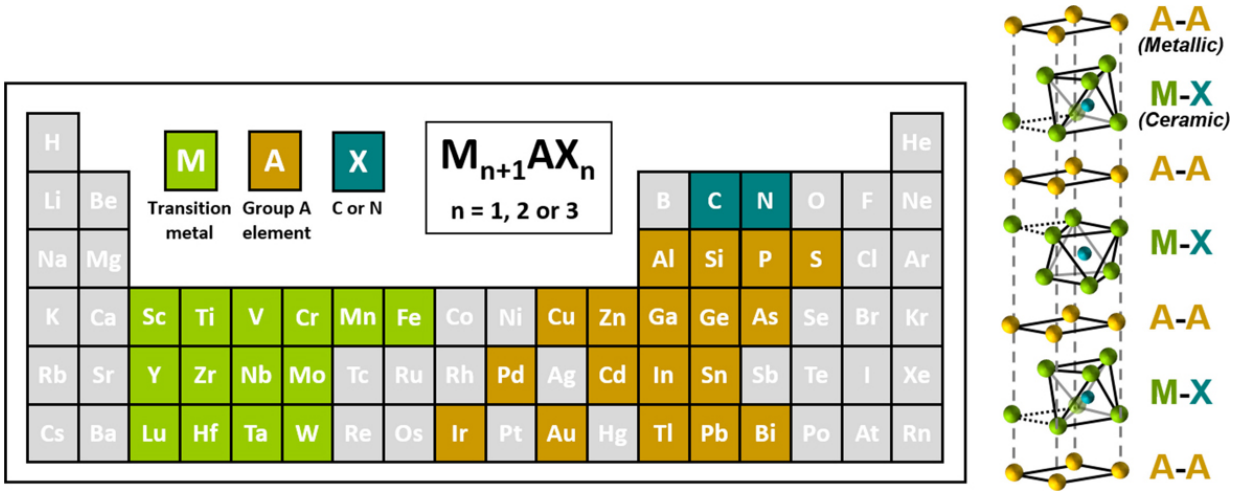



**Figure 10.** Elements of the Periodic Table found in MAX phases and unit cell for $n$ = 1. This figure is adapted from Ref.[177]. Licensed under CC-BY 4.0. MAX: MAX phases, a family of layered ternary carbides and nitrides generally represented by the formula $M_{n+1}AX_n$.

Among them, $Ti_3SiC_2$ and $Ti_2AlC$ are the most extensively investigated for Ti alloy coatings. $Ti_3SiC_2$ exhibits dual metallic-ceramic characteristics. Its weakly bonded Si layers readily undergo shear and selective delamination, forming graphite-like lubricating films with low shear strength. In laser-cladded coatings, $Ti_3SiC_2$ participates in load sharing while simultaneously reducing friction through self-adaptive delamination[181]. It maintains relatively stable tribological performance from RT to 600 °C[171]. Wang *et al.*[171] demonstrated that $Ti_3SiC_2$-containing Ni60-based coatings exhibited significantly improved tribological behavior across this temperature range, as the lamellar structure reduced shear stress while hard phases inhibited plastic deformation. The key advantage of $Ti_3SiC_2$, therefore, lies in the coexistence of a load-bearing ceramic framework and a shear-accommodating lamellar substructure within the same phase architecture.

$Ti_2AlC$ also possesses a layered structure but relies on Al-layer plasticity and oxidation for lubrication. During sliding, Al layers migrate or oxidize, promoting the formation of Al-O-rich transfer films with low shear strength[172,182]. Compared with $Ti_3SiC_2$, $Ti_2AlC$ has a lower density and superior thermal shock resistance, making it attractive for lightweight high-temperature applications. Hua *et al.*[173] showed that laser-cladded TC4-$Ti_2AlC$ composites exhibited improved wear resistance through the formation of continuous $Ti_2AlC$-derived transfer films at the sliding interface. However, $Ti_2AlC$ generally provides weaker lubrication than $Ti_3SiC_2$ due to stronger interlayer bonding, and Al loss during cladding may reduce phase stability[172]. It is therefore often used as an auxiliary lubricating phase in combination with other soft metals or high-temperature lubricants. This indicates that the tribological role of $Ti_2AlC$ is strongly dependent on phase stability during cladding and on the retention of its layered structural characteristics during service.

The *in situ* formation of MAX phases further enhances their structural integration. Chu *et al.*[178] revealed that $Ti_2AlC$ formation occurs through both direct precipitation from Ti-Al-C melts and interfacial transformation of TiC via Al diffusion. Moderate Al additions improved melt fluidity and promoted uniform MAX phase distribution. Similarly, Sun *et al.*[182] demonstrated that coatings with optimized MAX phase fractions exhibited balanced phase distribution and enhanced wear resistance at both RT and 400 °C. These findings indicate that an optimal MAX phase fraction is critical because its effectiveness depends on the retention and distribution of the lamellar structure within the coating. At appropriate fractions, MAX phases can simultaneously contribute to load support and shear accommodation through their layered architecture, enabling a balance between strengthening and adaptive lubrication. However, when the phase fraction

deviates from this optimal range, either due to insufficient presence or structural degradation, the coordinated load-sharing and shear-relief mechanisms are disrupted, leading to diminished tribological performance.

Overall, MAX-phase-based self-lubricating coatings are typically characterized by a laminated ceramic architecture that intrinsically combines load-bearing capability with interlayer shear accommodation. Their tribological benefit mainly arises from the coexistence of structural reinforcement and adaptive lubrication, enabling transfer-film formation while preserving mechanical support. However, their effectiveness still depends on phase stability during cladding, the retention of lamellar structural features, and the control of MAX phase fraction and distribution within the coating. These characteristics make MAX phases an important bridge between conventional lubricant-containing coatings and more intrinsically coupled multifunctional surface systems.

Conventional wear-resistant coatings predominantly rely on hardness enhancement to mitigate material removal. However, under severe operating conditions involving high contact stress, elevated temperature, or dry sliding, excessive frictional heating and stress concentration can undermine structural stability and accelerate failure. The synergistic coating systems discussed above address these limitations by integrating structural reinforcement with active friction regulation. By integrating load-bearing frameworks and lubricating phases, these coatings simultaneously suppress abrasive and adhesive wear, thereby extending the applicability of laser cladding technology to complex service environments characterized by high sliding speeds and unlubricated contact.

Building upon this concept of multifunctional synergy, HEA coatings represent a further evolution in surface engineering strategies. By leveraging multi-principal-element alloying and tunable phase stability, these systems offer expanded opportunities for *in situ* phase regulation, structural adaptability, and potentially intrinsic friction modulation. Consequently, they provide a promising pathway toward next-generation multifunctional coatings that can sustain performance under increasingly demanding service conditions.

## EMERGING MULTI-PRINCIPAL ELEMENT COATINGS: HEA SYSTEMS

In high-temperature tribological applications, surface coatings must not only provide high hardness but also maintain structural stability and wear resistance under coupled thermal-mechanical conditions. Conventional precipitation-strengthened alloys, including Ni-based superalloys, have long served as benchmark materials for elevated-temperature strength and oxidation resistance[183-187]. Their performance is primarily governed by γ/γ'-type precipitate architectures, which ensure creep resistance under static or quasi-static conditions[188]. However, under sliding contact, frictional heating and cyclic shear can accelerate precipitate coarsening, localized softening, and oxidation-spallation processes near the surface, often leading to unstable adhesive wear and friction fluctuations at elevated temperatures[189-191]. This limitation highlights the difficulty of maintaining precipitation-controlled strengthening under tribological conditions, where repeated surface deformation, oxidation, and thermal cycling continuously disturb near-surface microstructural stability.

In contrast, HEA coatings provide exceptional compositional flexibility and an expanded solid-solution stability domain. Unlike precipitation-dependent systems, HEAs are fundamentally engineered materials for microstructure and phase stability. Their multi-principal-element design enables tunable phase constitution and microstructural evolution under laser-cladding conditions[192,193]. Lattice distortion and sluggish diffusion effects inherent to HEAs suppress grain coarsening and phase instability, contributing to dense microstructures and enhanced structural stability under cyclic frictional loading and thermal exposure[194-196].

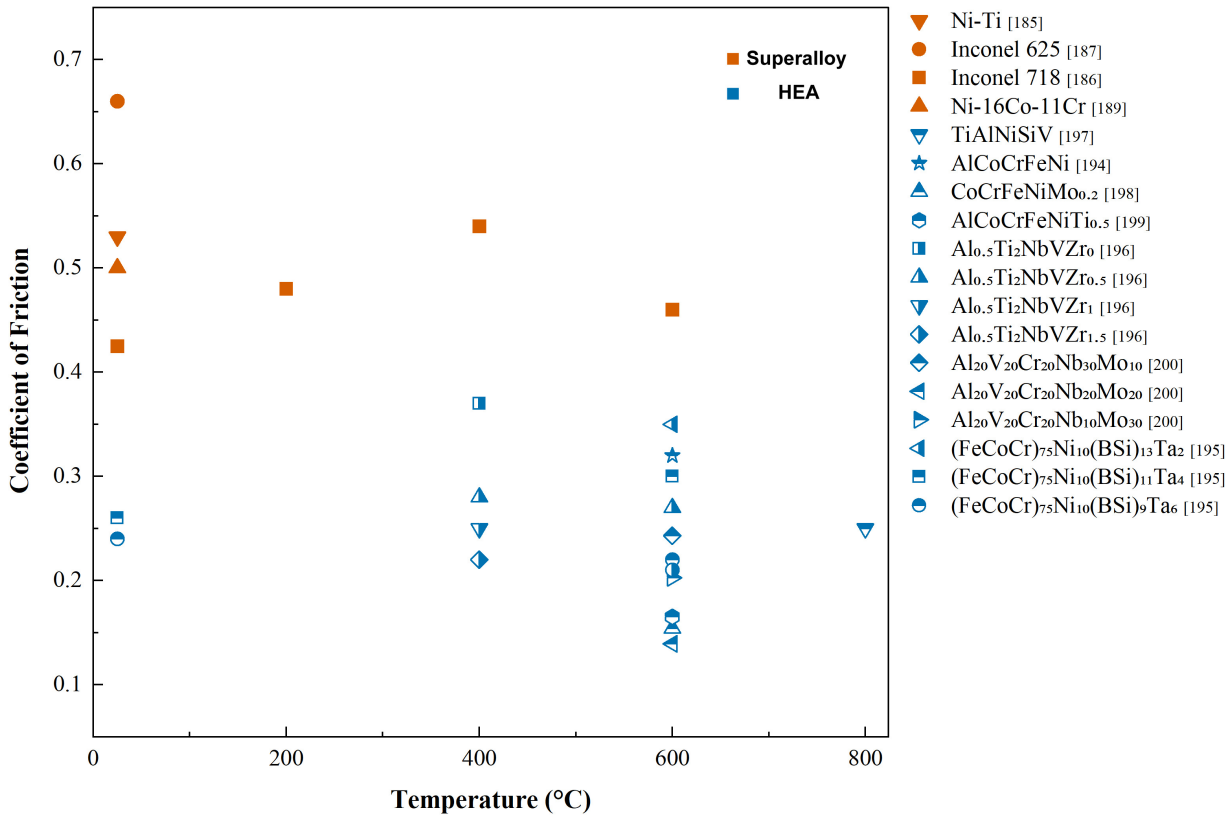



**Figure 11.** Comparison of high-temperature COF between conventional superalloys and representative laser-cladded HEA/RHEA coatings[185-187,189,194-200]. COF: Coefficient of friction; HEA: high-entropy alloy; RHEA: refractory high-entropy alloy.

Also, rapid solidification during laser cladding allows HEAs to access non-equilibrium phase combinations and hierarchical microstructures that are difficult to achieve in conventional alloy systems. As illustrated in Figure 11, representative laser-cladded HEA and Refractory high-entropy alloy (RHEA) coatings generally exhibit lower, more stable COF at intermediate-to-high temperatures compared with those of conventional superalloys, particularly around 600 °C. This behavior reflects improved high-temperature wear stability and suggests a transition in dominant wear mechanisms from severe adhesive tearing toward oxidation-assisted mild wear regimes, facilitated by the formation of dense Cr- or Al-rich tribofilms.

During rapid solidification processes such as laser cladding, HEAs exhibit diverse microstructural configurations, with phase constitution and secondary-phase formation playing decisive roles in mechanical and tribological performance. For surface modification of Ti alloys, several representative design paradigms have emerged. A primary strategy involves high-strength systems based on body-centered cubic (BCC) solid-solution matrices strengthened by intermetallic compounds such as Laves phases. RHEAs have been further developed to enhance high-temperature phase stability, hardness retention, and oxidation resistance. In addition, multifunctional approaches incorporate hard ceramic phases, stable oxides, or lubricating constituents into HEA matrices to achieve synergistic reinforcement and tribochemical regulation. These design routes are distinguished not simply by composition, but by how laser-cladding-induced solidification, segregation behavior, and phase selection are used to construct different load-bearing and damage-tolerant microstructures.

Overall, these strategies form a hierarchical material design framework capable of addressing diverse service requirements across different temperature and load regimes. More specifically, they represent distinct microstructural design pathways for controlling phase stability, deformation accommodation, oxidation

behavior, and wear degradation in laser-cladded Ti-alloy coatings. The following sections systematically examine the microstructural characteristics, phase stability, friction and wear mechanisms, and application potential of these HEA-based design routes.

The tribological performance of representative laser-cladded HEA coatings and HEA-based composite coatings on Ti alloy substrates is summarized in Tables 8 and 9. Overall, HEA coatings provide substantial improvements in hardness and wear resistance, whereas HEA-based composite coatings further extend this advantage through multifunctional coupling of reinforcement, interfacial regulation, and lubrication-related effects. These data also indicate that superior tribological performance is governed not only by hardness, but also by phase architecture, interface integrity, and crack resistance.

## Phase-structure-dominated HEA coatings

### *BCC-dominated high-strength HEA coatings*

BCC solid-solution-dominated HEA coatings constitute one of the most widely adopted systems for Ti alloy surface modification. Their microstructures are primarily composed of a BCC multi-principal-element solid solution, with secondary phases present only in limited or finely dispersed fractions. These alloys are typically enriched in BCC-stabilizing elements such as Al, Ti, Cr, V, Fe, and Mo. Under the rapid solidification conditions of laser cladding, these elements form chemically homogeneous BCC solid solutions characterized by pronounced lattice distortion. Furthermore, dilution from the Ti substrate can further stabilize the BCC phase, which is favorable for phase continuity across the coating/substrate region and for maintaining metallurgical compatibility during processing.

The improvement in wear resistance of this system originates mainly from the intrinsic strengthening mechanisms of the BCC solid solution. Severe atomic size mismatch and chemical disorder generate strong lattice distortion, increasing resistance to dislocation motion and enhancing solid-solution hardening. Simultaneously, the relatively high elastic modulus and lattice friction stress of BCC structures suppress matrix plastic flow under sliding contact. Consequently, near-surface deformation is more effectively constrained, and the coating is less prone to deep plowing grooves or large-scale material displacement during sliding. As a result, coatings exhibit enhanced load-bearing capacity, which mitigates plowing groove formation and promotes a transition in dominant wear mechanisms from severe abrasive wear toward mild abrasive or oxidation-assisted wear.

For example, Ren *et al.*[201] prepared an NbMoTaWTi HEA coating on TC4 via laser cladding. The coating exhibited a single-phase BCC structure with a microhardness of approximately 600 HV. The wear rate was reduced to $1.37 \times 10^{-4}$ $mm^3/(N \cdot m)$, and the worn surface became smoother than the substrate, indicating a shift from severe abrasive wear to a mixed oxidation and adhesive wear mechanism. Here, the smoother worn morphology is consistent with a reduced tendency toward localized plastic collapse, characteristic of a structurally stable BCC matrix under tribological loading.

At the microstructural level, the merit of BCC-dominated HEAs lies in their ability to retain a relatively simple phase constitution while still providing substantial hardness through lattice distortion and solid-solution stabilization. From a broader performance perspective, BCC-dominated HEA coatings typically increase substrate hardness from approximately 300-350 HV to 500-700 HV or higher, while reducing wear rates by one to two orders of magnitude[198,202,203]. Although their COF are not necessarily minimal, these coatings maintain stable tribological behavior under medium-to-high loads and exhibit superior resistance to micro-cutting and plowing compared with uncoated Ti alloys. Liu *et al.*[207] reported that lightweight $(Ti_{50}Nb_{15}V_{15}Zr_5Cr_5)100_{-x}Al_x$ coatings dominated by a BCC solid solution increased hardness from 431 HV to 538 HV and reduced wear rate by approximately 45% relative to the substrate.

**Table 8. Summary of tribological properties of laser-cladded HEA coatings on Ti alloy substrates**

| Substrate | HEAs | Main phases | Tribological results of substrate | | | | Tribological results of coatings | | | | Ref. |
|---|---|---|---|---|---|---|---|---|---|---|---|
| | | | Microhardness | COF | Wear losses | Mechanism | Microhardness | COF | Wear losses | Mechanism | |
| Ti6Al4V | $AlCoCrFeNiTi_{0.5}$ | FCC, BCC | 304 HV | 0.3995 | 0.6311 $mm^3$ | Abrasive Oxidative | 706 HV | 0.1653 | 0.0497 $mm^3$ | Adhesive Oxidative | [199] |
| Ti6Al4V | NbMoTaWTi | BCC | 350 HV | ~0.7 | $3.04 \times 10^{-4}$ $mm^3/(N·m)$ | Abrasive Adhesive | 600 HV | ~0.45 | $1.37 \times 10^{-4}$ $mm^3/(N·m)$ | Adhesive Oxidative | [201] |
| Ti6Al4V | $CoCrFeNiMo_{0.2}$ | BCC, σ | N/A | 0.578 | $1.54 \times 10^{-3}$ $mm^3/(N·m)$ (RT) | Abrasive Adhesive | N/A | 0.442 | $1.33 \times 10^{-3}$ $mm^3/(N·m)$(RT) | Abrasive | [198] |
| | | | | 0.17 | $5.83 \times 10^{-4}$ $mm^3/(N·m)$ (600 °C) | Abrasive Oxidative | | 0.154 | $2.08 \times 10^{-4}$ $mm^3/(N·m)$ (600 °C) | Abrasive Oxidative | |
| Ti6Al4V | TiZrNbCrCo | BCC, Laves | 318 $HV_{0.1}$ | ~0.3 | ~0.8 $mm^3$ | Abrasive Oxidative | 748 $HV_{0.1}$ | ~0.45 | ~0.2 $mm^3$ | Abrasive Oxidative | [202] |
| Ti6Al4V | TiAlNiSiV | BCC(NiAl), $(Ti,V)_5Si_3$, TiN | 340 HV | 0.37 | 10.25 $mm^3$ | Abrasive Adhesive | 1,151~1,357 HV | 0.45 | ~2.5 $mm^3$ | Abrasive | [197] |
| Ti6Al4V | AlTiVCrNb | BCC, Laves, $Ti_2AlNb$ | 349 $HV_{0.1}$ | 0.58 | $2.74 \times 10^7$ $\mu m^3$ | Abrasive Adhesive Oxidative | 549 $HV_{0.1}$ | 0.69 | $1.74 \times 10^7$ $\mu m^3$ | Adhesive Oxidative | [203] |
| Ti6Al4V | WMoTaNbV | BCC, Ti-rich | 341 $HV_{0.3}$ | 0.58 | $6.09 \times 10^7$ $\mu m^3$ | Abrasive Adhesive Oxidative | 671 $HV_{0.3}$ | 0.42 | $1.75 \times 10^7$ $\mu m^3$ | Abrasive Adhesive Oxidative | [204] |
| Pure Ti | $CoCrFeNiNb_x$, x = 0 | BCC, Laves ($Cr_2Ti$, $Cr_2Nb$) | 122 HV | N/A | N/A | N/A | 790 HV | N/A | N/A | N/A | [205] |
| | $CoCrFeNiNb_x$, x = 1 | | | | | | 1,008 HV | | | | |
| Ti6Al4V | $AlNbTiVB_x$, x = 0.05 | BCC, $TiB_2$ | 363 HV | 0.49 | $2.52 \times 10^7$ $\mu m^3$ | Abrasive Adhesive Oxidative | 435 HV | 0.65 | $1.91 \times 10^7$ $\mu m^3$ | Abrasive Adhesive Oxidative | [206] |
| | $AlNbTiVB_x$, x = 0.10 | | | | | | 457 HV | 0.67 | $1.81 \times 10^7$ $\mu m^3$ | | |
| | $AlNbTiVB_x$, x = 0.15 | | | | | | 487 HV | 0.65 | $1.77 \times 10^7$ $\mu m^3$ | | |
| Ti6Al4V | $(Ti_{50}Nb_{15}V_{15}Zr_5Cr_5)_{100-x}Al_x$, x = 10 | BCC | 342 $HV_{0.2}$ | 0.35 | $8.78 \times 10^{-4}$ $mm^3/(N·m)$ | Abrasive | 431 $HV_{0.2}$ | 0.60 | $7.33 \times 10^{-4}$ $mm^3/(N·m)$ | Fatigue Oxidative | [207] |
| | $(Ti_{50}Nb_{15}V_{15}Zr_5Cr_5)_{100-x}Al_x$, x = 15 | | | | | | 484 $HV_{0.2}$ | 0.56 | $6.20 \times 10^{-4}$ $mm^3/(N·m)$ | | |
| | $(Ti_{50}Nb_{15}V_{15}Zr_5Cr_5)_{100-x}Al_x$, x = 20 | | | | | | 515 $HV_{0.2}$ | 0.55 | $5.71 \times 10^{-4}$ $mm^3/(N·m)$ | | |
| | $(Ti_{50}Nb_{15}V_{15}Zr_5Cr_5)_{100-x}Al_x$, x = 25 | | | | | | 538 $HV_{0.2}$ | 0.51 | $4.83 \times 10^{-4}$ $mm^3/(N·m)$ | | |

| | | | | | | | | | | | |
|---|---|---|---|---|---|---|---|---|---|---|---|
| Ti6Al4V | $(AlCrFeTiV)_{100-x}Ni_x$, x = 0 | BCC, Laves | 361 $HV_{0.3}$ | 0.35 | 3.45 × $10^{-4}$ $mm^3/(N·m)$ | Abrasive Oxidative | 759 $HV_{0.3}$ | 0.64 | 2.89 × $10^{-4}$ $mm^3/(N·m)$ | Adhesive Oxidative | [208] |
| | $(AlCrFeTiV)_{100-x}Ni_x$, x = 10 | | | | | | 835 $HV_{0.3}$ | 0.63 | 1.84 × $10^{-4}$ $mm^3/(N·m)$ | | |
| | $(AlCrFeTiV)_{100-x}Ni_x$, x = 20 | | | | | | 879 $HV_{0.3}$ | 0.71 | 1.25 × $10^{-4}$ $mm^3/(N·m)$ | | |
| | $(AlCrFeTiV)_{100-x}Ni_x$, x = 30 | | | | | | 798 $HV_{0.3}$ | 0.44 | 0.44 × $10^{-4}$ $mm^3/(N·m)$ | Abrasive Adhesive Oxidative | |
| TC6 | $FeCrCoNiAlTi_x$, x = 0 | FCC, BCC, B2 | 380 $HV_{0.1}$ | ~0.82 | 12.1 μm | Abrasive Adhesive Oxidative | ~600 $HV_{0.1}$ | ~0.63 | 6.0 μm | Abrasive Adhesive Oxidative | [209] |
| | $FeCrCoNiAlTi_x$, x = 0.3 | | | | | | ~650 $HV_{0.1}$ | ~0.57 | 5.1 μm | | |
| | $FeCrCoNiAlTi_x$, x = 0.5 | | | | | | ~730 $HV_{0.1}$ | ~0.46 | 4.0 μm | | |
| | $FeCrCoNiAlTi_x$, x = 0.8 | | | | | | ~770 $HV_{0.1}$ | ~0.41 | 2.2 μm | | |
| | $FeCrCoNiAlTi_x$, x = 1.0 | | | | | | 848 $HV_{0.1}$ | ~0.51 | 4.8 μm | | |
| Ti6Al4V | $(TiZrNbCu)_{1-x}Ni_x$, x = 0 | FCC, BCC, $Cu_{10}Zr_7$ | ~360 $HV_{0.2}$ | 0.58 | 4.3 × $10^{-4}$ $mm^3/(N·m)$ | Abrasive Adhesive | 576 $HV_{0.2}$ | 0.45 | 1.7 × $10^{-4}$ $mm^3/(N·m)$ | Abrasive Adhesive | [210] |
| | $(TiZrNbCu)_{1-x}Ni_x$, x = 0.15 | | | | | | 625$HV_{0.2}$ | 0.22 | 0.52 × $10^{-4}$ $mm^3/(N·m)$ | | |
| | $(TiZrNbCu)_{1-x}Ni_x$, x = 0.25 | | | | | | 673 $HV_{0.2}$ | 0.25 | 1.4 × $10^{-4}$ $mm^3/(N·m)$ | | |
| | $(TiZrNbCu)_{1-x}Ni_x$, x = 0.35 | | | | | | 719 $HV_{0.2}$ | 0.42 | 2.0 × $10^{-4}$ $mm^3/(N·m)$ | | |
| Ti6Al4V | $Al_{20}V_{20}Cr_{20}Nb_{40-x}Mo_x$, x = 10 | BCC | N/A | 0.1692 | 107.2 × $10^{-6}$ $mm^3/(N·m)$ | Fatigue Adhesive | N/A | 0.2431 | 246.7 × $10^{-6}$ $mm^3/(N·m)$ | Oxidative | [200] |
| | $Al_{20}V_{20}Cr_{20}Nb_{40-x}Mo_x$, x = 20 | | | | | | | 0.1393 | 3.574 × $10^{-6}$ $mm^3/(N·m)$ | | |
| | $Al_{20}V_{20}Cr_{20}Nb_{40-x}Mo_x$, x = 30 | | | | | | | 0.2026 | 1.769 × $10^{-6}$ $mm^3/(N·m)$ | | |
| Ti6Al4V | $TiZrHfNbTaMo_x$, x = 0 | HCP, BCC | 353 HV | 1.22 | N/A | Abrasive Adhesive Oxidative | 553 HV | 1.13 | N/A | Abrasive Adhesive Oxidative | [211] |
| | $TiZrHfNbTaMo_x$, x = 0.25 | | | | | | 600 HV | 1.04 | | | |
| | $TiZrHfNbTaMo_x$, x = 0.5 | | | | | | 656 HV | 0.97 | | | |
| | $TiZrHfNbTaMo_x$, x = 0.75 | | | | | | 718 HV | 0.78 | | | |
| | $TiZrHfNbTaMo_x$, x = 1 | | | | | | 755 HV | 0.89 | | | |
| Ti6Al4V | $AlNbTaZr_x$, x = 0.2 | HCP, BCC | 330 $HV_{0.5}$ | N/A | 2.41 × $10^{-4}$ $mm^3/(N·m)$ | N/A | 561 $HV_{0.5}$ | ~0.82 | 2.06 × $10^{-4}$ $mm^3/(N·m)$ | Microcutting | [212] |
| | $AlNbTaZr_x$, x = 0.4 | | | | | | 596 $HV_{0.5}$ | | 1.85 × $10^{-4}$ $mm^3/(N·m)$ | | |
| | $AlNbTaZr_x$, x = 0.6 | | | | | | 611 $HV_{0.5}$ | | 1.62 × $10^{-4}$ $mm^3/(N·m)$ | Microcutting Oxidative | |
| | $AlNbTaZr_x$, x = 0.8 | | | | | | 624 $HV_{0.5}$ | ~0.72 | 1.16 × $10^{-4}$ $mm^3/(N·m)$ | | |
| | $AlNbTaZr_x$, x = 1.0 | | | | | | 654 $HV_{0.5}$ | | 1.60 × $10^{-4}$ $mm^3/(N·m)$ | Microcutting Oxidative Brittle debonding | |

HCP: Hexagonal close-packed; COF: coefficient of friction; HEA: high-entropy alloy; FCC: face-centered cubic; BCC: body-centered cubic.

**Table 9. Tribological properties of laser-cladded HEA-based composite coatings on Ti alloy substrates**

| Substrate | HEAs | Coating material | Main phases | Tribological results of substrate | | | | Tribological results of coatings | | | | Ref. |
|---|---|---|---|---|---|---|---|---|---|---|---|---|
| | | | | Microhardness | COF | Wear losses | Mechanism | Microhardness | COF | Wear losses | Mechanism | |
| Ti6Al4V | $FeNiCrTi_{0.3}Al_{0.3}$ | 0 wt.% $B_4C$ + 0 wt.% $LaB_6$ | BCC, $Ti_2Ni$ TiC, $TiB_2$, TiB, $La_2O_3$ | 370 $HV_{0.2}$ | ~0.5 | ~33 × $10^{-6}$ $mm^3/(N·m)$ | Adhesive | 530 $HV_{0.2}$ | ~0.45 | ~12 × $10^{-6}$ $mm^3/(N·m)$ | Plough furrow | [213] |
| | | 0.05 wt.% $B_4C$ + 0.5 wt.% $LaB_6$ | | | | | | 635 $HV_{0.2}$ | ~0.40 | ~6 × $10^{-6}$ $mm^3/(N·m)$ | Abrasive | |
| | | 0.10 wt.% $B_4C$ + 1.0 wt.% $LaB_6$ | | | | | | 698 $HV_{0.2}$ | ~0.37 | ~1 × $10^{-6}$ $mm^3/(N·m)$ | Slight grooves | |
| | | 0.15 wt.% $B_4C$ + 1.5 wt.% $LaB_6$ | | | | | | 786 $HV_{0.2}$ | ~0.39 | ~4 × $10^{-6}$ $mm^3/(N·m)$ | N/A | |
| | | 0.20 wt.% $B_4C$ + 2.0 wt.% $LaB_6$ | | | | | | 875 $HV_{0.2}$ | ~0.42 | ~11 × $10^{-6}$ $mm^3/(N·m)$ | Plough furrow | |
| Ti6Al4V | AlCoCrFeNiTi | 0 wt.% $CeO_2$ | BCC, FCC, laves | 340 $HV_{0.2}$ | N/A | N/A | N/A | 957 $HV_{0.2}$ | 0.55 (dry friction) | 173 × $10^{-6}$ $mm^3/(N·m)$ | Abrasive Adhesive Oxidative Fatigue | [214] |
| | | 1 wt.% $CeO_2$ (50 nm) | | | | | | 733 $HV_{0.2}$ | 0.39 | 152.4 × $10^{-6}$ $mm^3/(N·m)$ | | |
| | | 1 wt.% $CeO_2$ (0.5 μm) | BCC | | | | | 675 $HV_{0.2}$ | 0.32 | 77.6 × $10^{-6}$ $mm^3/(N·m)$ | | |
| | | 1 wt.% $CeO_2$ (5 μm) | | | | | | 706 $HV_{0.2}$ | 0.48 | 86.2 × $10^{-6}$ $mm^3/(N·m)$ | | |
| Ti6Al4V | MoNbTaW | 0.5 wt.% $Si_3N_4$ | BCC, TiN, $(Nb, Ti)_5Si_3$ | 337 $HV_{0.1}$ | 0.58 | 2.74 × $10^7$ $μm^3$ | Abrasive Adhesive Oxidative | N/A | N/A | N/A | Abrasive Adhesive Oxidative | [215] |
| | | 1.0 wt.% $Si_3N_4$ | | | | | | 503 $HV_{0.1}$ | 0.70 | 1.44 × $10^7$ $μm^3$ | | |
| | | 1.5 wt.% $Si_3N_4$ | | | | | | 537 $HV_{0.1}$ | 0.59 | 1.41 × $10^7$ $μm^3$ | | |
| | | 2.0 wt.% $Si_3N_4$ | | | | | | 628 $HV_{0.1}$ | 0.58 | 0.95 × $10^7$ $μm^3$ | | |
| Ti6Al4V | CuNiTiCrNb | 1 wt.% Graphite | FCC, TiC, NbC, $Cr_3C_2$ $Ti_xAl_y$, $TiCu_2$ $Ti_2AlC$ | 360 $HV_{0.5}$ | 0.400 | 30.96 × $10^{-5}$ $mm^3/(N·m)$ | N/A | 587 $HV_{0.5}$ | 0.196 | 3.60 × $10^{-5}$ $mm^3/(N·m)$ | Oxidative | [216] |
| | | 2 wt.% Graphite | | | | | | 607 $HV_{0.5}$ | 0.106 | 3.22 × $10^{-5}$ $mm^3/(N·m)$ | | |
| | | 3 wt.% Graphite | | | | | | 683 $HV_{0.5}$ | 0.155 | 2.47 × $10^{-5}$ $mm^3/(N·m)$ | | |
| Ti6Al4V | FeCoNiCrMo | 0 wt.% $CeO_2$ | BCC | 350 $HV_{0.3}$ | N/A | N/A | N/A | 850 $HV_{0.3}$ | N/A | N/A | N/A | [217] |
| | | 2 wt.% $CeO_2$ | | | | | | 950 $HV_{0.3}$ | | | | |
| Ti6Al4V | AlCrTiNbMo $(AlCrTiNbMo)N_x$ | $N_2$ | BCC, TiN | 340 $HV_{0.3}$ | 0.444 (600 °C) | 4.49 × $10^{-4}$ $mm^3/(N·m)$ (600 °C) | Abrasive Adhesive Oxidative | 591 $HV_{0.3}$ | 0.398 | 1.77 × $10^{-4}$ $mm^3/(N·m)$ | Oxidative | [218] |
| | | | | | | | | 1,070 $HV_{0.3}$ | 0.275 | 0.06 × $10^{-4}$ $mm^3/(N·m)$ | | |
| Ti6Al4V | CoCrFeNiTiNb | 0 wt.% $Y_2O_3$ | HCP, BCC | 340 $HV_{0.2}$ | 0.65 | 0.54 $mm^3$ | Abrasive Adhesive | 1,052 $HV_{0.2}$ | 0.48 | ~0.32 $mm^3$ | Abrasive Adhesive Oxidative | [219] |
| | | 2 wt.% $Y_2O_3$ | | | | | | 1,281 $HV_{0.2}$ | ~0.44 | ~0.22 $mm^3$ | | |

HCP: Hexagonal close-packed; COF: coefficient of friction; HEA: high-entropy alloy; FCC: face-centered cubic; BCC: body-centered cubic.

Even so, a single-phase BCC architecture does not eliminate all tribological constraints, because resistance to plastic deformation alone is insufficient to guarantee optimal wear resistance when interfacial instability, local cracking, or unstable tribofilm formation become dominant damage factors. Once contact stress becomes sufficiently high, the absence of additional toughening or secondary load-sharing units limits further improvement, and damage tends to concentrate within the solid-solution matrix itself. In other words, a chemically stable BCC phase can efficiently resist plastic deformation, yet it offers only limited structural redundancy when local contact conditions become more severe. This challenge has motivated the development of composite architectures that introduce intermetallic compounds or hard reinforcing phases to construct enhanced load-bearing frameworks. In parallel, FCC-BCC dual-phase designs have emerged as an effective strategy to balance strength and ductility, combining the high stiffness of BCC matrices with the stress-relief capacity of FCC phases under complex loading conditions.

### *BCC-Laves/B2 synergistically strengthened HEA coatings*

Building on BCC solid-solution-dominated systems, the introduction of intermetallic phases to construct BCC-Laves or BCC-B2 synergistic architectures represents an effective strategy to further enhance the load-bearing capacity of HEA coatings on Ti alloys. These coatings typically consist of a BCC matrix combined with a controlled volume fraction of Laves or ordered B2 phases, which commonly precipitate in interdendritic regions or form semi-continuous network morphologies. Such architectures differ from single-phase BCC coatings in that strengthening is no longer derived solely from lattice distortion within the matrix, but from microstructural partitioning between a continuous solid-solution framework and harder intermetallic domains.

A representative BCC-B2 phase-partitioned architecture is shown in Figure 12. In laser-deposited $AlCoCrFeNiTi_{0.5}$ HEA coatings on Ti6Al4V, the coating consists of disordered A2 and ordered B2 BCC phases, with Fe/Cr enrichment in the A2 regions and Al/Ni/Ti enrichment in the B2 regions. This phase partitioning demonstrates how elemental segregation during rapid solidification can construct a dual-BCC architecture that differs from single-phase BCC solid-solution coatings.

For example, Meng *et al.*[202] laser-cladded a TiZrNbCrCo coating on Ti6Al4V and observed that while the coating was predominantly BCC, increasing cladding layer number and reducing substrate dilution promoted the formation of Zr/Co-enriched C14-type Laves phases in interdendritic regions, resulting in a characteristic BCC-Laves dual-phase microstructure. This result shows that the phase balance in such coatings is highly sensitive to solidification conditions and dilution history, both of which directly affect interdendritic segregation and intermetallic precipitation.

The improved wear resistance of such dual-phase systems arises from synergistic load sharing between the BCC matrix and intermetallic phases. The BCC matrix provides a continuous load-transfer pathway, whereas high-hardness phases such as Laves or B2 preferentially sustain contact stresses, thereby suppressing plastic plowing and micro-cutting. Consequently, the dominant wear mechanism transitions toward a mixed abrasive-oxidative or an adhesive-oxidative regime. Hao *et al.*[203] reported that an AlTiVCrNb coating composed of disordered BCC, Laves phases, and dispersed $Ti_2AlNb$ nanoscale precipitates exhibited increased hardness and approximately 1.58-fold improved wear resistance compared with the substrate. This improvement can be attributed to the formation of a hierarchical load-bearing architecture across multiple length scales. The key feature here is not simply phase coexistence, but the establishment of a hierarchical stress-bearing network in which nanoscale precipitates, interdendritic intermetallics, and the BCC matrix operate at different structural levels during sliding.

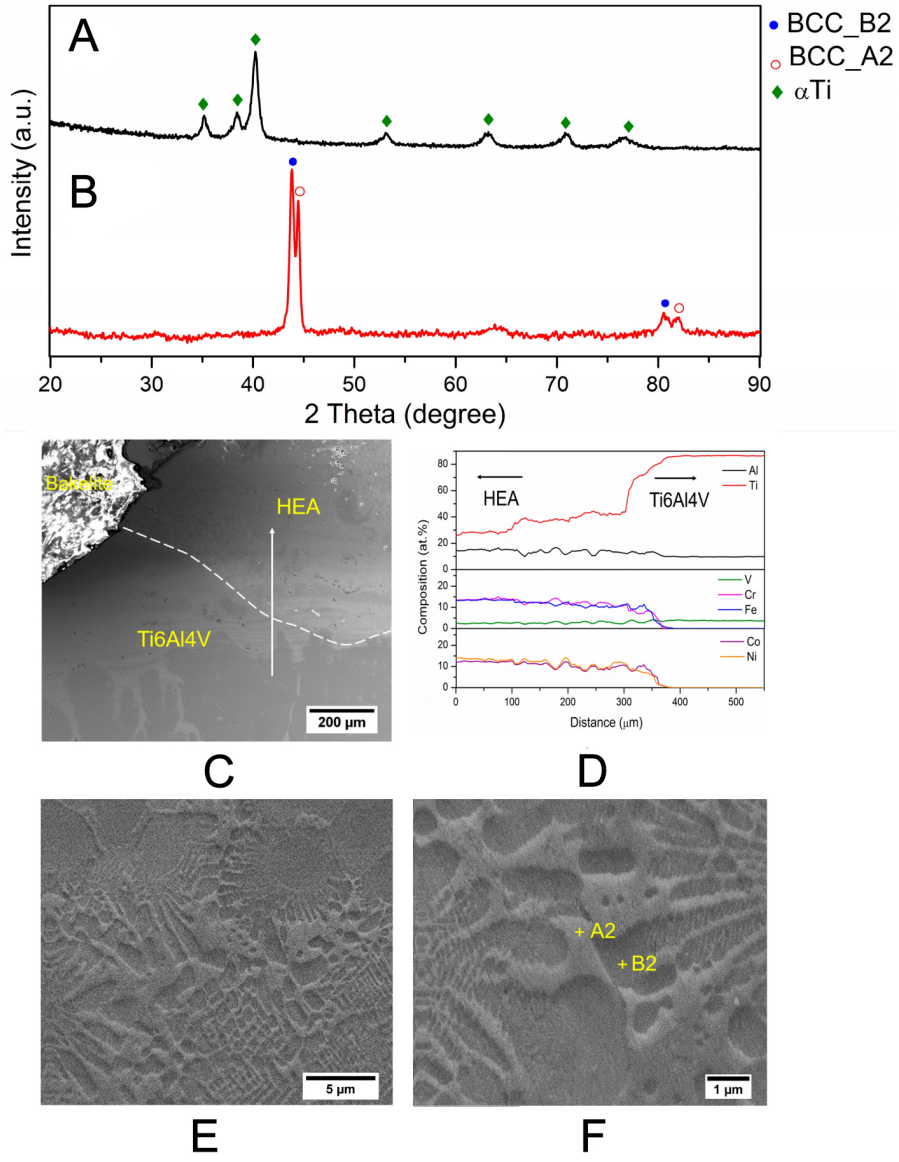



**Figure 12.** Representative BCC-B2 phase architecture and interfacial microstructure of a laser-deposited $AlCoCrFeNiTi_{0.5}$ HEA coating on Ti6Al4V. (A and B) XRD patterns of the Ti6Al4V substrate and as-deposited HEA coating, respectively; (C) coating/substrate interfacial morphology; (D) EDS line-scan profile across the HEA/Ti6Al4V interface; (E and F) SEM microstructures showing A2/B2 phase partitioning in the HEA coating. This figure is adapted from Ref.[220]. Licensed under CC-BY 4.0. BCC: Body-centered cubic; HEA: high-entropy alloy; EDS: energy-dispersive X-ray spectroscopy; XRD: X-ray diffraction; SEM: scanning electron microscopy.

From a performance standpoint, BCC-Laves/B2 systems often outperform single-phase BCC coatings in hardness and, under properly controlled phase fractions and morphologies, can also exhibit superior wear resistance. Meng *et al.*[202] reported an average hardness of approximately 748 HV for TiZrNbCrCo multiphase coatings, with a wear-volume reduction of 68.6% relative to the substrate. In addition, Zhang *et al.*[221] prepared $FeCrAlMoSi_x$ coatings containing B2 and μ phases, achieving hardness values up to approximately 805 HV at x = 0.10. This improvement is closely related to the introduction of ordered or topologically close-packed strengthening units that reduce local deformation compatibility but markedly increase resistance to penetration and plowing.

The advantages of BCC-intermetallic systems become more pronounced at elevated temperatures, especially when intermetallic-assisted oxidation promotes the formation of dense and adherent protective films that reduce interface damage and suppress oxidation-assisted cracking. The incorporation of Cr-rich or Al-rich

intermetallic phases facilitates the formation of dense, adherent oxide films during sliding or thermal exposure, thereby reducing oxidation wear and enhancing service stability. Deng *et al.*[198] demonstrated that a $CoCrFeNiMo_{0.2}$ coating composed of BCC and σ phases exhibited hardness of approximately 900 HV and superior wear resistance at 600 °C due to the formation of a protective Cr-rich oxide layer. In addition, Yang *et al.*[208] reported that increasing Ni content in $(AlCrFeTiV)_{100-x}Ni_x$ coatings transformed the phase constitution from BCC/Laves to BCC+NiAl-type B2+Laves, resulting in improved oxidation resistance at 800 °C due to the formation of a compact spinel oxide film. In other words, intermetallic phases influence high-temperature tribological behavior not only through direct hardening, but also through their effect on oxidation pathways and the chemistry of protective surface scales.

Despite these benefits, excessive volume fractions or continuous networks of intermetallic phases may introduce brittleness and increase susceptibility to crack initiation, particularly under thermal cycling or impact loading. For instance, an overly high μ-phase content in $FeCrAlMoSi_x$ coatings was shown to promote stress concentration and microcrack formation[221]. Once the intermetallic constituent evolves from a dispersed strengthening unit into a continuous brittle path, the same microstructural feature that improves hardness begins to accelerate crack propagation and structural instability. As a result, while BCC-Laves/B2 synergistic strengthening enhances load-bearing capability and wear resistance, careful control of phase fraction, morphology, and distribution is essential to balance mechanical strength with structural reliability. The design problem in this class of coatings is therefore not how to maximize intermetallic content, but how to confine hard phases to morphologies and length scales that strengthen the matrix without converting the coating into a brittle interconnected framework. This inherent trade-off has motivated further exploration of coatings with enhanced thermal stability and multifunctional composite architectures capable of sustaining performance under complex and extreme service conditions.

### *FCC-BCC dual-phase HEA coatings*

In high-strength systems dominated by BCC solid solutions or by BCC-intermetallic synergistic strengthening, improvements in wear resistance are often accompanied by reduced plasticity and an elevated risk of brittle failure. This limitation becomes particularly pronounced under high contact stresses, repeated sliding, or localized impact loading, where single high-strength architectures are susceptible to stress concentration and crack propagation. To address this trade-off between strength and toughness, FCC-BCC dual-phase HEA coatings have been proposed as an alternative design strategy. In these systems, the BCC phase retains the primary load-bearing function, while the FCC phase introduces plastic deformation capability and stress-relief pathways, thereby enhancing structural stability under complex wear conditions. The design logic of this class therefore lies in partitioning mechanical roles between two crystal structures rather than relying on a single hard phase to resist all forms of tribological damage.

Under laser cladding conditions, FCC-BCC dual-phase coatings typically exhibit a heterogeneous microstructure in which one phase forms a semi-continuous framework while the other is distributed in interdendritic or island-like regions. For example, Zeng *et al.*[199] reported that an $AlCoCrFeNiTi_{0.5}$ coating fabricated on Ti6Al4V displayed a characteristic dual-phase structure, with dendritic regions enriched in the FCC phase and interdendritic regions dominated by the BCC phase. This architecture provided balanced mechanical properties and stable performance under high-temperature and oxidative wear environments. Such spatial partitioning is important because it allows the two phases to respond differently to local contact stresses, with the harder skeleton resisting penetration and the more deformable regions accommodating local strain.

The formation of dual-phase microstructures is governed by compositional design and the tendency of constituent elements to stabilize crystal structures. Elements such as Ni, Co, and Cu favor FCC stabilization, whereas Ti, V, Cr, Nb, and Mo promote BCC formation[222,223]. During rapid solidification in laser cladding,

compositional partitioning occurs under non-equilibrium conditions, leading to local enrichment of FCC-stabilizing elements and preferential FCC formation in specific regions, while BCC-stabilizing elements contribute to a continuous BCC framework. Although Ti does not intrinsically stabilize the FCC structure, substrate dilution influences the overall phase balance and indirectly affects the compositional window for dual-phase formation. Through careful alloy design and process control, controllable FCC-BCC architectures can therefore be constructed on Ti alloy surfaces. What distinguishes these coatings from simpler solid-solution systems is not merely the coexistence of two phases, but the deliberate use of segregation-assisted phase separation to construct a heterogeneous deformation microstructure.

During friction and wear, the mechanical synergy between the two phases governs performance. The BCC phase provides high load-bearing capacity and resistance to plastic indentation, whereas the FCC phase, characterized by lower lattice friction stress and greater slip activity, accommodates localized deformation and redistributes stresses. Wu *et al.*[209] reported that in FeCrCoNiAlTi$_x$ coatings, the coexistence of FCC and BCC/B2 phases enabled high hardness while improving resistance to fatigue and adhesive wear. Moreover, Liu *et al.*[210] demonstrated that increasing Ni content modified the deformation mechanism from slip-band-dominated to dislocation-entanglement-dominated behavior, enhancing work hardening and wear resistance. In practical terms, the FCC constituent acts less as a soft phase and more as a deformation buffer that delays strain localization within the harder regions of the coating.

Compared with single-phase BCC or BCC-intermetallic systems, FCC-BCC dual-phase coatings are not primarily optimized for maximum hardness or the lowest wear rate. Instead, their advantage lies in improved structural reliability under complex service conditions involving cyclic loading, repeated sliding, or impact. By reducing dependence on high fractions of brittle intermetallic phases, dual-phase architectures mitigate crack susceptibility and delay catastrophic failure. Their main benefit emerges when wear damage is governed by instability and crack evolution rather than by insufficient hardness alone. However, under extremely high contact stresses or severe abrasive erosion, their wear resistance is typically lower than that of HEA composite coatings reinforced with *in situ*-formed hard phases.

### *In situ hard-phase-reinforced HEA coatings*

Building upon BCC solid-solution-dominated and BCC-intermetallic synergistically strengthened systems, the *in situ* formation of high-hardness ceramic phases during laser cladding has emerged as a key strategy for constructing HEA-based composite architectures capable of extreme wear resistance on Ti alloy surfaces[224]. In these systems, a HEA matrix is combined with reaction-induced hard phases, such as carbides, borides, nitrides, or composites. These reinforcing phases typically precipitate as particles, short rods, or semi-continuous networks within interdendritic regions or along GBs, thereby establishing a rigid load-supporting framework within the coating. Relative to dual-phase metallic HEAs, this approach pushes the microstructure toward a more strongly partitioned architecture in which stress-bearing and damage-arresting functions are distributed between the metallic matrix and ceramic constituents.

The superior wear resistance of such HEA composites arises from the synergistic interaction between the ductile HEA matrix and the *in situ*-generated hard phases, but not from hardness enhancement alone; rather, it also depends on whether the matrix/reinforcement interfaces remain stable, local stress concentration is controlled, and crack initiation is effectively suppressed during sliding. The ceramic phases preferentially sustain contact stress during sliding, effectively suppressing matrix plowing and severe plastic deformation. Simultaneously, their dispersion refines the microstructure and promotes dislocation accumulation, resulting in combined solid-solution, dispersion, and GB strengthening within the HEA matrix. Zhang *et al.*[206] reported that in AlNbTiVB$_x$ coatings, increasing B content led to the *in situ* formation of $TiB_2$, which

significantly enhanced load-bearing capacity. At a B content of 0.15, the wear volume was reduced by approximately 44% relative to the substrate, underscoring the critical role of reaction-induced ceramic reinforcement.

Here, the strengthening effect is tied not only to the intrinsic hardness of the ceramic phase, but also to how its morphology and spacing constrain local deformation within the surrounding HEA matrix.

In terms of performance, HEA composite coatings containing *in situ* hard phases generally exhibit substantially higher hardness and wear resistance than single BCC or BCC-Laves/B2 systems. Reported microhardness values frequently exceed 900-1,200 HV, accompanied by markedly reduced wear rates under high-load or elevated-temperature conditions. For example, Zhang *et al.*[197] fabricated a TiAlNiSiV HEA coating on Ti6Al4V in which the *in situ* formation of $(Ti, V)_5Si_3$, TiN, and B2-NiAl phases increased hardness to approximately 1,150-1,357 HV. The coating demonstrated superior wear resistance at both RT and 800 °C. This level of performance reflects the establishment of a multiscale reinforcing framework rather than the contribution of any single strengthening phase in isolation.

However, the introduction of *in situ* hard phases inevitably increases microstructural heterogeneity and the risk of brittleness. Excessive volume fractions, continuous networks, or non-uniform spatial distributions can induce stress concentration, interfacial decohesion, and microcrack initiation, particularly under thermal cycling or impact loading. Once the reinforcing phase evolves from a dispersed barrier into a connected brittle pathway, damage can propagate through the coating much more rapidly than in metallic-only HEA systems. Consequently, achieving an optimal balance between reinforcement fraction and structural continuity is essential. Precise control over phase content, morphology, and distribution is required to maximize wear resistance while maintaining coating integrity and long-term service reliability. For this reason, the central issue in these coatings is not simply how many hard phases can be generated, but how they are embedded within the HEA matrix and whether the resulting architecture remains damage tolerant under service conditions.

### *Tribological performance of RHEA coatings*

With the expanding application of Ti alloys in aerospace, energy systems, and high-temperature tribological components, surface-modification requirements have progressively shifted from room- and intermediate-temperature wear resistance toward service conditions involving elevated temperatures, high contact stresses, and coupled oxidation-wear environments. Under such conditions, conventional HEA coatings dominated by FCC or BCC phases may experience microstructural softening, phase instability, or accelerated oxidation. In response, RHEA coatings, mainly composed of refractory elements with high melting points, have emerged as a promising solution. The central design philosophy of RHEAs is to exploit strong atomic bonding, sluggish diffusion, and exceptional thermal stability to maintain wear resistance at elevated temperatures. What sets this class apart is that coating design is no longer centered mainly on ambient-strength enhancement, but on preserving phase constitution and near-surface microstructural stability during prolonged thermal-mechanical exposure.

From a phase-structure standpoint, RHEA coatings are typically characterized by a BCC solid-solution matrix, occasionally accompanied by minor secondary phases or localized segregation. Although this configuration resembles conventional BCC-type HEAs, the design emphasis is fundamentally different. Whereas BCC-type HEAs are often optimized for room- or intermediate-temperature load-bearing enhancement, RHEAs prioritize phase stability and mechanical property retention under high-temperature exposure. The distinction therefore lies less in the nominal crystal structure itself than in the extent to which

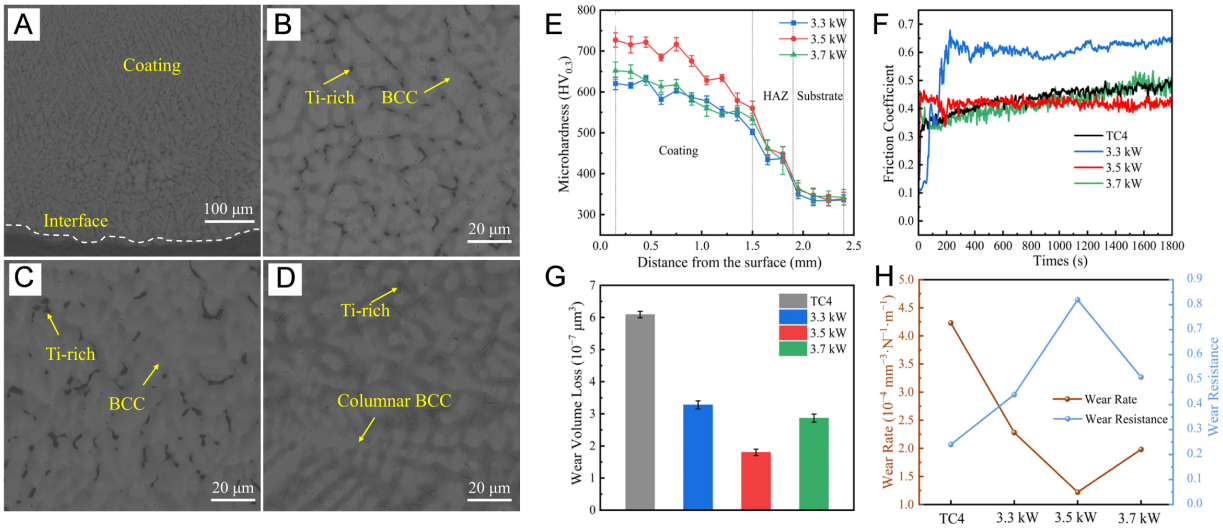



**Figure 13.** Cross-sectional microstructure and tribological properties of laser-cladded WMoTaNbV refractory high-entropy alloy coatings on TC4 substrate. (A-D) Cross-sectional SEM images of the coating fabricated at 3.7 kW, showing (A) the overall coating morphology and the microstructures of the (B) top, (C) middle, and (D) bottom regions; (E-H) Tribological results of the TC4 substrate and coatings fabricated at different laser powers, including (E) microhardness profiles, (F) friction coefficient curves, (G) wear-volume loss, and (H) wear rate and wear resistance. This figure is adapted from Ref.[204]. Licensed under CC-BY 4.0. BCC: Body-centered cubic; SEM: scanning electron microscopy.

that structure can resist thermally induced softening, diffusion-assisted coarsening, and oxidation-related degradation. Representative microstructures and tribological properties of laser-cladded WMoTaNbV RHEA coatings on Ti6Al4V are shown in Figure 13, illustrating the relationship between BCC-based refractory microstructures, coating hardness, friction stability, and wear resistance.

BCC structures enriched with refractory elements such as Nb, Mo, Ta, W, and V possess high melting points and elastic moduli, rendering them less susceptible to softening or microstructural degradation during high-temperature sliding. This intrinsic stability provides a robust load-bearing framework for elevated-temperature wear resistance. For example, Hu *et al.*[225] reported that a lightweight AlNbTiVZr RHEA coating fabricated on Ti6Al4V exhibited a predominantly BCC microstructure with a minor fraction of C14-type Laves phase, achieving enhanced hardness and wear resistance while maintaining reduced density. Here, the presence of only a limited amount of secondary phase is important, because it preserves the thermal stability of the BCC framework without introducing excessive brittle connectivity. In the same way, Du *et al.*[211] demonstrated that in $TiZrHfNbTaMo_x$ RHEA coatings, Mo addition stabilized the BCC structure and improved hardness retention at elevated temperatures, establishing a structural basis for reliable service in complex environments.

In terms of tribological behavior, the advantages of RHEA coatings become particularly evident at medium to high temperatures. During elevated temperature sliding or fretting, these coatings generally exhibit lower wear rates and more stable COF. Their performance derives not only from high hardness but also from the suppression of microstructural degradation. Strong atomic bonding and relatively low diffusion rates among refractory elements effectively inhibit dislocation recovery and grain coarsening, thereby delaying near-surface softening and preventing the wear mechanism from transitioning to severe adhesive or spallation modes. Liu *et al.*[200] reported that at 600 °C, the wear rate of $Al_{20}V_{20}Cr_{20}Nb_{40-x}Mo_x$ RHEA coatings decreased by nearly two orders of magnitude, primarily due to the rapid formation of a dense oxide film and the mechanical anchoring effect of Mo-rich oxides at the friction interface. In this temperature regime, wear resistance is governed by the combined persistence of the refractory matrix and the development of a

compact oxide-bearing surface layer, rather than by matrix hardness alone; in particular, the mechanical integrity, adhesion, and continuity of the oxide layer are critical in determining whether oxidation becomes protective or damage-accelerating.

Because high-temperature wear is often strongly coupled with oxidation, the compositional design of RHEAs frequently incorporates elements such as Cr and Al that form dense, adherent oxide scales. These oxide layers serve dual functions: they retard further matrix oxidation and participate in load sharing and friction modulation at the sliding interface. However, performance does not improve monotonically with increasing alloying content or temperature. Zhao *et al.*[212] observed that in $AlNbTaZr_x$ RHEA coatings, increasing Zr content induced a transition from a single BCC phase to a BCC + hexagonal close-packed (HCP) dual-phase structure, accompanied by a shift in wear mechanism from micro-cutting to oxidation-assisted brittle spallation. Similarly, Liu *et al.*[226] reported that $TiZrNbAl_x$ lightweight RHEA coatings exhibited inferior wear resistance at 500 °C compared with RT, which was associated with enhanced thermal vibration and strain accumulation at elevated temperatures. Once phase stability is disrupted or the oxide layer loses mechanical integrity, the same high-temperature environment that favors protective oxidation can instead accelerate embrittlement and surface damage.

Although RHEA coatings exhibit pronounced advantages in high-temperature wear resistance and oxidation resistance, their design is often associated with relatively high density, increased material cost, and potentially insufficient room-temperature plasticity. These constraints mean that RHEAs are better viewed as environment-specific coating solutions than as universally optimal systems for Ti-alloy surfaces. Consequently, RHEAs are better suited to specific service conditions that demand exceptionally high-temperature stability and long-term durability, rather than serving as general-purpose surface modification solutions for Ti alloys.

Overall, RHEA coatings represent a significant extension of HEA design for Ti alloy surface engineering, marking a shift from phase-centered strengthening strategies toward service-environment-driven optimization. Together with BCC-type, BCC-intermetallic, FCC-BCC dual-phase, and *in situ* hard-phase-reinforced systems, RHEAs complete a hierarchical material design framework capable of addressing diverse combinations of load, temperature, and environmental conditions. Within this framework, their defining contribution lies in coupling refractory phase stability with oxidation-assisted interfacial protection under severe thermal tribological conditions.

## HEA-based composite coatings with ceramic reinforcements, rare-earth oxides, and lubricating phases

While monolithic HEA coatings provide enhanced structural stability and load-bearing capacity, their performance under extreme wear, corrosion, or high-temperature environments may still be limited by insufficient hardness, interfacial instability, or frictional heat accumulation. To overcome these limitations, recent research has increasingly focused on HEA-based composite coatings that integrate ceramic reinforcements, rare-earth oxides, and lubricating phases within a high-entropy matrix, thereby constructing multifunctional microstructural architectures with coupled strengthening, stabilization, and friction-regulation mechanisms.

### *HEA-ceramic composite architectures*

In HEA-based ceramic composite systems, the HEA matrix serves as a tough, compositionally stable platform, while *in situ*-formed carbides, borides, or nitrides form an independent load-bearing skeleton. The role of the matrix in such systems is not merely to bind the reinforcement, but to provide a deformation-tolerant framework that accommodates local stress around hard phases and delays catastrophic cracking. For

example, He *et al.*[213] reported that $LaB_6$ + $B_4C$ additions in $FeNiCrTi_{0.3}Al_{0.3}$ HEA coatings promoted the *in situ* formation of TiC and $TiB_x$ phases during laser cladding. The rare-earth-containing precursor not only enhanced ceramic precipitation but also altered melt-pool convection and promoted heterogeneous nucleation, resulting in microstructural refinement and improved hardness, with a maximum microhardness of 875 $HV_{0.2}$, approximately 2.36 times that of the Ti6Al4V substrate.

Similarly, Hao *et al.*[215] demonstrated that nano-$Si_3N_4$ additions in MoNbTaWTi refractory HEA coatings triggered *in situ* formation of TiN and $(Nb, Ti)_5Si_3$ ceramic phases. The exothermic Ti-N reaction facilitated densification and phase stabilization, significantly improving hardness and wear resistance. Reliability here is governed by the spatial relationship between the lattice-distorted HEA matrix and the ceramic domains. When the reinforcing phase remains discrete and well distributed, the coating can combine local hardness with crack deflection and stress redistribution. Once ceramic connectivity becomes excessive, however, the composite begins to lose the damage-tolerant character that makes the HEA matrix advantageous in the first place. Consequently, the value of HEA-ceramic systems lies in preserving a hierarchical load-sharing architecture rather than in simply maximizing ceramic content.

### *HEA-rare-earth hybrid architectures*

Rare-earth oxides incorporated into HEA coatings primarily function as microstructural regulators rather than direct load-bearing phases. Cui *et al.*[217] showed that $CeO_2$ additions in FeCoNiCrMo HEA coatings reduced crack sensitivity and refined grain structure without altering the dominant BCC phase constitution. The microhardness increased to approximately 2.7 times that of the TC4 substrate, and corrosion resistance improved due to the formation of a denser passive film.

Likewise, Li *et al.*[219] reported that $Y_2O_3$-modified CoCrFeNiTiNb HEA coatings exhibited significant grain refinement and enhanced oxidation and hot-corrosion resistance. The fine-grain strengthening effect increased microhardness and wear resistance by over 20%, while oxidation and hot-corrosion rates were markedly reduced. In these hybrids, rare-earth oxides act mainly through kinetic and interfacial pathways: they retard grain growth, suppress defects, and improve the stability of oxide or passive films formed during service. Moderate additions therefore improve both structural cohesion and environmental durability. By contrast, excessive segregation or over-addition can disturb local phase evolution, create chemically heterogeneous regions, and reintroduce brittleness at precisely the interfaces meant to be stabilized. Rare-earth modification in HEA systems should therefore be regarded as a tool for regulating solidification and interfacial chemistry, rather than as a conventional hardening route.

### *HEA-lubricating phase synergistic systems*

To further enhance service performance in high-temperature or dry-sliding environments, lubricating phases have been incorporated into HEA matrices to enable simultaneous load-bearing and friction modulation. Tang *et al.*[216] prepared graphite/CuNiTiCrNb HEA coatings in which graphite decomposition generated TiC and $Ti_2AlC$/$Ti_3AlC$ phases. The layered graphite and MAX-derived phases contributed to the formation of dense oxide layers composed of $Cr_2O_3$ and $TiO_2$, reducing both wear and oxidation rates at elevated temperatures.

In this class of coatings, the HEA matrix functions as a thermally stable support for tribofilm evolution, whereas the lubricating phases govern local shear accommodation at the contact interface. Performance is therefore controlled not only by whether lubricating species are present, but by how they are retained, transformed, and redistributed during sliding. Non-uniform dispersion, excessive decomposition, or uncontrolled coarsening of lubricating phases may weaken the supporting framework and introduce

preferred sites for stress concentration. As temperature or contact stress rises, the balance between matrix rigidity and interfacial compliance becomes increasingly delicate: insufficient lubrication promotes adhesive damage, whereas excessive local softening undermines load support.

Consequently, HEA-lubricant composite systems must balance structural stiffness with controlled interfacial compliance, ensuring that friction reduction does not occur at the expense of mechanical stability. The central challenge is not compositional addition itself, but the coordination of phase evolution, interfacial coherence, and tribochemical response over the course of service.

To sum up, HEA-based composite coatings represent a transition from single-phase strengthening toward integrated multi-mechanism design. Their performance depends on the coordinated contributions of matrix stabilization, ceramic reinforcement, microstructural regulation, and friction control. However, these benefits can only be realized when phase fractions, spatial distributions, and interface stability are carefully controlled, because uncontrolled segregation or phase connectivity may convert synergistic constituents into competing damage-initiation pathways. Future development should therefore emphasize the coordinated design of phase evolution, interfacial coherence, and tribochemical response rather than the simple addition of functional phases.

## COMPARATIVE DISCUSSION OF DESIGN LOGICS ACROSS DIFFERENT COATING SYSTEMS

Although different coating systems are often discussed as independent material categories, they can be more fundamentally understood as distinct microstructural design routes developed to address the same underlying challenge in Ti-alloy surface engineering: the need to simultaneously enhance load-bearing capacity, suppress damage evolution, maintain interfacial stability, and accommodate service-induced structural and chemical changes. From this perspective, the differences among coating systems do not arise from composition alone, but from how each system prioritizes and resolves competing requirements in microstructural design and service response.

Self-fluxing alloy coatings represent the baseline strengthening-dominated route. Their core design logic lies in constructing a metallurgically bonded metallic framework in which a relatively continuous matrix cooperates with *in situ* formed hard phases to resist plastic deformation and material removal. The intrinsic connection of this system to others lies in its direct attempt to improve load-bearing capacity, which is a common objective across all coating types. However, its essential limitation arises from the need to balance reinforcement with structural integrity: increasing hard-phase fraction enhances wear resistance but also promotes brittle phase continuity, interfacial stress concentration, and crack initiation. Therefore, self-fluxing alloys are fundamentally governed by a strength-toughness trade-off within a metallic matrix-dominated architecture.

Ceramic-particle-reinforced coatings represent a shift toward rigid load-bearing frameworks. While sharing the same objective of enhancing resistance to deformation and wear, these systems differ fundamentally from self-fluxing alloys in that the primary load-bearing role is transferred from the metallic matrix to hard ceramic phases. As a result, wear resistance is more directly controlled by the continuity, morphology, and spatial connectivity of the ceramic framework. This leads to a higher strengthening efficiency but also introduces greater sensitivity to brittle fracture, interfacial decohesion, and crack propagation along rigid phase networks. Thus, the essential difference lies in the relocation of the dominant load-bearing unit, which transforms the governing mechanism from matrix-supported reinforcement to skeleton-controlled load transfer.

Rare-earth-modified coatings follow a fundamentally different design route by targeting microstructural evolution rather than directly redefining the load-bearing architecture. Their intrinsic connection to other systems lies in the improvement of coating performance through enhanced structural stability and reduced defect sensitivity. However, their essential distinction is that rare-earth elements primarily act by modifying solidification behavior, refining microstructures, suppressing defect formation, and stabilizing coating/substrate interfaces. Consequently, the strengthening effect is indirect and mediated through improved microstructural quality, rather than through the introduction of dominant reinforcing phases or rigid frameworks. This makes rare-earth-modified systems less sensitive to brittle failure but also less capable of providing substantial load-bearing enhancement on their own.

Self-lubricating coatings represent a transition from bulk strengthening to interfacial shear regulation. While still requiring sufficient load-bearing capacity from the underlying microstructure, their primary design focus shifts toward controlling frictional behavior at the sliding interface through the formation and evolution of low-shear tribofilms. The intrinsic connection with other systems lies in the need to maintain structural integrity under load; however, the essential difference is that performance is no longer governed solely by resistance to deformation, but by the ability to reduce shear stress and stabilize tribochemical films during service. As a result, these systems are particularly sensitive to the stability, continuity, and regeneration capability of lubricating phases, and their failure is often associated with tribofilm breakdown rather than bulk structural collapse.

HEA-based coatings represent a higher-level architectural design approach, in which compositional complexity and phase stability are deliberately utilized to achieve multifunctional microstructural optimization. Their intrinsic connection to other systems lies in addressing the same combined requirements of strength, stability, and service adaptability. However, their essential distinction is that they do not rely on a single dominant mechanism, but instead aim to coordinate multiple strengthening and stabilization effects - such as solid-solution strengthening, phase stability, and defect tolerance - within a unified compositional and structural framework. This enables greater flexibility in tailoring performance but also introduces new challenges related to phase evolution, compositional segregation, and long-term stability under service conditions.

In summary, these coating systems should not be regarded as parallel solutions of equivalent nature, but as fundamentally different microstructural strategies that operate at different levels of intervention: from matrix-dominated strengthening, to rigid skeleton construction, to solidification and interface regulation, to interfacial shear control, and finally to compositional and architectural design. This hierarchical distinction provides a clearer basis for understanding their intrinsic connections and essential differences, and forms the conceptual bridge toward a unified microstructure-oriented design framework.

## UNIFIED MICROSTRUCTURE-ORIENTED DESIGN STRATEGY FOR LASER-CLADDED WEAR-RESISTANT COATINGS ON TI ALLOYS

Laser-cladded wear-resistant coatings on Ti alloys are governed by coupled relationships among processing conditions, phase selection, microstructural architecture, interfacial stability, and tribological degradation. Although a wide variety of coating systems have been developed, their design principles are often discussed separately according to material category or performance outcome. A more unified interpretation can be established by recognizing that the performance of these coatings is ultimately controlled by how laser-cladding-induced solidification constructs and destabilizes specific microstructural features during service. Rather than introducing a completely new individual mechanism, the value of this framework lies in integrating these previously separated considerations into a unified design logic that connects processing, phase formation, microstructural architecture, interface stability, and service-related degradation.

The first requirement is the establishment of a mechanically effective load-bearing architecture. Hard phases such as carbides, borides, nitrides, intermetallic compounds, and stable oxides improve resistance to plowing, indentation, and material removal, but their benefit depends on morphology, continuity, and spatial distribution rather than on content alone. Discrete or hierarchically distributed reinforcing phases can share contact stresses and constrain local deformation, whereas excessive phase continuity readily converts strengthening units into brittle crack-initiation paths. For this reason, the optimal coating is not the hardest possible structure, but a microstructurally balanced architecture in which a relatively tough matrix and a controlled reinforcing framework operate cooperatively.

The second requirement involves interfacial and compositional compatibility. Because Ti substrates are highly reactive and sensitive to thermal-expansion mismatch, the coating/substrate region often becomes a critical source of brittle intermetallic formation, residual stress accumulation, and crack nucleation. Interfacial reliability therefore depends on controlling dilution, chemical gradients, and reaction pathways during cladding. Approaches such as transition layers, graded composition design, and rare-earth-mediated interfacial regulation are effective because they reduce local incompatibility and stabilize metallurgical bonding rather than simply increasing coating hardness.

The third requirement is control over microstructural refinement and defect evolution during rapid solidification. Laser cladding can generate fine grains, metastable phases, and heterogeneous phase distributions that are beneficial for strengthening, but steep thermal gradients and non-equilibrium segregation may also introduce pores, brittle networks, and local chemical inhomogeneity. As a result, wear durability is closely tied to whether the solidification path produces a dense and damage-tolerant microstructure or a structurally unstable one. GB pinning, melt-pool regulation, and phase-transformation control are therefore central design tools, especially in systems modified by rare-earth oxides, HEA matrices, or *in situ* reaction-induced reinforcements.

The fourth requirement is adaptive control of the sliding interface. Tribological performance is not determined by hardness alone, but by the evolution of near-surface deformation layers, oxide scales, transfer films, and tribochemical products during service. Dense oxides, lubricating films, and mechanically supported tribolayers can shift wear from severe adhesive tearing or brittle spallation toward milder and more stable regimes. By contrast, unstable film formation, oxide fragmentation, or lubricant depletion can rapidly accelerate damage even in hard coatings. Effective coating design must therefore integrate bulk load-bearing support with interfacial shear accommodation and tribofilm stability.

Importantly, these factors are not independent. Processing conditions govern phase selection and defect evolution; phase constitution and microstructural architecture determine load-bearing capability and crack sensitivity; interfacial stability influences stress transfer and damage initiation; and tribolayer evolution ultimately controls the transition between mild and severe wear during service.

Taken together, these considerations suggest that the design of next-generation laser-cladded coatings on Ti alloys should be framed not as a search for individual high-performance additives, but as the coordinated control of five linked factors: processing thermodynamics, phase constitution, microstructural architecture, interfacial stability, and tribolayer evolution. In this sense, a unified strategy is possible because different coating families ultimately solve the same problem through different microstructural routes. Ceramic-reinforced systems emphasize hard-phase load support, rare-earth-modified systems emphasize solidification and interface regulation, self-lubricating systems emphasize adaptive interfacial shear control, and HEA-based systems emphasize phase stability and multifunctional microstructural design. Accordingly, the contribution of this unified strategy is not to replace existing mechanistic understanding, but to provide a

common interpretive framework through which different coating families can be compared, connected, and designed according to the same microstructure-mechanism-service logic.

## CONCLUSIONS

This review systematically summarizes recent progress in laser-cladded wear-resistant coatings on Ti alloys, covering self-fluxing alloys, ceramic-particle-reinforced composites, rare-earth-modified coatings, self-lubricating systems, and HEAs. Rather than treating these systems as isolated material categories, the discussion has been organized around the coupled roles of phase formation, microstructural evolution, interfacial stability, and tribological degradation.

The results demonstrate that different coating families improve tribological performance through distinct microstructural routes, including hard-phase load support, solidification and interface regulation, adaptive tribofilm formation, and multiphase architectural stabilization. Across these systems, wear resistance is governed not by hardness alone, but by the coordinated control of phase morphology, damage tolerance, interfacial compatibility, and tribolayer stability.

In general, these findings highlight a transition in coating design from single-mechanism strengthening toward microstructure-oriented, service-environment-specific multifunctional engineering. A unified design strategy linking processing thermodynamics, phase constitution, microstructural architecture, interfacial stability, and tribolayer evolution is proposed to guide future development. In this framework, different coating systems can be understood as distinct microstructural design routes for solving the same fundamental problem, namely how to reconcile load-bearing capacity, damage tolerance, and interfacial stability under complex tribological conditions.

Looking ahead, gradient architectures, multifunctional materials systems, and data-driven design methodologies are expected to play key roles in advancing high-performance laser-cladded coatings for Ti alloys. Equally important will be the integration of advanced microstructural characterization, crystallography-informed phase design, and *in situ* studies of oxidation and tribofilm evolution, so that future coating development can move from empirical composition optimization toward mechanism-guided microstructural engineering.

## PERSPECTIVES

Despite significant progress in laser-cladded wear-resistant coatings on Ti alloys, several fundamental challenges remain unresolved, limiting their structural reliability and long-term service performance. Future research should therefore move beyond incremental compositional optimization toward microstructure-informed, mechanism-driven, and service-oriented design strategies.

First, achieving a balanced combination of hardness, toughness, and interfacial stability remains a central challenge. Excessive reliance on rigid ceramic reinforcements or brittle intermetallic phases often leads to crack initiation and premature failure under complex thermo-mechanical loading. Future efforts should place greater emphasis on damage-tolerant microstructural architectures, in which load-bearing phases, ductile matrices, and lubricating constituents are spatially distributed to mitigate stress concentration and enhance damage tolerance. In particular, the regulation of residual stress, brittle interfacial reaction layers, and thermomechanical compatibility across coating-substrate interfaces represents a critical yet underexplored research direction. Future studies should pay greater attention to how Ti-related interfacial reactions, dilution behavior, and thermal-stress evolution jointly determine crack initiation, interfacial delamination, and long-term wear failure.

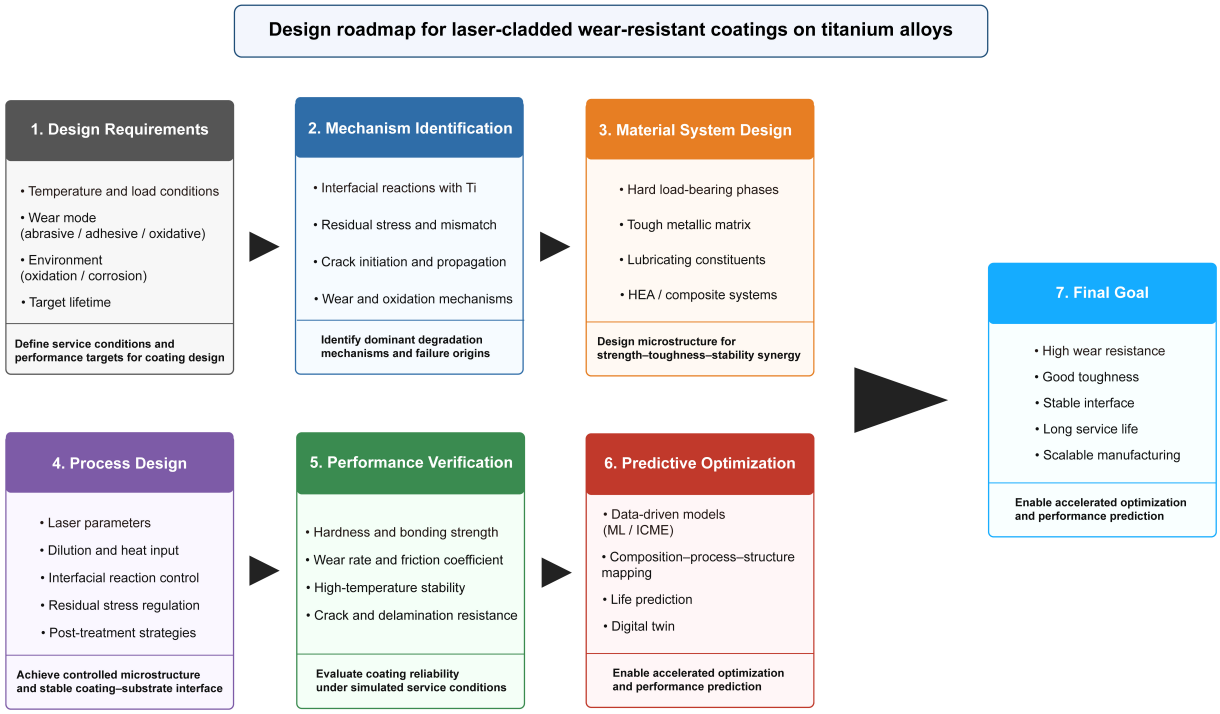



**Figure 14.** Design roadmap for laser-cladded wear-resistant coatings on Ti alloys. ML: Machine learning; HEA: high-entropy alloy; ICME: integrated computational materials engineering.

Second, the fundamental physics governing interfacial reactions and failure evolution during laser cladding requires a deeper understanding. Ti alloys exhibit strong chemical affinity with many alloying elements, and rapid solidification can readily lead to segregation, metastable phases, and non-equilibrium interfacial reactions. Future progress will depend heavily on advanced characterization approaches capable of tracking microstructural evolution across multiple length scales, including *in situ* or quasi-*in situ* observation of melt-pool behavior, phase transformation, oxidation, and tribofilm formation. Combining such experiments with multiscale simulations will be essential for clarifying how the solidification path, local chemistry, residual stress, and defect accumulation jointly control coating degradation during both processing and service.

Third, emerging materials concepts should be pursued not as isolated additions, but as routes toward structurally integrated multifunctionality. High-entropy and multi-principal-element coating offer promising pathways for improving thermal stability and mechanical reliability, yet their phase stability, interfacial compatibility, and wear mechanisms under realistic service conditions remain insufficiently understood. In addition, hybrid strategies combining laser cladding with additive manufacturing, surface texturing, or post-processing treatments may enable hierarchical structural control and multifunctional performance optimization.

Finally, the next stage of development will increasingly require integrating data-driven methods with physically informed coating design. Machine learning and integrated computational materials engineering (ICME) frameworks can accelerate composition screening, process optimization, and performance prediction, but their real value will lie in linking processing conditions to phase constitution, microstructural architecture, and long-term service response. In this regard, digital twins for coating systems may become especially valuable if they are built not only on empirical property databases, but also on mechanistic descriptors such as phase stability, defect sensitivity, oxide-scale integrity, and tribofilm persistence.

Based on these considerations, Figure 14 summarizes a design roadmap for future laser-cladded wear-resistant coatings on Ti alloys, linking service requirements, failure mechanisms, material system design, process control, performance verification, and predictive optimization.

Overall, future advances in laser-cladded wear-resistant coatings on Ti alloys will increasingly rely on the synergistic integration of microstructural design, interfacial engineering, and predictive modeling. The most important shift will be from empirical optimization of composition and hardness toward controllable design of phase constitution, structural heterogeneity, and damage evolution under service conditions. Such a transition is essential for developing next-generation coating systems capable of sustained operation in extreme tribological environments.

## DECLARATIONS

### Authors' contributions

Writing - original draft; data extraction: Zhao, Y.; Wang, K.
Writing - review & editing: Gu, J.; Li, Y.; Li, Z.; Pang, X.
Writing - review & editing; supervision: Shen, Z.; Dong, A.; Wang, J.; Sun, B.
Writing - review and editing; supervision; resources; project administration; funding acquisition; conceptualization: Wang, K.; Ju, J.

### Availability of data and materials

Not applicable.

### AI and AI-assisted tools statement

Not applicable.

### Financial support and sponsorship

The authors would like to acknowledge the financial support for this work from the National Natural Science Foundation of China (52205334), Natural Science Foundation of Hunan Province (2025JJ40039), and the Tribology Science Fund of the State Key Laboratory of Tribology in Advanced Equipment (SKLTKF24B18).

### Conflicts of interest

Gu, J. is affiliated with State Grid Electric Power Engineering Research Institute Co., Ltd. The other authors declare that there are no conflicts of interest.

### Ethical approval and consent to participate

Not applicable.

### Consent for publication

Not applicable.

### Copyright

© The Author(s) 2026.

## REFERENCES

1. Wang, H.; Dan, X.; Chao, Q.; et al. Impact of hierarchical martensitic structure on deformation twinning in titanium alloys during additive manufacturing. *Microstructures* **2026**, *6*, 2026047. DOI
2. Zhang, X.; Chen, Y.; Hu, J. Recent advances in the development of aerospace materials. *Prog. Aerosp. Sci.* **2018**, *97*, 22-34. DOI
3. Pasang, T.; Budiman, A. S.; Wang, J.; et al. Additive manufacturing of titanium alloys - enabling re-manufacturing of aerospace and biomedical components. *Microelectron. Eng.* **2023**, *270*, 111935. DOI
4. Yue, D.; Jiang, X.; Yu, H.; Sun, D. In-situ fabricated hierarchical nanostructure on titanium alloy as highly stable and durable super-lubricated surface for anti-biofouling in marine engineering. *Chem. Eng. J.* **2023**, *463*, 142389. DOI
5. Xu, J.; Zhang, J.; Shi, Y.; et al. Surface modification of biomedical Ti and Ti alloys: a review on current advances. *Materials* **2022**, *15*, 1749. DOI PubMed PMC

6. Marin, E.; Lanzutti, A. Biomedical applications of titanium alloys: a comprehensive review. *Materials* **2023**, *17*, 114. DOI PubMed PMC
7. Najafizadeh, M.; Yazdi, S.; Bozorg, M.; et al. Classification and applications of titanium and its alloys: a review. *J. Alloys. Compd. Commun.* **2024**, *3*, 100019. DOI
8. Wang, H.; Ma, K.; Tang, J.; et al. Additively manufactured Ti6Al4V/Ta bimetal: from neutron diffraction residual stress analysis to wear and bioproperty testings. *Microstructures* **2026**, *5*, 2026036. DOI
9. Blanco, D.; Rubio, E. M.; Lorente-Pedreille, R. M.; Sáenz-Nuño, M. A. Sustainable processes in aluminium, magnesium, and titanium alloys applied to the transport sector: a review. *Metals* **2022**, *12*, 9. DOI
10. Zhang, F. F.; Feng, C.; Zhu, L. J.; Song, W. W. Research progress on corrosion resistance of titanium alloy oil well tubing. *Mater. Sci. Forum.* **2021**, *1035*, 528-33. DOI
11. Li, G.; Huang, Y.; Zhao, C.; et al. Strong yet ductile heat-resistant aluminum alloy by additive manufacturing. *Nat. Commun.* **2026**, *17*, 5230. DOI
12. Su, J.; Jiang, F.; Teng, J.; et al. Laser additive manufacturing of titanium alloys: process, materials and post-processing. *Rare. Met.* **2024**, *43*, 6288-328. DOI
13. Chen, Y.; Zhang, H.; Wang, B.; et al. A review of research on improving wear resistance of titanium alloys. *Coatings* **2024**, *14*, 786. DOI
14. Bai, H.; Zhong, L.; Kang, L.; et al. A review on wear-resistant coating with high hardness and high toughness on the surface of titanium alloy. *J. Alloys. Compd.* **2021**, *882*, 160645. DOI
15. Wang, C.; Huang, H.; Wu, H.; Hong, J.; Zhang, L.; Yan, J. Ultra-low wear of titanium alloy surface under lubricated conditions achieved by laser texturing and simultaneous nitriding. *Surf. Coat. Technol.* **2023**, *474*, 130083. DOI
16. Zhang, H.; Zhang, S.; Zhang, M.; An, J. Carburizing of Ti6Al4V alloy: structure, growth mechanism and wear performance. *J. Mater. Res. Technol.* **2023**, *27*, 7059-71. DOI
17. Thirumalvalavan, S.; Senthilkumar, N. Optimising the wear performance of HVOF thermal spray coated Ti6Al4V alloy by grey relational approach. *Int. J. Rapid. Manuf.* **2020**, *9*, 25. DOI
18. Danışman, Ş.; Odabaş, D.; Teber, M. The effect of TiN, TiAlN, TiCN thin films obtained by reactive magnetron sputtering method on the wear behavior of Ti6Al4V alloy: a comparative study. *Coatings* **2022**, *12*, 1238. DOI
19. Gabor, R.; Cvrček, L.; Doubková, M.; et al. Hybrid coatings for orthopaedic implants formed by physical vapour deposition and microarc oxidation. *Mater. Des.* **2022**, *219*, 110811. DOI
20. Huang, J.; Ma, J.; Wu, L.; Wei, J.; Li, H. Microstructure and wear resistance of $WS_2$/W composite coating on TC4 titanium alloy surface. *J. Phys. Conf. Ser.* **2021**, *1885*, 032046. DOI
21. Xiang, D.; Liu, Y.; Yu, T.; et al. Review on wear resistance of laser cladding high-entropy alloy coatings. *J. Mater. Res. Technol.* **2024**, *28*, 911-34. DOI
22. Wang, Z.; Zhang, S. Research progress of laser cladding coating on titanium alloy surface. *Coatings* **2024**, *14*, 1495. DOI
23. Li, G.; Zhang, X.; Li, H.; Zhu, B.; Yu, H.; Chen, C. The strategies for enhancing the wear resistance of titanium alloy via laser cladding: a review. *Int. J. Refract. Met. Hard. Mater.* **2026**, *136*, 107607. DOI
24. Wang, K.; Zhang, Z.; Xiang, D.; Ju, J. Research and progress of laser cladding: process, materials and applications. *Coatings* **2022**, *12*, 1382. DOI
25. Wang, K.; Liu, W.; Hong, Y.; et al. An overview of technological parameter optimization in the case of laser cladding. *Coatings* **2023**, *13*, 496. DOI
26. Liu, Z.; Zhao, D.; Wang, P.; et al. Additive manufacturing of metals: microstructure evolution and multistage control. *J. Mater. Sci. Technol.* **2022**, *100*, 224-36. DOI
27. Zhu, L.; Xue, P.; Lan, Q.; et al. Recent research and development status of laser cladding: a review. *Opt. Laser. Technol.* **2021**, *138*, 106915. DOI
28. Gao, K.; Zhang, Y.; Yi, J.; Dong, F.; Chen, P. Overview of surface modification techniques for titanium alloys in modern material science: a comprehensive analysis. *Coatings* **2024**, *14*, 148. DOI
29. Tisov, O.; Łępicka, M.; Tsybrii, Y.; Yurchuk, A.; Kindrachuk, M.; Dukhota, O. Duplex aging and gas nitriding process as a method of surface modification of titanium alloys for aircraft applications. *Metals* **2022**, *12*, 100. DOI
30. Qadir, D.; Sharif, R.; Nasir, R.; Awad, A.; Mannan, H. A. A review on coatings through thermal spraying. *Chem. Pap.* **2024**, *78*, 71-91. DOI
31. Borowski, P.; Myśliwiec, J. Recent advances in magnetron sputtering: from fundamentals to industrial applications. *Coatings* **2025**, *15*, 922. DOI
32. Deng, Y.; Chen, W.; Li, B.; Wang, C.; Kuang, T.; Li, Y. Physical vapor deposition technology for coated cutting tools: a review. *Ceram. Int.* **2020**, *46*, 18373-90. DOI
33. Fan, M.; Du, P.; Wen, K.; Zhang, R.; Yu, S.; Chen, T. Tribological properties of laser-cladded NiCrBSi coatings undergoing friction with Ti6Al4V alloys. *Coatings* **2024**, *14*, 813. DOI

34. Fan, Z.; Ren, W.; Zuo, W.; Wang, Y. Comparative study on the reinforcement effects of WC and TiC in the laser cladding layer of Ti6Al4V alloy. *J. Manuf. Process.* **2025**, *134*, 589-602. DOI
35. Zhang, T.; Zhuang, H.; Zhang, Q.; Yao, B.; Yang, F. Influence of $Y_2O_3$ on the microstructure and tribological properties of Ti-based wear-resistant laser-clad layers on TC4 alloy. *Ceram. Int.* **2020**, *46*, 13711-23. DOI
36. Liu, Y.; Li, J.; Xu, Q.; et al. Microstructure and wear behavior of TC4 laser cladding modified via SiC and $MoS_2$. *Coatings* **2022**, *12*, 792. DOI
37. Liu, J.; Lv, H.; Xie, S.; et al. Solidification microstructure prediction of Ti6Al4V alloy produced by laser melting deposition. *Coatings* **2022**, *12*, 1610. DOI
38. Zhong, M.; Liu, W. Laser surface cladding: the state of the art and challenges. *Proc. Inst. Mech. Eng. C. J. Mech. Eng. Sci.* **2010**, *224*, 1041-60. DOI
39. Liu, Y.; Yang, L.; Yang, X.; Zhang, T.; Sun, R. Optimization of microstructure and properties of composite coatings by laser cladding on titanium alloy. *Ceram. Int.* **2021**, *47*, 2230-43. DOI
40. Bermingham, M.; Stjohn, D.; Krynen, J.; Tedman-Jones, S.; Dargusch, M. Promoting the columnar to equiaxed transition and grain refinement of titanium alloys during additive manufacturing. *Acta. Mater.* **2019**, *168*, 261-74. DOI
41. Cui, C.; Wu, M.; Han, J.; et al. Preparation of FeCoNiCrMo high entropy alloy coatings by laser cladding on Ti6Al4V surface: evolution of columnar - equiaxed crystal transition and longitudinal comparison of mechanical properties. *J. Mater. Res. Technol.* **2025**, *38*, 4414-36. DOI
42. Debroy, T.; Wei, H.; Zuback, J.; et al. Additive manufacturing of metallic components - process, structure and properties. *Prog. Mater. Sci.* **2018**, *92*, 112-224. DOI
43. Liu, Y.; Wang, Y.; Yang, X.; et al. Research on microstructure and properties of Ti-based coating prepared by laser cladding on titanium alloy: simulation and experiment. *J. Mater. Res. Technol.* **2022**, *20*, 3667-82. DOI
44. Ye, Z.; Zhao, K.; Yu, Z.; et al. Understanding the solute segregation and redistribution behavior in rapidly solidified binary Ti-X alloys fabricated through non-equilibrium laser processing. *Addit. Manuf.* **2024**, *96*, 104561. DOI
45. Pinomaa, T.; Laukkanen, A.; Provatas, N. Solute trapping in rapid solidification. *MRS. Bull.* **2020**, *45*, 910-5. DOI
46. Ren, N.; Li, J.; Zhang, R.; et al. Solute trapping and non-equilibrium microstructure during rapid solidification of additive manufacturing. *Nat. Commun.* **2023**, *14*, 7990. DOI PubMed PMC
47. Chen, J.; Zheng, P.; Gong, X.; et al. Restoring the ductility of in-situ alloying additively manufactured Ti-Fe alloy via short-time heat treatment. *Mater. Sci. Eng. A.* **2025**, *948*, 149320. DOI
48. Weng, F.; Chen, C.; Yu, H. Research status of laser cladding on titanium and its alloys: a review. *Mater. Des.* **2014**, *58*, 412-25. DOI
49. Zhao, H.; Zhao, C.; Xie, W.; et al. Research progress of laser cladding on the surface of titanium and its alloys. *Materials* **2023**, *16*, 3250. DOI PubMed PMC
50. Liu, Y.; Sun, R.; Niu, W.; Zhang, T.; Lei, Y. Effects of $CeO_2$ on microstructure and properties of TiC/$Ti_2Ni$ reinforced Ti-based laser cladding composite coatings. *Opt. Lasers. Eng.* **2019**, *120*, 84-94. DOI
51. Zhao, X.; Lyu, P.; Fang, S.; et al. Microstructure and wear behavior of Ti-xFe-SiC in situ composite ceramic coatings on TC4 substrate from laser cladding. *Materials* **2023**, *17*, 100. DOI PubMed PMC
52. Cui, B.; Zhou, P.; Lv, Y. Research progress in and defect improvement measures for laser cladding. *Materials* **2025**, *18*, 3206. DOI PubMed PMC
53. Cui, D.; Aggarwal, A.; Leparoux, M. Laser metal deposition of titanium on stainless steel with high powder flowrate for high interfacial strength. *Int. J. Mater. Form.* **2024**, *17*, 1820. DOI
54. Preuß, B.; Lindner, T.; Kaur, S.; et al. Development of CoCr0.65FeNi-BSiC as a self-fluxing high-entropy alloy for thermal spraying. *Surf. Coat. Technol.* **2024**, *476*, 130259. DOI
55. Pereira, J. C.; Taboada, M. C.; Niklas, A.; Rayón, E.; Rocchi, J. Influence of the chemical composition on the solidification path, strengthening mechanisms and hardness of Ni-Cr-Si-Fe-B self-fluxing alloys obtained by laser-directed energy deposition. *J. Manuf. Mater. Process.* **2023**, *7*, 110. DOI
56. Meng, Q.; Wang, C.; Liu, T.; Song, Q.; Xue, B.; Cui, H. Microstructure and performance optimization of laser cladding nano-TiC modified nickel-based alloy coatings. *Surf. Coat. Technol.* **2024**, *479*, 130583. DOI
57. Jin, F.; Zhang, S.; Wu, C. L.; Zhang, C. H.; Sun, X. Y.; Bai, X. L. Comparative study on the microstructure, wear behavior, and corrosion performance of iron-based and cobalt-based coatings fabricated by laser cladding. *J. Mater. Eng. Perform.* **2024**, *33*, 12398-412. DOI
58. Zhang, H.; Zhang, S.; Wu, H.; et al. Mechanical properties and corrosion resistance of laser cladding iron-based coatings with two types of NbC reinforcement. *Surf. Coat. Technol.* **2024**, *479*, 130558. DOI

59. Jie, G.; Yan, S.; Kangning, W.; Qiang, S.; Canming, W. Effect of Fe content on microstructure and corrosion resistance of Ni-based alloy formed by laser cladding. *Surf. Coat. Technol.* **2022**, *446*, 128761. DOI
60. Li, R.; Feng, A.; Zhao, J.; et al. Study on process optimization of WC-Ni60A cermet composite coating by laser cladding. *Mater. Today. Commun.* **2023**, *37*, 107400. DOI
61. Wang, F.; Li, X.; Peng, J.; Liu, Z.; Feng, X. The Microstructure and properties of Ni60 cladding layer by laser cladding on TC4 alloy surface. *J. Phys. Conf. Ser.* **2023**, *2566*, 012070. DOI
62. Zhang, T.; Yan, X.; Zhen, H.; Zhang, Q.; Zhang, Z. Influence of Cu addition on the microstructure and tribological properties of Ti-based laser cladded composite coatings on TC4. *Mater. Today. Commun.* **2024**, *40*, 110220. DOI
63. Shi, Z.; Pang, M. Study on the effect of Co12 content variation on the properties of Co12/TC4 composite coating with in situ reinforced phase under nitrogen protective atmosphere. *J. Mater. Sci.* **2023**, *58*, 10166-88. DOI
64. Weng, F.; Yu, H.; Chen, C.; Dai, J. Microstructures and wear properties of laser cladding Co-based composite coatings on Ti6Al4V. *Mater. Des.* **2015**, *80*, 174-81. DOI
65. Liu, X.; Wang, H.; Liu, C.; et al. Microstructural characteristics and properties of stellite 6 coatings on TC4 titanium alloy processed at different laser powers. *Mater. Today. Commun.* **2026**, *50*, 114415. DOI
66. Kazamer, N.; Muntean, R.; Vălean, P. C.; Pascal, D. T.; Mărginean, G.; Șerban, V. A. Comparison of Ni-based self-fluxing remelted coatings for wear and corrosion applications. *Materials* **2021**, *14*, 3293. DOI PubMed PMC
67. Simunovic, K.; Saric, T.; Simunovic, G. Different approaches to the investigation and testing of the Ni-based self-fluxing alloy coatings-a review. Part 2: microstructure, adhesive strength, cracking behavior, and residual stresses investigations. *Tribol. Trans.* **2014**, *57*, 980-1000. DOI
68. Wang, Y.; Feng, C.; Lin, T.; et al. A review of wear-resistant coatings for steel substrates: applications and challenges. *Metals* **2025**, *15*, 1231. DOI
69. Górka, J.; Lont, A.; Poloczek, T. The microstructure and properties of laser-cladded Ni-based self-fluxing alloy coatings reinforced by TiC particles. *Coatings* **2025**, *15*, 527. DOI
70. Fu, J.; Yang, Q.; Devojno, O.; Kardapolava, M.; Kasiakova, I.; Wang, C. Wear resistance design of laser cladding Ni-based self-fluxing alloy coating using machine learning. *Materials* **2024**, *17*, 5651. DOI PubMed PMC
71. Baydoun, S.; Moul-el-ksour, F.; Fouvry, S.; et al. Tribological investigation of new self-fluxing nickel alloys for high temperature application: the effect of silicon distribution on glaze layer formation. *Wear* **2025**, *564-565*, 205631. DOI
72. Liu, X.; Meng, L.; Zeng, X.; et al. Studies on high power laser cladding stellite 6 alloy coatings: metallurgical quality and mechanical performances. *Surf. Coat. Technol.* **2024**, *481*, 130647. DOI
73. Singla, Y. K.; Maughan, M. R.; Arora, N.; Dwivedi, D. Enhancing the wear resistance of iron-based alloys: a comprehensive review of alloying element effects. *J. Manuf. Process.* **2024**, *120*, 135-60. DOI
74. Feng, Y.; Pang, X.; Feng, K.; Feng, Y.; Li, Z. Study on microstructure and compressive properties of Fe-C-W-Cr-V-Nb coating with boron addition. *J. Alloys. Compd.* **2022**, *904*, 163986. DOI
75. Liu, L.; Lin, Y.; Peng, L.; Kang, X.; Wang, X. Progress in microstructure design and control of high-hardness Fe-based alloy coatings via laser cladding. *Coatings* **2024**, *14*, 1351. DOI
76. Prasanthi, T. N.; Sudha, C.; Saroja, S. An overview on the microstructure and properties of Fe/Ti based dissimilar joints. *Mater. Sci. Technol.* **2023**, *39*, 2595-615. DOI
77. Xiao, Q.; Xia, J.; Gao, X.; et al. Investigation of the microstructure and wear properties of conventional laser cladding and ultra-high-speed laser cladding alloy coatings for wheel materials. *Coatings* **2023**, *13*, 949. DOI
78. Fang, Y.; Jiang, X.; Song, T.; Mo, D.; Luo, Z. Interfacial reaction and microstructure investigation of TC4/Co/4J29 diffusion-bonded joints. *Mater. Lett.* **2019**, *253*, 59-62. DOI
79. Mou, G.; Hua, X.; Wang, M.; Li, F. Effects of Ni addition on removing Fe-Ti intermetallic compounds in cold metal transfer arc-brazed TC4/304L dissimilar joints. *J. Manuf. Process.* **2019**, *38*, 104-12. DOI
80. Liu, J.; Chen, G.; Ma, Y.; et al. Formation mechanism and control of welding cracks in dissimilar materials of $Ni_{50}Ti_{50}$ SMA and Ti6Al4V. *J. Manuf. Process.* **2022**, *75*, 552-64. DOI
81. Li, M.; Huang, K.; Yi, X. Crack formation mechanisms and control methods of laser cladding coatings: a review. *Coatings* **2023**, *13*, 1117. DOI
82. Li, J.; Chen, Y.; Guan, C.; Zhang, C.; Zhao, J.; Yu, T. Microstructure and wear resistance of in situ synthesized Ti(C, N) ceramic-reinforced nickel-based coatings by laser cladding. *Materials* **2024**, *17*, 3878. DOI PubMed PMC
83. Wen, M.; Jiang, B.; Duan, X.; Xiang, D. Research progress on microstructure, mechanical properties, and strengthening mechanisms of in situ-synthesized ceramic-reinforced titanium matrix composite coatings via laser cladding. *Coatings* **2025**, *15*, 815. DOI
84. Li, N.; He, D.; Liu, D.; et al. In-situ TiB reinforced titanium matrix composite coatings prepared by laser cladding: effect of $TiB_2$ content on microstructure, hardness and wear properties. *J. Alloys. Compd.* **2025**, *1010*, 178215. DOI

85. Yang, Y.; Ma, S.; Li, K.; Han, H.; Lei, J. Boosted wear and electrochemical corrosion resistance properties of Ti6Al4V alloy via graphene nanoplatelets and titanium particles. *J. Manuf. Process.* **2024**, *124*, 818-33. DOI
86. Chen, H.; Yu, D.; Mao, J.; et al. Microstructure and tribo-corrosion behavior of TC4 composites reinforced by in situ synthesized TiC ceramics particles through laser cladding. *Ceram. Int.* **2025**, *51*, 31719-33. DOI
87. Wang, H.; Wu, A.; Wu, M.; Miao, X. SiC reinforced Ti-based coatings: in-situ generation of TiC and strengthening mechanism. *Ceram. Int.* **2025**, *51*, 46514-25. DOI
88. Heng, W.; Pang, M. Microstructure and wear resistance of laser cladding NiCrAlY/TC4 composite coatings with in-situ synthesized transition layer by modulating thermal boundary in nitrogen atmosphere. *J. Mater. Sci.* **2023**, *58*, 16119-43. DOI
89. Chen, T.; Li, W.; Liu, D.; Xiong, Y.; Zhu, X. Effects of heat treatment on microstructure and mechanical properties of TiC/TiB composite bioinert ceramic coatings in-situ synthesized by laser cladding on Ti6Al4V. *Ceram. Int.* **2021**, *47*, 755-68. DOI
90. Mi, H.; Chen, T.; Deng, Z.; Li, S.; Liu, J.; Liu, D. Microstructure and mechanical properties of TiC/TiB composite ceramic coatings in-situ synthesized by ultrasonic vibration-assisted laser cladding. *Coatings* **2022**, *12*, 99. DOI
91. Wang, L.; Yang, L.; Huang, Y.; Yuan, Y.; Jia, C. Effects of $Y_2O_3$ addition on the microstructure and wear-resistant performance of TiN/TiB-reinforced Ti-based laser-clad coatings on Ti-6Al-4V alloys. *Mater. Today. Commun.* **2021**, *29*, 102752. DOI
92. Wen, H.; Pang, M.; Hu, Y. Study on fabrication of multi-phase reinforcement coatings on Ti6Al4V by laser cladding for enhanced tribological performance. *Mater. Today. Commun.* **2024**, *41*, 110566. DOI
93. Xu, S.; Cai, Q.; Li, G.; Lu, X.; Zhu, X. Effect of scanning speed on microstructure and properties of TiC/Ni60 composite coatings on Ti6Al4V alloy by laser cladding. *Opt. Laser. Technol.* **2022**, *154*, 108309. DOI
94. Feng, M.; Ma, Y.; Tian, Y.; Cao, H. Microstructure and wear resistance of Ti6Al4V titanium alloy laser-clad Ni60/WC composite coating. *Materials* **2024**, *17*, 264. DOI PubMed PMC
95. Jiang, T.; Kim, H. S. Simultaneous improvement in the hardness and friction characteristics of Ti6Al4V through laser cladding with nanoscale SiC particles in an air environment. *Int. J. Adv. Manuf. Technol.* **2021**, *116*, 1041-51. DOI
96. Liu, D.; He, D.; Li, H.; et al. Multi-ceramic phases synergistically reinforced titanium matrix composite coating deposited by laser cladding: effect of B4C content on the microstructure and wear properties. *Surf. Coat. Technol.* **2025**, *496*, 131648. DOI
97. Liu, Y.; Zhu, L.; Liu, X.; et al. Microstructure and properties of Ni-TiCN composite coatings on Ti6Al4V substrate by laser cladding. *J. Therm. Spray. Tech.* **2025**, *34*, 1915-25. DOI
98. Li, Y.; Su, K.; Bai, P.; et al. Effect of TiBCN content on microstructure and properties of laser cladding Ti/TiBCN composite coatings. *Met. Mater. Int.* **2019**, *25*, 1366-77. DOI
99. Lin, Y.; Wang, H.; Zhang, M.; et al. Gradient coating of laser cladding $TiB_2$/Ti-based alloy on titanium alloy surface. *Coatings* **2023**, *13*, 743. DOI
100. Zhang, Y.; Liu, Z.; Lv, Z.; et al. Effect of SiC and TiC content on microstructure and wear behavior of Ni-based composite coating manufactured by laser cladding on Ti6Al4V. *Wear* **2024**, *552-553*, 205431. DOI
101. Shi, H.; Gao, Z.; Li, Y.; Li, X.; Wang, L.; Zhan, X. Morphological characteristics of precipitated phases in laser cladding (Nano WC + Micron TiC)/Ti6Al4V coatings with different composite ceramic contents. *Met. Mater. Int.* **2024**, *30*, 2581-94. DOI
102. Tang, J.; Wang, K.; Fu, H. Laser cladding in situ carbide-reinforced iron-based alloy coating: a review. *Metals* **2024**, *14*, 1419. DOI
103. Jiang, D.; Wang, G.; Dong, W.; Hong, X.; Guo, C. Recent advance on metal carbides reinforced laser cladding coatings. *Molecules* **2025**, *30*, 1820. DOI PubMed PMC
104. Zhang, Y.; Liu, Z.; Yang, C.; et al. Microstructure and wear behavior of laser-cladded WC matrix composite coatings with different TiC/Ni contents on titanium alloys. *Ceram. Int.* **2025**, *51*, 27229-42. DOI
105. Chen, C.; Li, W.; Wang, S. Interlayer laser cladding SiC regulates microstructure and mechanical properties of Ti6Al4V arc-directed energy deposited components. *Virtual. Phys. Prototyp.* **2024**, *19*, e2399183. DOI
106. Wei, M.; Yu, H.; Song, Z.; et al. Microstructural evolution, mechanical properties and wear behavior of in-situ TiC-reinforced Ti matrix composite coating by induction cladding. *Surf. Coat. Technol.* **2021**, *412*, 127048. DOI
107. Wang, Y.; Tan, H.; Feng, Z.; et al. Enhanced mechanical properties of in situ synthesized TiC/Ti composites by pulsed laser directed energy deposition. *Mater. Sci. Eng. A.* **2022**, *855*, 143935. DOI
108. Ou, B.; Lu, L.; Wang, Q.; He, Q.; Xie, Y.; Yan, J. Mechanical properties of TC11 titanium alloy and graphene nanoplatelets/TC11 composites prepared by selective laser melting. *Int. J. Mol. Sci.* **2022**, *23*, 6134. DOI PubMed PMC
109. Mihai, S.; Baciu, F.; Radu, R.; Chioibasu, D.; Popescu, A. C. In situ fabrication of TiC/Ti-matrix composites by laser directed energy deposition. *Materials* **2024**, *17*, 4284. DOI PubMed PMC
110. Jiang, Q.; Li, S.; Guo, S.; Fu, M.; Zhang, B. Comparative study on process-structure-property relationships of TiC/Ti6Al4V and Ti6Al4V by selective laser melting. *Int. J. Mech. Sci.* **2023**, *241*, 107963. DOI
111. Maurya, P.; Kota, N.; Gibmeier, J.; Wanner, A.; Roy, S. Review on study of internal load transfer in metal matrix composites using diffraction techniques. *Mater. Sci. Eng. A.* **2022**, *840*, 142973. DOI

112. Gülenç, İT.; Bai, M.; Mitchell, R. L.; Todd, I.; Inkson, B. J. In situ TiC reinforced Ti6Al4V matrix composites manufactured via selective laser melting. *RPJ* **2024**, *30*, 378-92. DOI
113. Wang, H.; Hu, Y.; Wang, L.; et al. Enhancing the wearing resistance of TC17 alloy by nano/micro-TiC ceramic through directed energy deposition. *Mater. Today. Commun.* **2024**, *39*, 109083. DOI
114. Cai, Q.; Li, G.; Wu, B.; Xu, S.; Wang, L.; Guo, Y. Effect of TiC content on microstructure and properties of TiC/Ni60 coatings on Ti6Al4V alloy deposited by laser cladding. *Opt. Laser. Technol.* **2024**, *168*, 109854. DOI
115. Wu, Y.; Ma, L.; Duan, Y.; et al. Constructing serrated boride composite layer for enhancing wear resistance of Ti6Al4V alloy. *Rare. Metals.* **2026**, *45*, e70025. DOI
116. Konstantinov, A.; Bazhin, P.; Stolin, A.; Kostitsyna, E.; Ignatov, A. Ti-B-based composite materials: properties, basic fabrication methods, and fields of application (review). *Compos. Part. A. Appl. Sci. Manuf.* **2018**, *108*, 79-88. DOI
117. Singh, H.; Hayat, M.; Zhang, H.; Das, R.; Cao, P. Effect of $TiB_2$ content on microstructure and properties of in situ Ti-TiB composites. *Int. J. Miner. Metall. Mater.* **2019**, *26*, 915-24. DOI
118. Kurita, H.; Suzuki, S.; Kikuchi, S.; Yodoshi, N.; Gourdet, S.; Narita, F. Strengthening mechanism of titanium boride whisker-reinforced Ti6Al4V alloy matrix composites with the TiB orientation perpendicular to the loading direction. *Materials* **2019**, *12*, 2401. DOI PubMed PMC
119. Zhang, Q.; Sun, W.; Xu, S.; Zhang, X.; Wang, J.; Si, C. Nano-TiB whiskers reinforced Ti-6Al-4 V matrix composite fabricated by direct laser deposition: microstructure and mechanical properties. *J. Alloys. Compd.* **2022**, *922*, 166171. DOI
120. Ma, F.; Liu, P.; Li, W.; et al. The mechanical behavior dependence on the TiB whisker realignment during hot-working in titanium matrix composites. *Sci. Rep.* **2016**, *6*, 36126. DOI PubMed PMC
121. Li, B.; Shang, J.; Guo, J.; Fu, H. In situ observation of fracture behavior of in situ TiBw/Ti composites. *Mater. Sci. Eng. A.* **2004**, *383*, 316-22. DOI
122. Shen, X.; Zhang, Z.; Wei, S.; Wang, F.; Lee, S. Microstructures and mechanical properties of the in situ TiB-Ti metal-matrix composites synthesized by spark plasma sintering process. *J. Alloys. Compd.* **2011**, *509*, 7692-6. DOI
123. Zhou, Z.; Liu, Y.; Liu, X.; Wu, L. High-temperature tensile and creep properties of TiB-reinforced Ti6Al4V composite fabricated by laser powder bed fusion. *Mater. Charact.* **2023**, *200*, 112859. DOI
124. Zhao, X.; Lu, X.; Zuo, H.; Ma, S.; Wang, C.; Li, M. V. TiBw reinforced titanium matrix composites fabricated by selective laser melting: influence of energy density on microstructure and tribological performance. *Ceram. Int.* **2023**, *49*, 28920-33. DOI
125. Cai, C.; He, S.; Li, L.; et al. In-situ TiB/Ti6Al4V composites with a tailored architecture produced by hot isostatic pressing: microstructure evolution, enhanced tensile properties and strengthening mechanisms. *Compos. Part. B. Eng.* **2019**, *164*, 546-58. DOI
126. Zheng, Y.; Xu, L.; Chi, D.; et al. Tensile and creep properties under different temperature conditions of titanium matrix composites reinforced by TiB and TiC. *Mater. Sci. Eng. A.* **2022**, *860*, 144279. DOI
127. Zhang, Z.; Han, Q.; Liu, Z.; et al. Influence of the $TiB_2$ content on the processability, microstructure and high-temperature tensile performance of a Ni-based superalloy by laser powder bed fusion. *J. Alloys. Compd.* **2022**, *908*, 164656. DOI
128. Wang, H.; Zhao, L.; Peng, Y.; Cai, X.; Tian, Z. Microstructure and mechanical properties of $TiB_2$ reinforced tial-based alloy coatings prepared by laser melting deposition. *Acta. Met. Sin.* **2023**, *59*, 226-36. DOI
129. Ammisetti, D. K.; Kruthiventi, S. S. H.; Vinjavarapu, S.; Babu, N. N.; Gandepudi, J. R.; Battula, S. K. A review on reinforcements, fabrication methods, and mechanical and wear properties of titanium metal matrix composites. *J. Eng. Appl. Sci.* **2024**, *71*, 392. DOI
130. Jeje, S. O.; Shongwe, M. B. Wear and oxidation behavior of Ti-7Al-1Mo/TiN composites fabricated via spark plasma sintering. *Int. J. Adv. Manuf. Technol.* **2024**, *133*, 559-69. DOI
131. Morton, P.; Taylor, H.; Murr, L.; Delgado, O.; Terrazas, C.; Wicker, R. In situ selective laser gas nitriding for composite TiN/Ti6Al4V fabrication via laser powder bed fusion. *J. Mater. Sci. Technol.* **2020**, *45*, 98-107. DOI
132. Sahasrabudhe, H.; Soderlind, J.; Bandyopadhyay, A. Laser processing of in situ TiN/Ti composite coating on titanium. *J. Mech. Behav. Biomed. Mater.* **2016**, *53*, 239-49. DOI PubMed
133. Mandal, V.; Tripathi, P.; Sharma, S.; et al. Fabrication of ex-situ TiN reinforced IN718 composites using laser powder bed fusion (L-PBF): experimental characterization and high-fidelity numerical simulations. *Ceram. Int.* **2023**, *49*, 14408-25. DOI
134. Zhang, H.; Cui, H.; Man, C.; et al. The tribocorrosion resistance of TiN+TiB/TC4 composite coatings and the synergistic strengthening effects of multi-level reinforcements. *Corros. Sci.* **2023**, *219*, 111224. DOI
135. Sánchez, de. Rojas. Candela. C.; Riquelme, A.; Rodrigo, P.; et al. A one-step novel method to fabricate multigrade Ti6Al4V/TiN composites using laser powder bed fusion. *Coatings* **2024**, *14*, 90. DOI
136. Huang, L.; Li, L.; Zhao, Y.; et al. Microstructure and properties of Ti6Al4V surface processed by continuous wave laser in different atmospheres. *Coatings* **2024**, *14*, 753. DOI

137. Zhang, L.; Shao, M.; Wang, Z.; et al. Comparison of tribological properties of nitrided Ti-N modified layer and deposited TiN coatings on TA2 pure titanium. *Tribol. Int.* **2022**, *174*, 107712. DOI
138. Zhao, Y.; Lu, M.; Yin, Y.; Lin, W.; Huang, H. Laser gas alloying of Ti6Al4V in air for tribological applications. *Appl. Surf. Sci.* **2021**, *570*, 151125. DOI
139. Li, G.; Yao, X.; Wood, R. J.; Guo, J.; Shi, Y. Laser surface nitriding of Ti6Al4V alloy in nitrogen-argon atmospheres. *Coatings* **2020**, *10*, 1009. DOI
140. Das, A. K. Effect of rare earth oxide additive in coating deposited by laser cladding: a review. *Mater. Today. Proc.* **2022**, *52*, 1558-64. DOI
141. Zhang, B.; Liu, K.; Li, J.; Chen, B.; Huang, C.; Soboleva, N. A comprehensive review on the rare earth elements improving microstructure and properties of laser cladded coatings. *J. Alloys. Compd.* **2025**, *1036*, 181761. DOI
142. Wang, H.; Chen, T.; Cong, W.; Liu, D. Laser cladding of Ti-based ceramic coatings on Ti6Al4V alloy: effects of $CeO_2$ nanoparticles additive on wear performance. *Coatings* **2019**, *9*, 109. DOI
143. Xia, K.; Feng, A.; Ye, Z. Effect of $Y_2O_3$ content on microstructure and wear resistance of laser cladding layer of stellite-6 alloy. *Processes* **2024**, *12*, 1119. DOI
144. Xu, S.; Han, K.; Wang, H.; Xi, Y.; Wang, L.; Dong, X. The influence of adding $B_4C$ and $CeO_2$ on the mechanical properties of laser cladding nickel-based coatings on the surface of TC4 titanium alloy. *Materials* **2024**, *17*, 3823. DOI PubMed PMC
145. Zhang, T.; Xiao, H.; Zhang, Z.; Yao, B.; Yang, F. Effect of $Y_2O_3$ addition on microstructural characteristics and microhardness of laser-cladded Ti6Al4V alloy coating. *J. Mater. Eng. Perform.* **2020**, *29*, 8221-35. DOI
146. Zhang, Z.; Yao, X.; Pei, X.; et al. Influence of $Y_2O_3$ addition amount on the microstructure and wide-temperature range tribological properties of wear-resistant and friction-reducing titanium-based coatings. *Surf. Coat. Technol.* **2025**, *515*, 132657. DOI
147. Wang, C.; Zhang, Q.; Zhang, T.; et al. Effects of $Y_2O_3$ content on the microstructure and tribological properties of WC-reinforced Ti-based coatings on TC4 surfaces. *Coatings* **2024**, *14*, 1110. DOI
148. Ding, M.; Zhang, Y.; Han, G.; Wang, Y.; Zhang, W. Mechanisms of microstructure refinement and wear resistance in laser-cladded $La_2O_3$/TiB composite coatings: experimental and numerical insights. *Modelling* **2025**, *6*, 163. DOI
149. Tong, W.; Xu, Q.; Liu, Y.; Qi, Z.; Wang, J.; Liu, J. The effect of $CeO_2$ content on the microstructure and properties of TiC/WC/Co composite cladding layers. *Coatings* **2025**, *15*, 530. DOI
150. Peera, S. G.; Kim, S. W. Rare Earth Ce/$CeO_2$ electrocatalysts: role of high electronic spin state of Ce and $Ce^{3+}/Ce^{4+}$ redox couple on oxygen reduction reaction. *Nanomaterials* **2025**, *15*, 600. DOI PubMed PMC
151. He, X.; Kong, D.; Song, R. Microstructures and properties of laser cladding Al-TiC-$CeO_2$ composite coatings. *Materials* **2018**, *11*, 198. DOI PubMed PMC
152. Zhang, L.; Zhang, M.; Zhu, Z.; Gao, M.; Gao, J.; Guo, Z. Effects of nano-$CeO_2$ on microstructure and properties of Ni625 alloy prepared by laser cladding. *J. Alloys. Compd.* **2022**, *918*, 165571. DOI
153. Zhuang, H.; Zhang, Q.; Zhang, D. Microstructure and tribological properties of Ni-based laser-clad coatings by rare earth modification. *J. Therm. Spray. Tech.* **2021**, *30*, 1410-31. DOI
154. Gong, Y.; Wu, M.; Miao, X.; Cui, C. Effect of $CeO_2$ on crack sensitivity and tribological properties of Ni60A coatings prepared by laser cladding. *Adv. Mech. Eng.* **2021**, *13*, 16878140211013125. DOI
155. Chen, T.; Liu, D.; Wu, F.; Wang, H. Effect of $CeO_2$ on microstructure and wear resistance of TiC bioinert coatings on Ti6Al4V alloy by laser cladding. *Materials* **2017**, *11*, 58. DOI PubMed PMC
156. Kurapova, O. Y.; Shugurov, S. M.; Vasil'eva, E. A.; Savelev, D. A.; Konakov, V. G.; Lopatin, S. I. Thermal prehistory, structure and high-temperature thermodynamic properties of $Y_2O_3$-$CeO_2$ and $Y_2O_3$-$ZrO_2$-$CeO_2$ solid solutions. *Ceram. Int.* **2021**, *47*, 11072-9. DOI
157. Zhang, Z.; Yang, Q.; Yu, Z.; Wang, H.; Zhang, T. Influence of $Y_2O_3$ addition on the microstructure of TiC reinforced Ti-based composite coating prepared by laser cladding. *Mater. Charact.* **2022**, *189*, 111962. DOI
158. Zhang, C.; Li, Z.; Liu, X.; et al. Development and wear performance of ceramic TiC reinforced Ni-based solid lubrication composite coatings by laser cladding. *Ceram. Int.* **2025**, *51*, 38884-98. DOI
159. Liu, K.; Yan, H.; Zhang, P.; Zhao, J.; Yu, Z.; Lu, Q. Wear behaviors of TiN/$WS_2$ + hBN/NiCrBSi self-lubricating composite coatings on TC4 alloy by laser cladding. *Coatings* **2020**, *10*, 747. DOI
160. Wang, C.; Yan, X.; Zhang, T.; Zhang, Q.; Zhang, Z. Microstructure and tribological properties of WC/Ni-$MoS_2$ titanium-based composite coating on TC4. *Coatings* **2024**, *14*, 1157. DOI
161. Zhang, T.; Zhen, H.; Liu, T.; Hou, X.; Zhang, Z. Microstructure and tribological properties of lubricating-reinforcing laser cladding composite coating with the $Ti_2SC$-$Ti_2Ni$ mosaic structure phase. *Coatings* **2022**, *12*, 876. DOI

162. Shi, Z.; Pang, M. Study on the performance of laser nitriding in situ enhanced Co12/TC4 composite Ag self-lubricating coating on TC4 surface. *J. Mater. Sci.* **2023**, *58*, 18207-27. DOI
163. Qu, C.; Li, J.; Juan, Y.; et al. Effects of the content of $MoS_2$ on microstructural evolution and wear behaviors of the laser-clad coatings. *Surf. Coat. Technol.* **2019**, *357*, 811-21. DOI
164. Gao, Q.; Yan, H.; Qin, Y.; et al. Laser cladding Ti-Ni/TiN/TiW+TiS/$WS_2$ self-lubricating wear resistant composite coating on Ti6Al4V alloy. *Opt. Laser. Technol.* **2019**, *113*, 182-91. DOI
165. Zhang, F.; Liu, X.; Chen, G.; et al. Microstructure evolution and tribological properties of laser cladding stellite6-Cu/Graphene composite coatings on TC4 alloy. *Tribol. Int.* **2025**, *204*, 110463. DOI
166. Miao, X.; Wu, M.; Cui, C.; Wang, H. Effect of graphene oxide on the performance of Co-based coatings on Ti6Al4V alloys by laser cladding. *Coatings* **2020**, *10*, 1048. DOI
167. Xiang, Z.; Liu, X.; Ren, J.; et al. Investigation of laser cladding high temperature anti-wear composite coatings on Ti6Al4V alloy with the addition of self-lubricant $CaF_2$. *Appl. Surf. Sci.* **2014**, *313*, 243-50. DOI
168. Gao, L.; Meng, W.; Pang, M. Effect of h-BN content on tribological properties of laser-cladded titanium-based self-lubricating coatings on TC4 surfaces. *J. Mater. Eng. Perform.* **2026**, *35*, 329-43. DOI
169. Qu, C.; He, B.; Cheng, X.; Wang, H. Microstructure and wear characteristics of laser-clad Ni-based self-lubricating coating incorporating $MoS_2$/Ag for use in high temperature. *J. Mater. Res. Technol.* **2024**, *33*, 4481-92. DOI
170. Zhu, Y.; Liu, X.; Liu, Y.; et al. Development and characterization of Co-Cu/$Ti_3SiC_2$ self-lubricating wear resistant composite coatings on Ti6Al4V alloy by laser cladding. *Surf. Coat. Technol.* **2021**, *424*, 127664. DOI
171. Wang, Y.; Liu, X.; Liu, Y.; Luo, Y.; Meng, Y. Microstructure and tribological performance of Ni60-based composite coatings on Ti6Al4V alloy with different $Ti_3SiC_2$ ceramic additions by laser cladding. *Ceram. Int.* **2020**, *46*, 28996-9010. DOI
172. Hua, S.; Pang, M.; Chen, J.; Ji, F. Effects of frictional loading on tribological properties of laser cladding Ti2AlC/TC4-coated TiC particle-reinforced coatings on Ti6Al4V. *J. Mater. Eng. Perform.* **2024**, *33*, 2077-92. DOI
173. Hua, S.; Pang, M.; Chen, J.; Zhao, J.; Ji, F. Microstructure and tribological performance of laser cladding $Ti_2AlC$ particle reinforced coatings on Ti6Al4V. *J. Mater. Eng. Perform.* **2023**, *32*, 8452-66. DOI
174. Ouyang, J.; Li, Y.; Zhang, Y.; Wang, Y.; Wang, Y. High-temperature solid lubricants and self-lubricating composites: a critical review. *Lubricants* **2022**, *10*, 177. DOI
175. Zhu, S.; Cheng, J.; Qiao, Z.; Yang, J. High temperature solid-lubricating materials: a review. *Tribol. Int.* **2019**, *133*, 206-23. DOI
176. Kumar, S.; Mandal, A.; Das, A. K.; Das, P. Development of a Cu/$MoS_2$/Ni Self-lubricating composite clad through laser additive approach over a Ti6Al4V substrate and its characterizations. *Langmuir* **2023**, *39*, 17201-15. DOI
177. Gonzalez-julian, J. Processing of MAX phases: From synthesis to applications. *J. Am. Ceram. Soc.* **2021**, *104*, 659-90. DOI
178. Chu, M.; Xiao, H.; Ren, L.; Mo, T.; Lin, B. Microstructure and properties of Ti-Al-C composite coatings prepared by laser cladding. *Ceram. Int.* **2024**, *50*, 12498-509. DOI
179. Lei, X.; Lin, N. Structure and synthesis of MAX phase materials: a brief review. *Crit. Rev. Solid. State. Mater. Sci.* **2022**, *47*, 736-71. DOI
180. Hua, S.; Pang, M.; Ji, F.; Chen, J.; Liu, G. Microstructure and tribological properties of $Ti_2AlC$-B particle-enhanced self-lubricating coatings on Ti6Al4V by ultrasonic impact treatment and laser cladding. *Mater. Today. Commun.* **2023**, *34*, 105165. DOI
181. Yan, H.; Liu, K.; Zhang, P.; et al. Fabrication and tribological behaviors of $Ti_3SiC_2$/$Ti_5Si_3$/TiC/Ni-based composite coatings by laser cladding for self-lubricating applications. *Opt. Laser. Technol.* **2020**, *126*, 106077. DOI
182. Sun, L.; Cao, Y.; Ding, H.; et al. Fabrication of composite coatings containing in-situ reacted $Ti_2AlC$/$Ti_2AlN$ MAX phases by laser cladding and investigation of fretting wear mechanism. *Ceram. Int.* **2024**, *50*, 39138-49. DOI
183. Wu, Y.; Zhao, X.; Chen, Q.; et al. Strengthening and fracture mechanisms of a precipitation hardening high-entropy alloy fabricated by selective laser melting. *Virtual. Phys. Prototyp.* **2022**, *17*, 451-67. DOI
184. Wang, K.; Yi, Z.; Song, Z.; et al. Wear behaviors of laser-directed energy deposited Inconel 625 alloys-based composite coating by different oscillating laser paths. *Opt. Laser. Technol.* **2025**, *192*, 113900. DOI
185. Liu, Y.; Yang, Y.; Chen, C. Microstructure and properties of Ni-Ti based gradient laser cladding layer of Ti6Al4V alloy by laser powder bed fusion. *Addit. Manuf.* **2024**, *79*, 103906. DOI
186. Lu, S.; Zhou, J.; Wang, L.; Liang, J. Effect of V and Cr transition layers on microstructure and mechanical properties of Ni-based coating on titanium alloy fabricated by laser cladding. *Surf. Coat. Technol.* **2021**, *405*, 126734. DOI
187. Cheng, H.; Shin, K.; Kim, H. S. Enhancement of mechanical and tribological performance of Ti6Al4V alloy by laser surface alloying with Inconel 625 and SiC precursor materials. *Friction* **2024**, *12*, 2089-107. DOI
188. Gong, L.; Li, Y.; Wang, X.; Li, S.; Yang, Z.; Chen, H. Progress in additive manufacturing of nickel-based superalloys: materials, processing, microstructures, properties and alloy design. *Rare. Metals.* **2025**, *44*, 7041-87. DOI

189. Konovalov, S.; Osintsev, K.; Golubeva, A.; et al. Surface modification of Ti-based alloy by selective laser melting of Ni-based superalloy powder. *J. Mater. Res. Technol.* **2020**, *9*, 8796-807. DOI
190. Sun, Z.; Ji, X.; Zhang, W.; et al. Microstructure evolution and high temperature resistance of Ti6Al4V/Inconel625 gradient coating fabricated by laser melting deposition. *Mater. Des.* **2020**, *191*, 108644. DOI
191. Sun, H.; Wang, D.; Zhao, H.; et al. Analysis of microstructure and properties of laser cladding Inconel625 on TC4 surface. *J. Phys. Conf. Ser.* **2025**, *3026*, 012043. DOI
192. Zamzu, C. O.; Jia, Z.; Shen, B. Advancing high-entropy alloy design: from experimental methods to machine-learning integration. *Rare. Metals.* **2026**, *45*, e70199. DOI
193. Zhang, W.; Wang, X.; Zhang, F.; et al. Frontiers in high entropy alloys and high entropy functional materials. *Rare. Metals.* **2024**, *43*, 4639-776. DOI
194. Liao, L.; Zhou, S.; Cheng, Y.; et al. Microstructure characteristics and high-temperature properties of AlCoCrFeNi high entropy alloy coating on TC4 alloy prepared by laser cladding. *Surf. Interfaces.* **2025**, *74*, 107717. DOI
195. Zhang, G.; Han, L.; Sun, Y.; et al. The high-temperature oxidation resistance and tribological properties of $(FeCoCr)_{75}Ni_{10}(BSi)_{15-x}Ta_x$ high-entropy alloy coating by laser cladding. *Phys. Scr.* **2025**, *100*, 095941. DOI
196. Dai, R.; Wang, H.; Wei, A.; et al. Phase and tribological behavior of $Al_{0.5}Ti_2NbVZr_x$ lightweight refractory HEA coatings. *Surf. Coat. Technol.* **2025**, *516*, 132731. DOI
197. Zhang, H.; Dai, J.; Sun, C.; Li, S. Microstructure and wear resistance of TiAlNiSiV high-entropy laser cladding coating on Ti6Al4V. *J. Mater. Process. Technol.* **2020**, *282*, 116671. DOI
198. Deng, C.; Wang, C.; Chai, L.; Wang, T.; Luo, J. Mechanical and chemical properties of $CoCrFeNiMo_{0.2}$ high entropy alloy coating fabricated on Ti6Al4V by laser cladding. *Intermetallics* **2022**, *144*, 107504. DOI
199. Zeng, X.; Liu, Z.; Wu, G.; et al. Microstructure and high-temperature properties of laser cladded $AlCoCrFeNiTi_{0.5}$ high-entropy coating on Ti 6Al-4V alloy. *Surf. Coat. Technol.* **2021**, *418*, 127243. DOI
200. Liu, H.; Huang, C.; Tu, J.; et al. Advanced wear protection at high temperatures: a study of $Al_{20}V_{20}Cr_{20}Nb_{(40-x)}Mo_x$ RHEA coatings on Ti6Al4V by laser cladding. *Appl. Surf. Sci.* **2024**, *673*, 160878. DOI
201. Ren, Z.; Hu, Y.; Tong, Y.; et al. Wear-resistant NbMoTaWTi high entropy alloy coating prepared by laser cladding on TC4 titanium alloy. *Tribol. Int.* **2023**, *182*, 108366. DOI
202. Meng, Y.; Yang, Z.; Shi, Y.; et al. Microstructural evolution and enhanced properties of multi-layer TiZrNbCrCo high entropy alloy coatings laser-clad onto Ti6Al4V alloy. *Intermetallics* **2024**, *173*, 108407. DOI
203. Hao, X.; Liu, H.; Zhang, X.; et al. Friction-wear behaviors and microstructure of AlTiVCrNb lightweight refractory high-entropy alloy coating prepared by laser cladding on Ti6Al4V substrate. *J. Mater. Res. Technol.* **2024**, *29*, 1-11. DOI
204. Liang, J.; Liu, H.; Zhang, Q.; Zhou, L.; Peng, Y. Microstructure and wear behavior of WMoTaNbV refractory high-entropy alloy coating on Ti6Al4V alloy surface prepared by laser cladding. *Materials* **2025**, *18*, 1770. DOI PubMed PMC
205. Xiang, K.; Chen, L.; Chai, L.; Guo, N.; Wang, H. Microstructural characteristics and properties of $CoCrFeNiNb_x$ high-entropy alloy coatings on pure titanium substrate by pulsed laser cladding. *Appl. Surf. Sci.* **2020**, *517*, 146214. DOI
206. Zhang, Q.; Liu, H.; Zhou, L.; et al. Microstructure and wear-resistance of $AlNbTiVB_x$ high entropy alloy coatings prepared by laser cladding on Ti6Al4V substrate. *Mater. Today. Commun.* **2025**, *44*, 112158. DOI
207. Liu, Q.; Miao, X.; Wu, M.; Wang, H.; Jie, D. Enhanced wear-corrosion synergy in lightweight $(Ti_{50}Nb_{15}V_{15}Zr_5Cr_5)_{100-x}Al_x$ high entropy alloy coatings via laser cladding. *Met. Mater. Int.* **2026**, *32*, 2307-22. DOI
208. Yang, C.; Liu, H.; Liu, Y.; Hao, X.; Wang, Y.; Liu, H. Wear and high-temperature oxidation resistance of $(AlCrFeTiV)_{100-x}Ni_x$ high-entropy alloy coatings prepared by laser cladding on Ti6Al4V alloy. *Surf. Coat. Technol.* **2024**, *489*, 131147. DOI
209. Wu, X.; Zhou, G.; Sun, D.; et al. Cultivating a comprehensive understanding of microstructural attributes and wear mechanisms in $FeCrCoNiAlTi_x$ high-entropy alloy coatings on TC6 substrates through laser cladding fabrication. *J. Alloys. Compd.* **2024**, *984*, 173865. DOI
210. Liu, M.; Song, X.; Zhu, Y.; et al. Properties of Ti-Zr-Nb-Cu-Ni multi-principal-component alloy coatings prepared by laser cladding on a Ti6Al4V surface. *Vacuum* **2023**, *217*, 112524. DOI
211. Du, Z.; Su, Y.; Li, J.; et al. Microstructure and properties of laser-cladded TiZrHfNbTaMox RHEA coating on TC4. *Surf. Coat. Technol.* **2025**, *513*, 132454. DOI
212. Zhao, P.; Li, J.; Zhang, Y.; Li, X.; Xia, M.; Yuan, B. Wear and high-temperature oxidation resistances of $AlNbTaZr_x$ high-entropy alloys coatings fabricated on Ti6Al4V by laser cladding. *J. Alloys. Compd.* **2021**, *862*, 158405. DOI
213. He, R.; Wu, M.; Cui, C.; Jie, D.; Miao, X. Laser cladding manufacturing of TiC + $TiB_x$ reinforced $FeNiCrTi_{0.3}Al_{0.3}$ high entropy alloy composite coating: effects on corrosion and tribology. *J. Alloys. Compd.* **2024**, *970*, 172631. DOI

214. Li, S.; Liu, D.; Liu, G.; et al. Study on the preparation of $CeO_2$-doped AlCoCrFeNiTi high entropy alloy bioinert coatings by laser cladding: the effect of $CeO_2$ particle size on the tribological properties of the coatings. *Surf. Coat. Technol.* **2023**, *475*, 130155. DOI
215. Hao, X.; Liu, H.; Zhang, X.; et al. Microstructure and wear resistance of in-situ TiN/$(Nb, Ti)_5Si_3$ reinforced MoNbTaWTi-based refractory high entropy alloy composite coatings by laser cladding. *Appl. Surf. Sci.* **2023**, *626*, 157240. DOI
216. Tang, J.; Li, Z.; Liu, X.; et al. Tribology and oxidation properties of graphite/CuNiTiCrNb HEA coatings produced by laser cladding. *Carbon* **2026**, *249*, 121261. DOI
217. Cui, C.; Wu, M.; Miao, X.; Zhao, Z.; Gong, Y. Microstructure and corrosion behavior of $CeO_2$/FeCoNiCrMo high-entropy alloy coating prepared by laser cladding. *J. Alloys. Compd.* **2022**, *890*, 161826. DOI
218. Liu, Y.; Cui, X.; Jin, G.; Wen, X.; Wang, S.; Zhang, Y. In-situ array TiN reinforced Al-Cr-Ti-Nb-Mo refractory high-entropy alloy coating on Ti6Al4V alloy by gas assisted laser nitriding. *J. Alloys. Compd.* **2024**, *981*, 173743. DOI
219. Li, Z.; Zhao, W.; Yu, K.; et al. Effect of $Y_2O_3$ on microstructure and properties of CoCrFeNiTiNb high entropy alloy coating on Ti6Al4V surface by laser cladding. *J. Rare. Earths.* **2024**, *42*, 586-99. DOI
220. Cui, W.; Li, W.; Chen, W.; Liou, F. Laser metal deposition of an $AlCoCrFeNiTi_{0.5}$ high-entropy alloy coating on a Ti6Al4V substrate: microstructure and oxidation behavior. *Crystals* **2020**, *10*, 638. DOI
221. Zhang, Z.; Hua, K.; Cao, Y.; et al. Microstructures and properties of FeCrAlMoSi high entropy alloy coatings prepared by laser cladding on a titanium alloy substrate. *Surf. Coat. Technol.* **2024**, *478*, 130437. DOI
222. Zhang, X.; Guo, C.; Huang, G.; et al. Study on microstructures and properties of FeCoNiCuAlSi$_x$ high-entropy alloy composite coatings by laser cladding. *Micromachines* **2025**, *16*, 1211. DOI PubMed PMC
223. Zhang, G.; Yang, X.; Qi, W.; et al. Effect of Co on phase stability and mechanical behavior of $Co_xCrFeNiMnAl_{0.3}$ high entropy alloys with micro/nano hierarchical structure. *Mater. Des.* **2022**, *215*, 110442. DOI
224. Zhang, F.; Liu, X.; Chen, G.; et al. Tribo-corrosion performance of laser cladding CuNiTiCrNb(h-BN)$_x$ high-entropy alloy coatings. *Tribol. Int.* **2026**, *214*, 111190. DOI
225. Hu, J.; Sun, L.; Dong, H.; et al. Laser-clad AlNbTiVZr lightweight refractory high-entropy alloy coating on Ti6Al4V: microstructural characterization and wear resistance. *J. Alloys. Compd.* **2025**, *1026*, 180425. DOI
226. Liu, Y.; Liu, H.; Chen, Y.; et al. Microstructure and high-temperature wear behavior of TiZrNbAl$_x$ light-weight refractory high-entropy alloy coatings prepared by laser cladding on Ti6Al4V titanium alloy. *Surf. Coat. Technol.* **2025**, *512*, 132297. DOI


**Disclaimer/Publisher's Note:** All statements, opinions, and data contained in this publication are solely those of the individual author(s) and contributor(s) and do not necessarily reflect those of OAE and/or the editor(s). OAE and/or the editor(s) disclaim any responsibility for harm to persons or property resulting from the use of any ideas, methods, instructions, or products mentioned in the content.

© The Author(s) 2026. Open Access This article is licensed under a Creative Commons Attribution 4.0 International License (https://creativecommons.org/licenses/by/4.0/), which permits unrestricted use, sharing, adaptation, distribution and reproduction in any medium or format, for any purpose, even commercially, as long as you give appropriate credit to the original author(s) and the source, provide a link to the Creative Commons license, and indicate if changes were made.